Supporting Information

for

Synthesis, coordination behavior, and catalytic properties of dppf congeners with an inserted carbonyl moiety

Petr Vosáhlo, Ivana Císařová, Petr Štěpnička*

Contents

X-ray Crystallography S-2
Copies of the NMR Spectra S-10
References S-54

X-ray Crystallography

The crystal structure of 15

Compound **15** crystallizes with the symmetry of the orthorhombic space group *Pbca* with one molecule per the asymmetric unit (Figure S1). The molecule contains symmetrically coordinated diimine ligand (Pd-N1 = 2.161(1), Pd-N1 = 2.155(1) Å), which forms a planar chelate ring (atoms Pd, N1, N2, C1, and C2 are coplanar within ca. 0.03 Å). The in-ring distances are as follows: N1-C1 1.277(2) Å, N2-C2 1.488(2) Å, and C1-C2 1.469(2) Å). Similar parameters were determined for [Pd{η^2-(*E*)-CH(CN)=CH(CN)}N^N)][1] and [Pd(η^2-$MeO_2CC{\equiv}CCO_2Me$)(N^N)][2] (N^N = *N*,*N*′-di-*t*-butylethanedialdiimine). The η^2-*N*-methylmaleimide (mi) is coordinated in side-on fashion with Pd-C41 = 2.067(1) Å, and Pd-C42 = 2.068(1) Å, essentially planar (the eight atoms are coplanar within 0.02 Å) and oriented nearly perpendicularly to the {Pd, N1, N2} plane (dihedral angle: 72.18(6)°). Such features are again similar to those determined for [Pd(η^2-mi){fc(P(*t*-Bu)R)$_2$-κ^2*P*,*P*′}] (fc = ferrocene-1,1'-diyl, R = Ph, 2-pyridyl).[3]

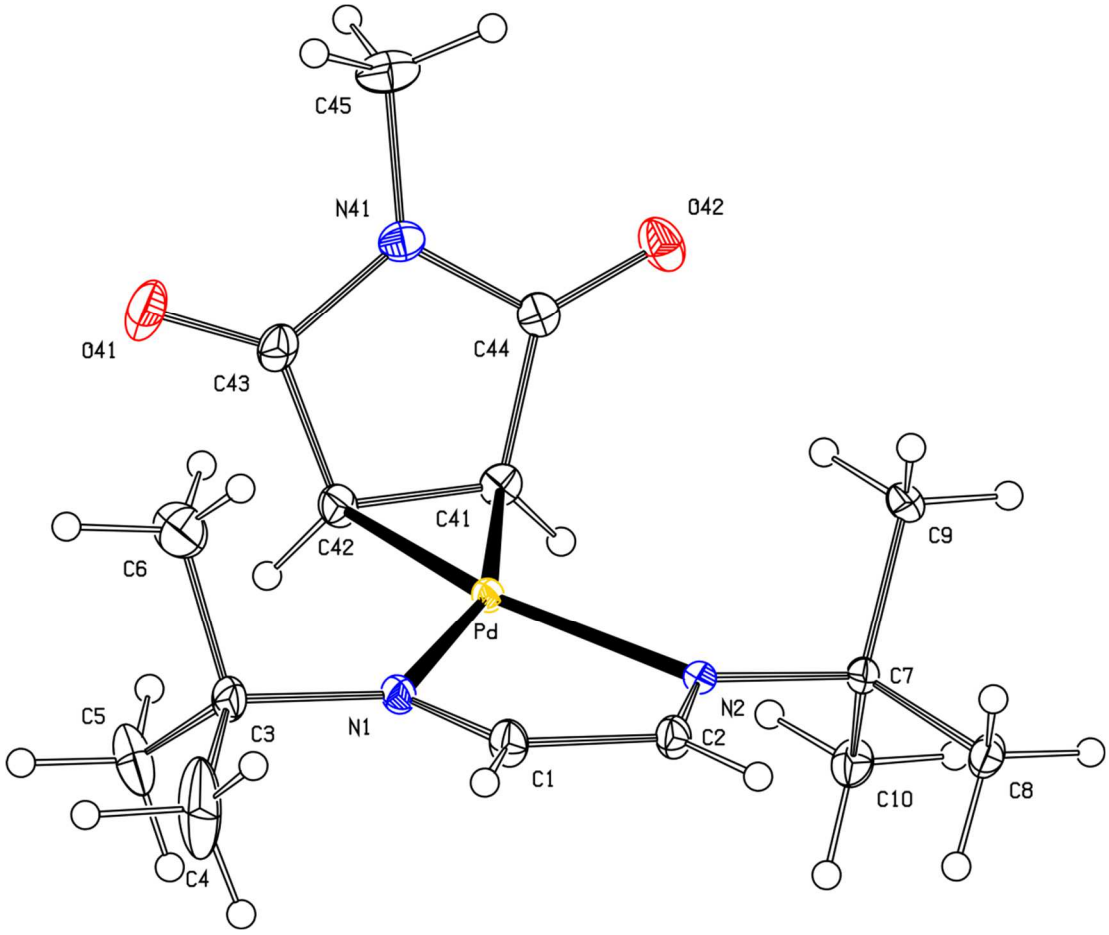

Figure S1. PLATON plot of the molecular structure of **15** showing 30% probability ellipsoids.

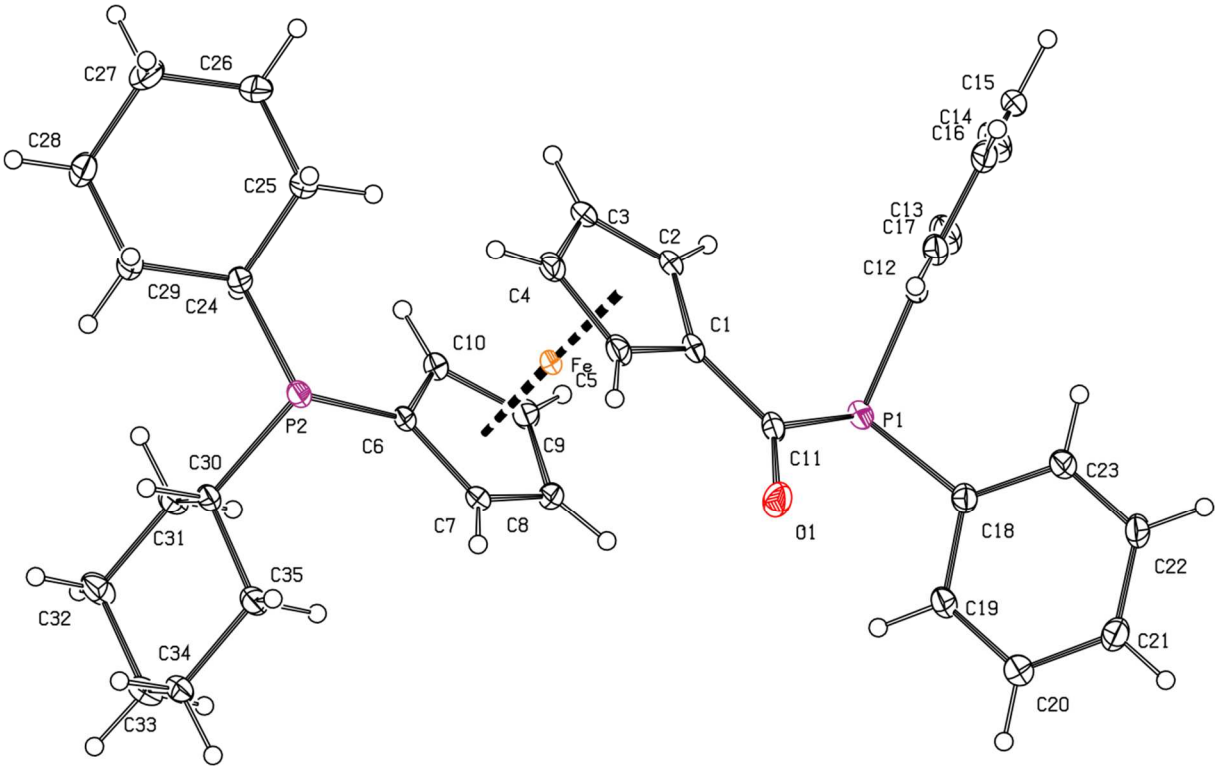

Figure S2. PLATON plot of the molecular structure of **3** showing 30% probability ellipsoids.

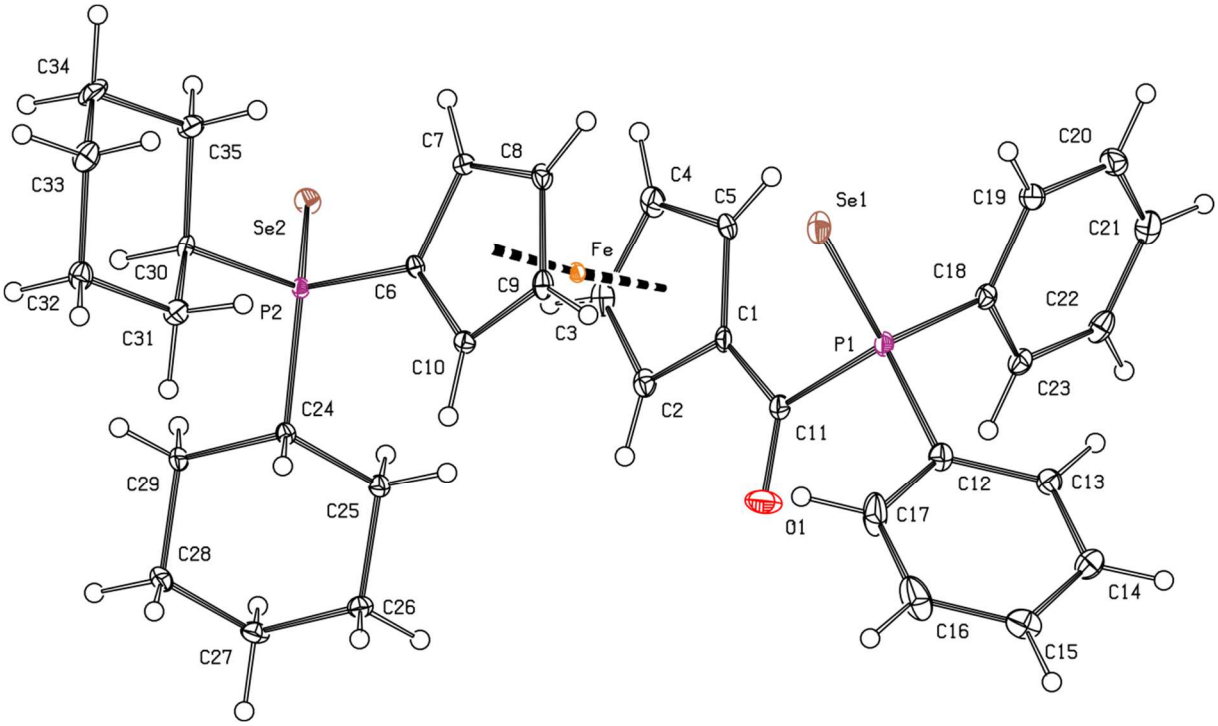

Figure S3. PLATON plot of the molecular structure of **9** showing 30% probability ellipsoids.

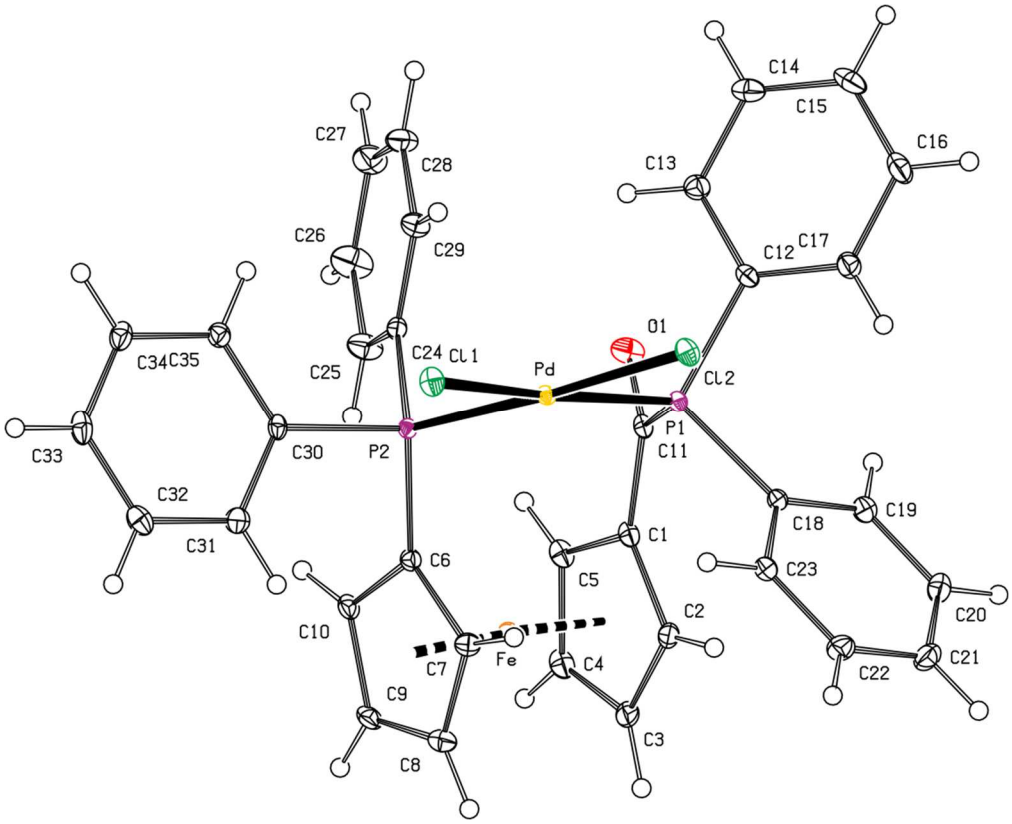

Figure S4. PLATON plot of the complex molecule in the structure of **11**·$3CH_2Cl_2$ showing 30% probability ellipsoids.

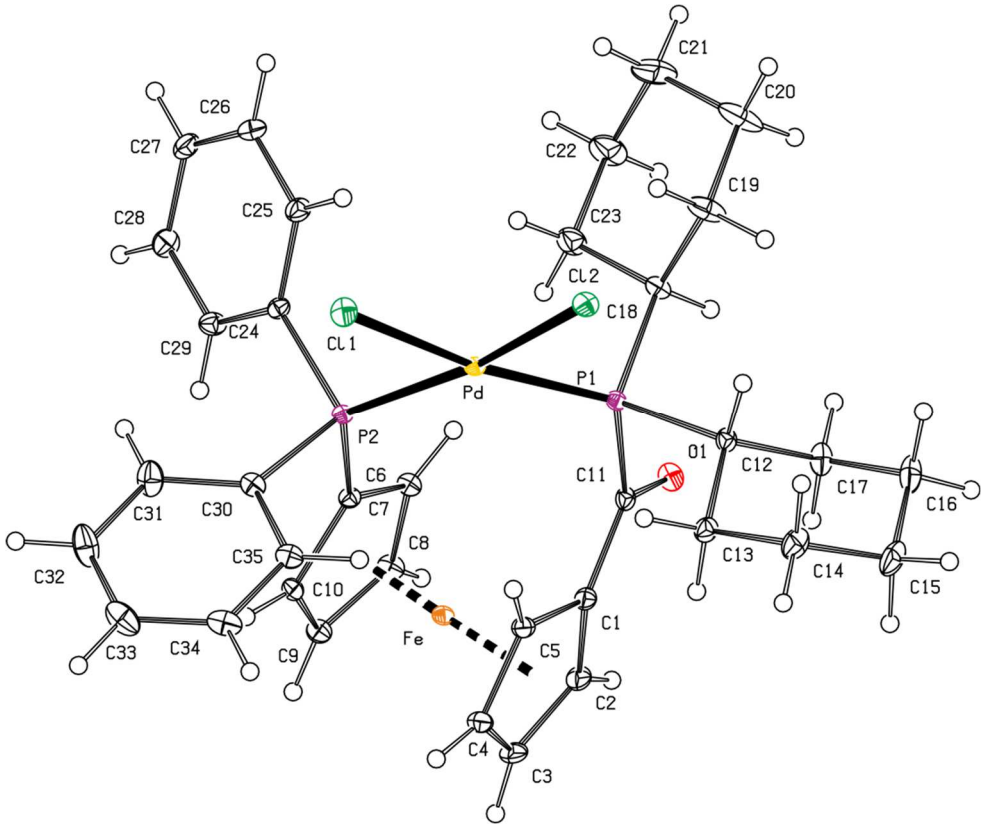

Figure S5. PLATON plot of the complex molecule in the structure of **12**·$CHCl_3$ showing 30% probability ellipsoids.

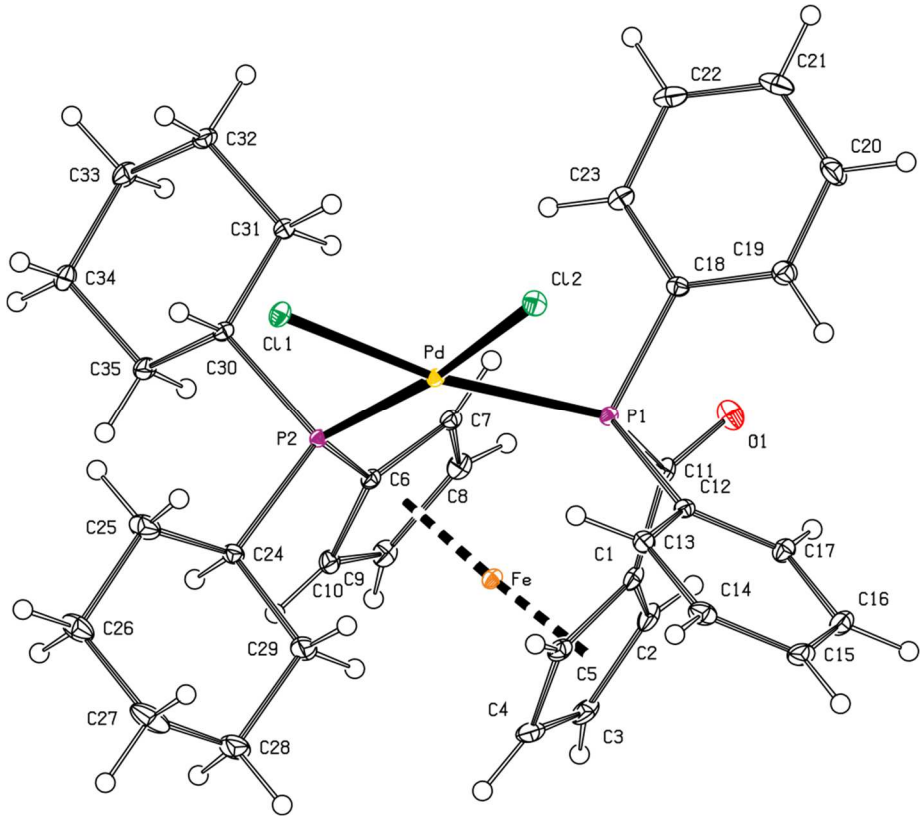

Figure S6. PLATON plot of the complex molecule in the structure of **12**·$3C_2H_4Cl_2$ showing 30% probability ellipsoids.

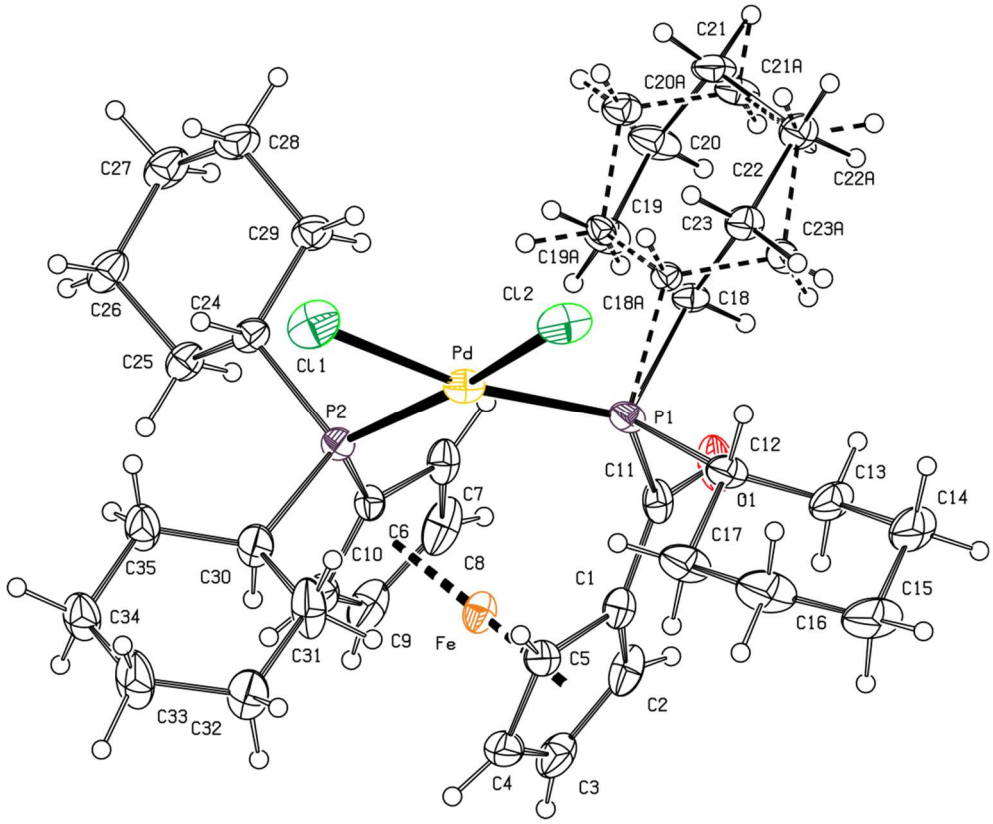

Figure S7. PLATON plot of the complex molecule in the structure of **14a**·$1.5Et_2O$ showing 30% probability ellipsoids.

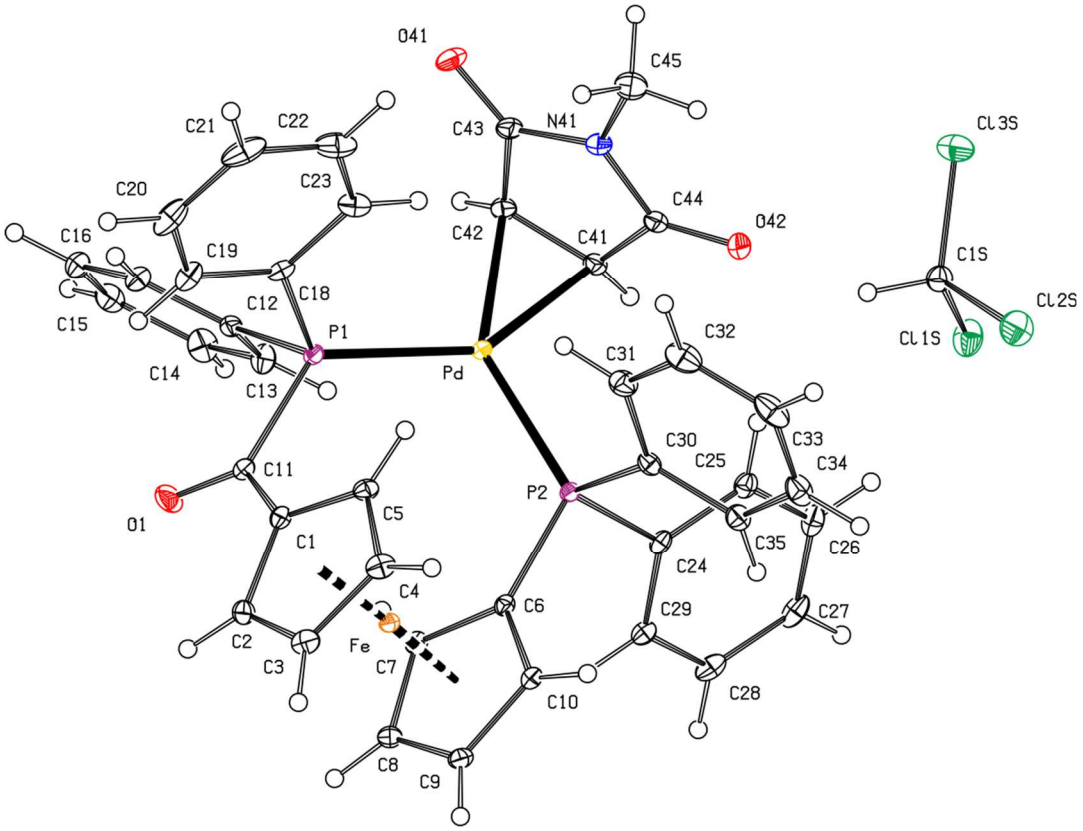

Figure S8. PLATON plot of the molecular structure of **16**·$CHCl_3$ showing 30% probability ellipsoids.

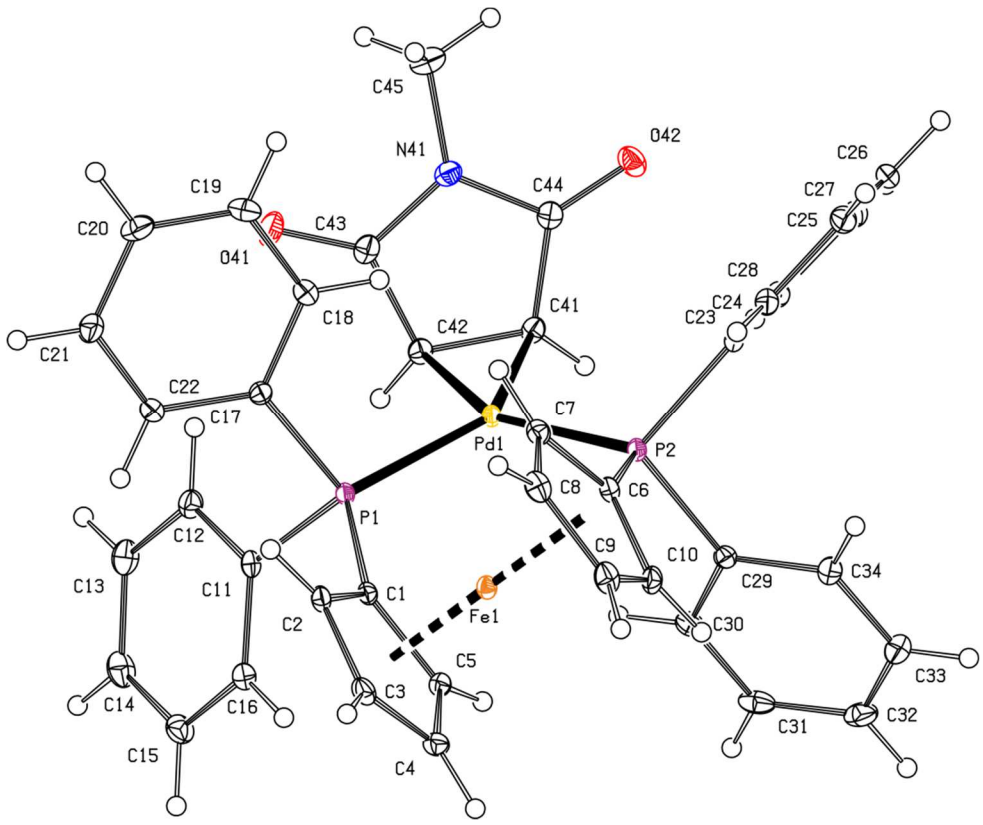

Figure S9. PLATON plot of the molecular structure of **20** showing 30% probability ellipsoids.

Table S2. Selected crystallographic data and structure refinement parameters.[a]

Compound	**3**	**9**	**11**·$3CH_2Cl_2$
Formula	$C_{35}H_{40}FeOP_2$	$C_{35}H_{40}FeOP_2Se_2$	$C_{38}H_{34}Cl_8FeOP_2Pd$
M	594.46	752.38	1014.44
Crystal system	triclinic	monoclinic	triclinic
Space group	*P*–1 (no. 2)	$P2_1$ (no. 4)	*P*–1 (no. 2)
T [K]	120(2)	120(2)	150(2)
a [Å]	6.0140(2)	10.3484(8)	10.6263(5)
b [Å]	11.4903(5)	13.291(1)	13.0647(6)
c [Å]	22.172(1)	11.8953(9)	16.3339(8)
α [°]	85.552(2)		110.403(2)
β [°]	84.954(1)	101.676(3)	104.240(2)
γ [°]	78.179(1)		98.716(2)
V [$Å^3$]	1491.1(1)	1602.3(2)	1988.5(2)
Z	2	2	2
μ(Mo Kα) [mm^{-1}]	0.640	2.870	1.467
Diffrns collected	62932	41498	55604
Independent diffrns	6841	7372	9147
Observed[a] diffrns	6135	7080	8196
R_{int}[b] [%]	3.25	3.43	2.89
No. of parameters	352	370	460
R[b] obsd diffrns [%]	2.91	1.92	2.49
R, *wR*[b] all data [%]	3.34, 7.61	2.14, 4.30	2.99, 6.13
Δρ [e $Å^{-3}$]	0.599, –0.243	0.225, –0.340	0.811, –0.817
CCDC deposition no.	2177221	2177222	2177223

[a] Diffractions with $I > 2\sigma(I)$. [b] Definitions: $R_{int} = \Sigma\,|F_o^2 - F_o^2(\text{mean})|/\Sigma F_o^2$, where F_o^2(mean) is the average intensity of symmetry-equivalent diffractions. $R = \Sigma\,||F_o| - |F_c||/\Sigma|F_o|$, $wR = [\Sigma\{w(F_o^2 - F_c^2)^2\}/\Sigma w(F_o^2)^2]^{1/2}$.

Table S2 continued

Compound	**12**·$CHCl_3$	**13**·$3C_2H_4Cl_2$	**14a**·$1.5Et_2O$
Formula	$C_{36}H_{41}Cl_5FeOP_2Pd$	$C_{37}H_{44}Cl_4FeOP_2Pd$	$C_{41}H_{67}Cl_2FeO_{2.5}P_2Pd$
M	891.13	870.71	895.03
Crystal system	triclinic	triclinic	monoclinic
Space group	*P*–1 (no. 2)	*P*–1 (no. 2)	$P2_1/c$ (no. 14)
T [K]	120(2)	120(2)	120(2)
a [Å]	10.4175(6)	10.3654(6)	11.7264(5)
b [Å]	14.4351(7)	11.5653(7)	19.7632(8)
c [Å]	14.8759(8)	16.703(1)	17.7941(8)
α [°]	62.941(2)	99.203(2)	
β [°]	83.906(2)	94.117(2)	98.506(2)
γ [°]	82.033(2)	113.043(2)	
V [$Å^3$]	1970.6(2)	1798.8(2)	4078.4(3)
Z	2	2	4
μ(Mo Kα) [mm^{-1}]	1.272	1.319	1.042
Diffrns collected	38683	40823	60155
Independent diffrns	9067	8278	9305
Observed[a] diffrns	8449	7645	8625
R_{int}[b] [%]	2.02	2.46	2.30
No. of parameters	379	419	434
R[b] obsd diffrns [%]	2.01	2.17	3.84
R, *wR*[b] all data [%]	2.23, 5.22	2.49, 5.26	4.20, 8.23
Δρ [e $Å^{-3}$]	0.398, –0.602	0.637, –0.787	0.727, –0.821
CCDC deposition no.	2177224	2177225	2177226

Table S2 continued

Compound	**15**	**16**·$CHCl_3$	**20**
Formula	$C_{15}H_{25}N_3O_2Pd$	$C_{41}H_{34}Cl_3FeNO_3P_2Pd$	$C_{39}H_{33}FeNO_2P_2Pd$
M	385.78	919.23	771.85
Crystal system	orthorhombic	triclinic	monoclinic
Space group	*P*bca (no. 61)	*P*–1 (no. 2)	$P2_1$/n (no. 14)
T [K]	120(2)	120(2)	120(2)
a [Å]	17.3887(4)	8.1762(3)	12.7157(3)
b [Å]	9.9535(3)	12.2017(4)	14.7205(4)
c [Å]	19.3374(5)	20.0739(6)	17.3222(4)
α [°]		81.262(1)	
β [°]		80.928(1)	103.817(1)
γ [°]		74.063(1)	
V [$Å^3$]	3346.9(2)	1889.1(1)	3148.6(1)
Z	8	2	4
μ(Mo Kα) [mm^{-1}]	1.117	1.198	1.172
Diffrns collected	38345	30799	42761
Independent diffrns	4852	8654	7219
Observed[a] diffrns	4472	8088	6865
R_{int}[b] [%]	2.17	2.11	2.07
No. of parameters	197	470	416
R[b] obsd diffrns [%]	1.93	2.12	1.94
R, *wR*[b] all data [%]	2.16, 4.70	2.40, 4.93	2.09, 4.82
Δρ [e $Å^{-3}$]	0.548, –0.485	0.434, –0.433	0.763, –0.389
CCDC deposition no.	2177227	2177228	2177229

Copies of the NMR spectra

(Note: solvent signals in the NMR spectra are denoted by an asterisk.)

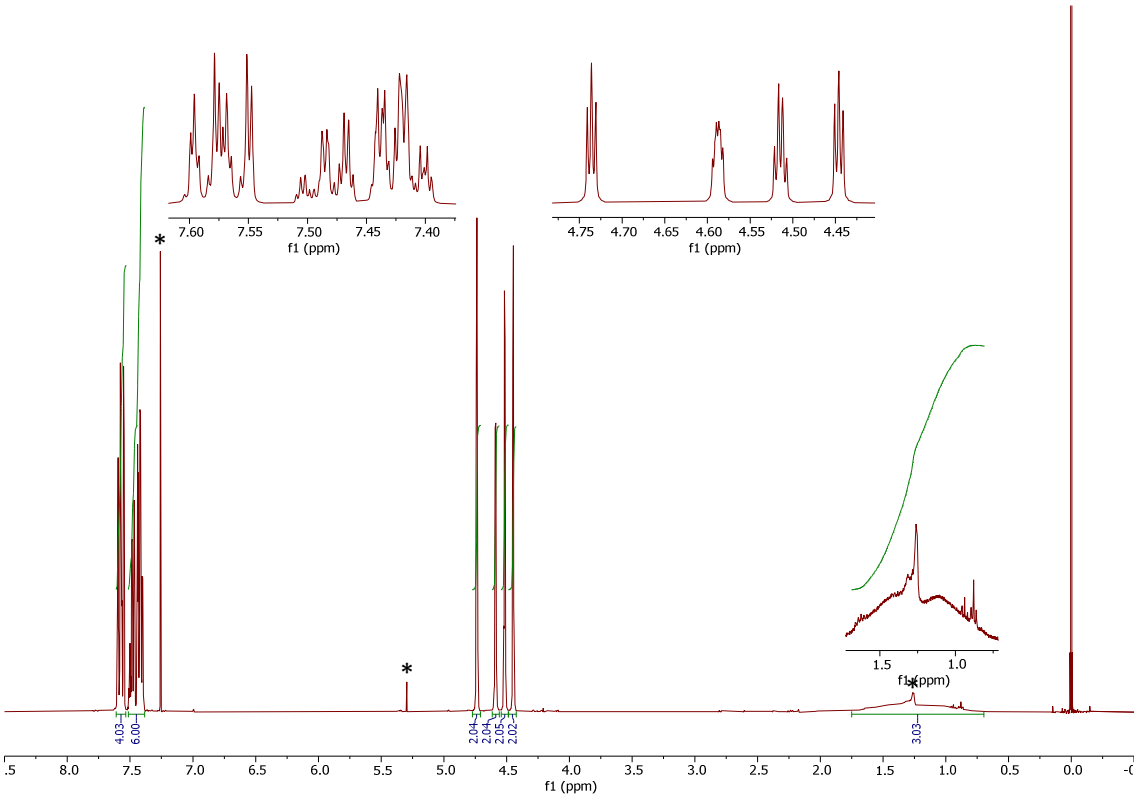

Figure S10. ^{1}H NMR spectrum (400 MHz, $CDCl_3$) of **5**.

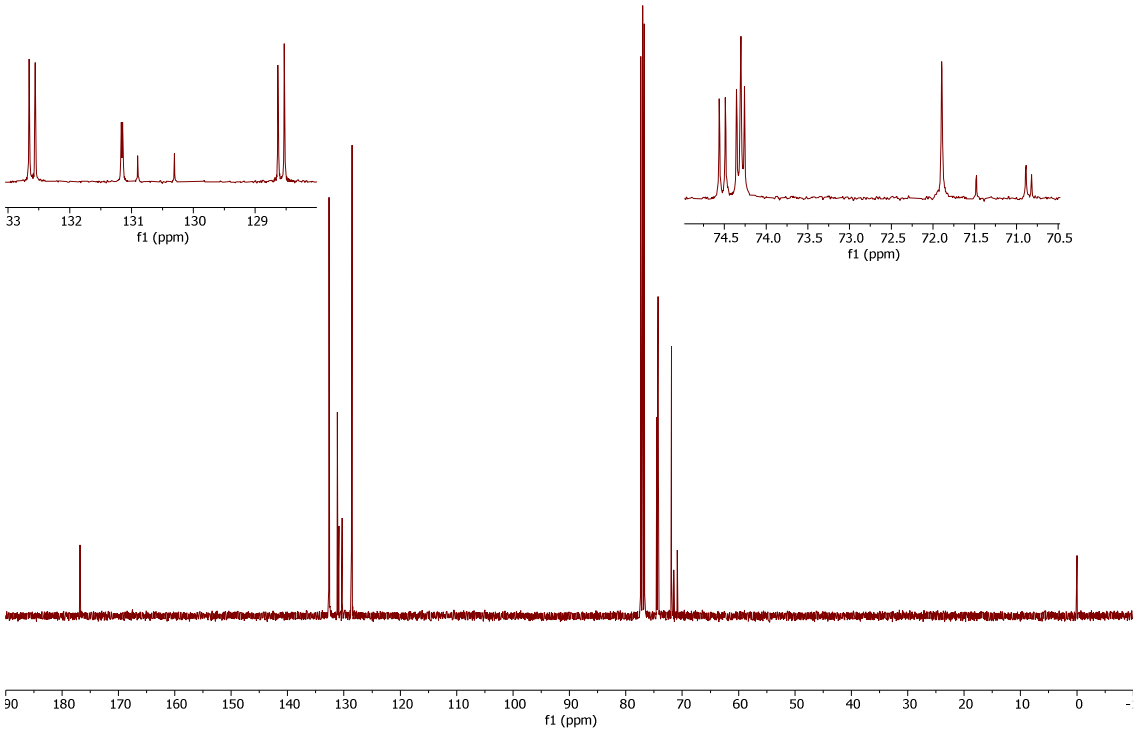

Figure S11. ^{13}C{^{1}H} NMR spectrum (101 MHz, $CDCl_3$) of **5**.

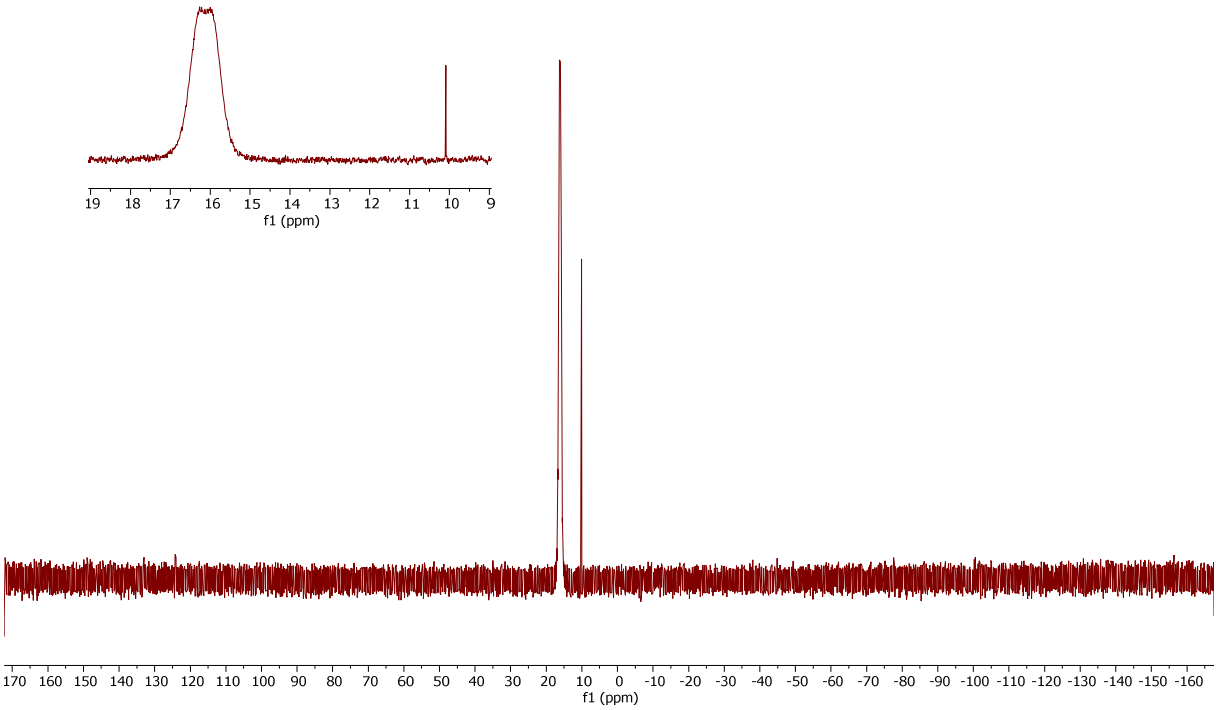

Figure S12. $^{31}P\{^{1}H\}$ NMR spectrum (162 MHz, $CDCl_3$) of **5**.

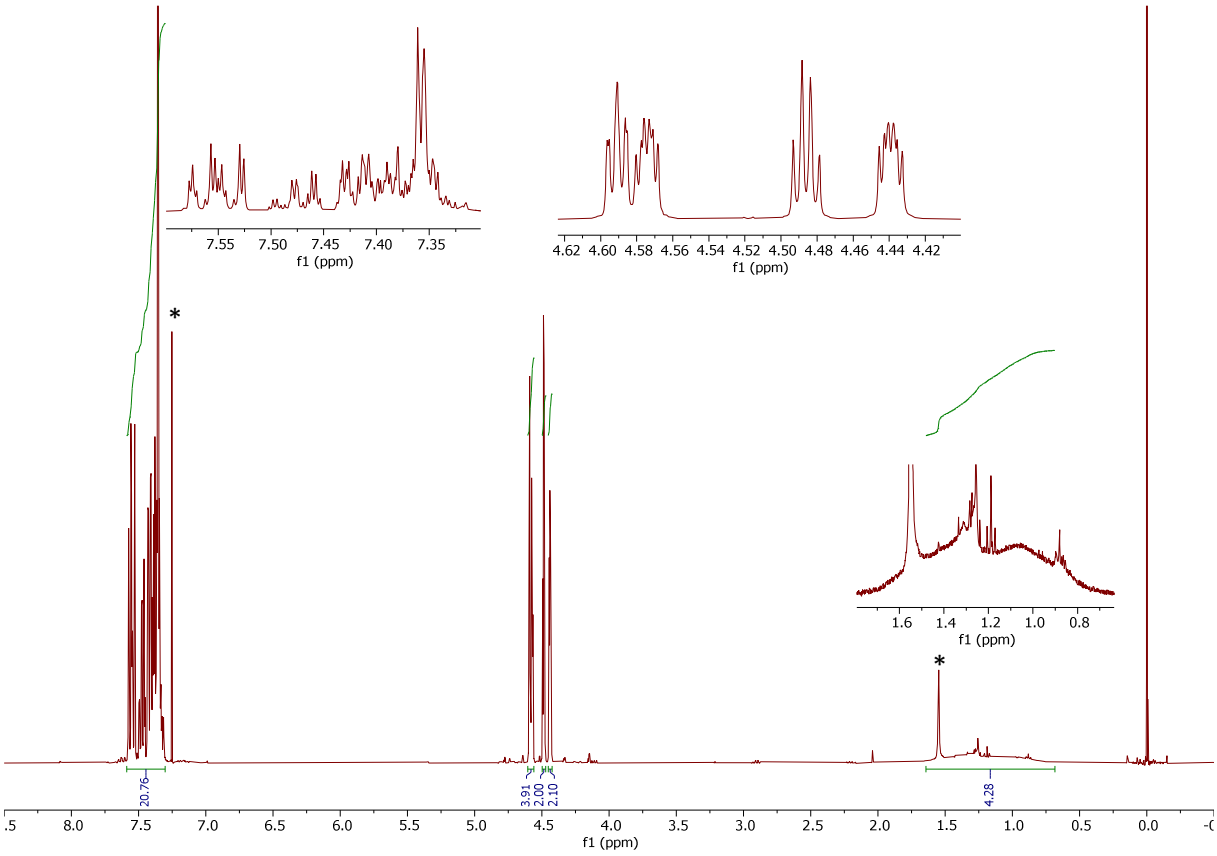

Figure S13. ^{1}H NMR spectrum (400 MHz, $CDCl_3$) of **1·BH$_3$**.

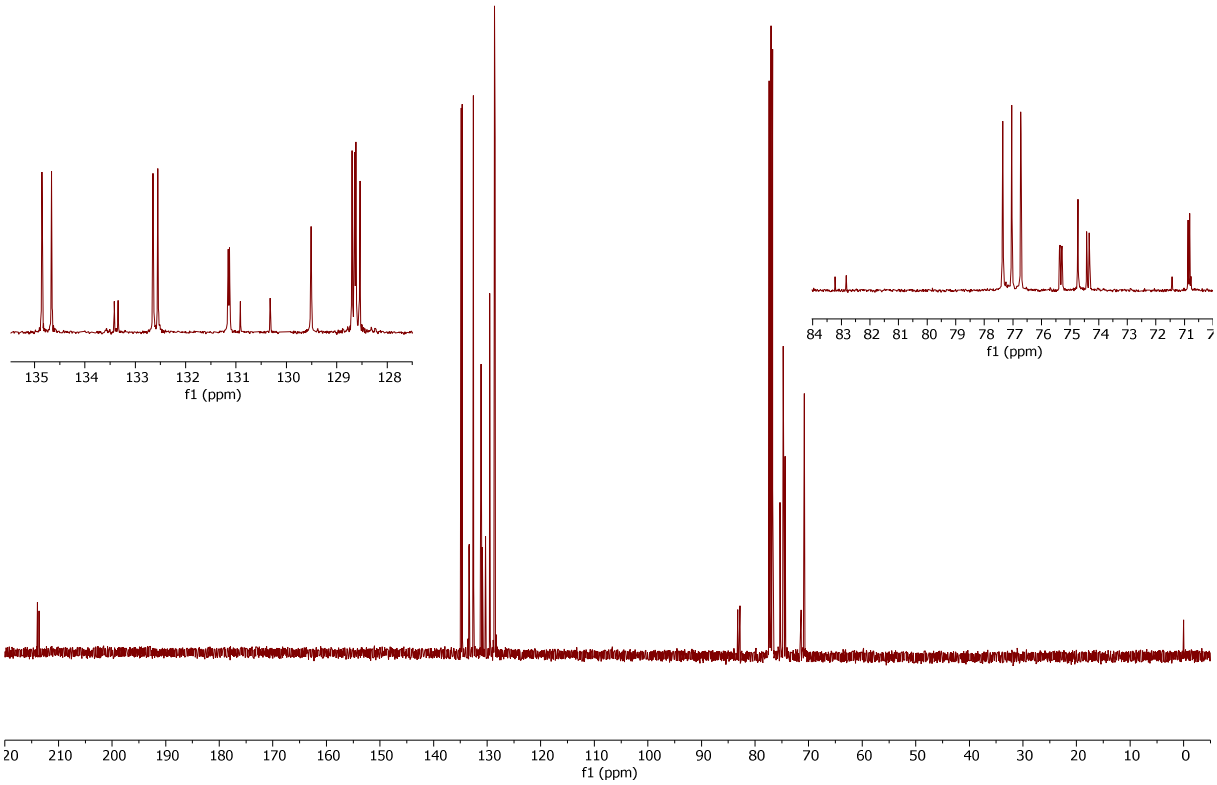

Figure S14. ^{13}C{^{1}H} NMR spectrum (101 MHz, $CDCl_3$) of **1·BH$_3$**.

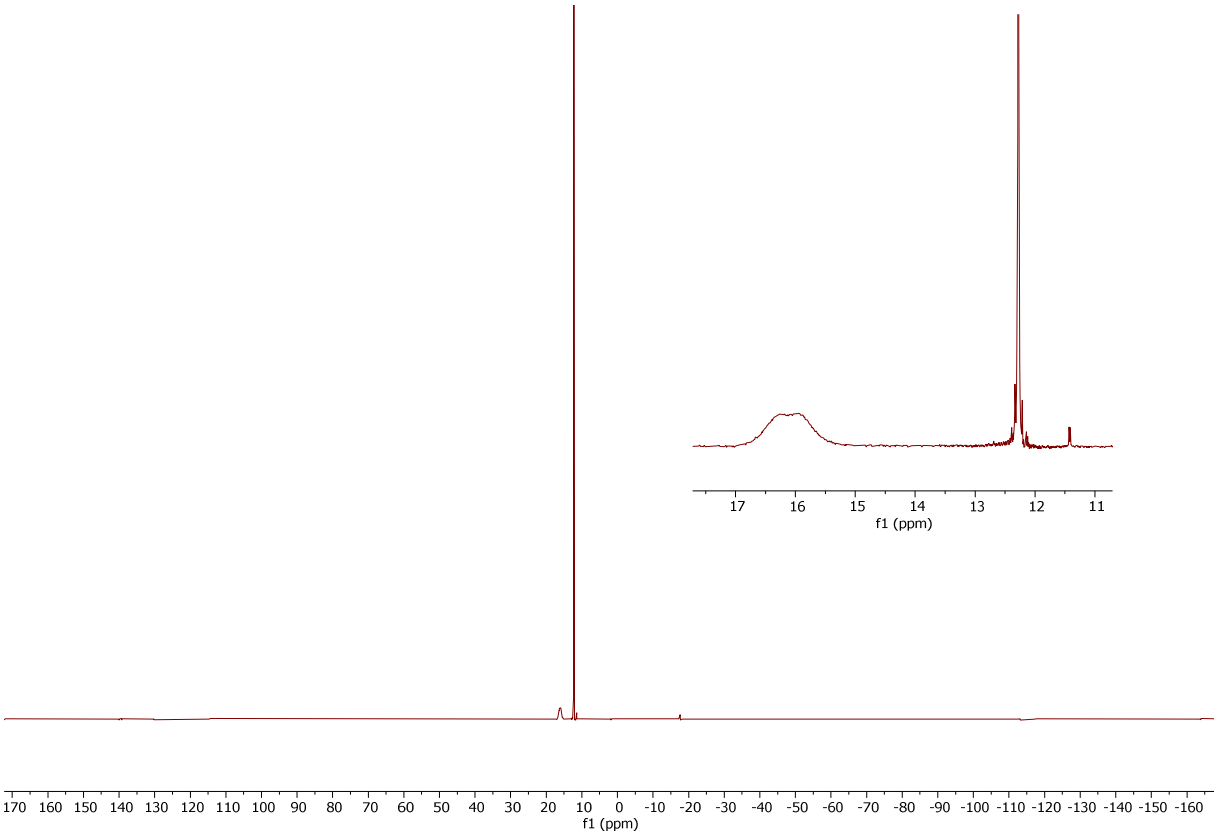

Figure S15. $^{31}P\{^{1}H\}$ NMR spectrum (162 MHz, $CDCl_3$) of **1·BH$_3$**.

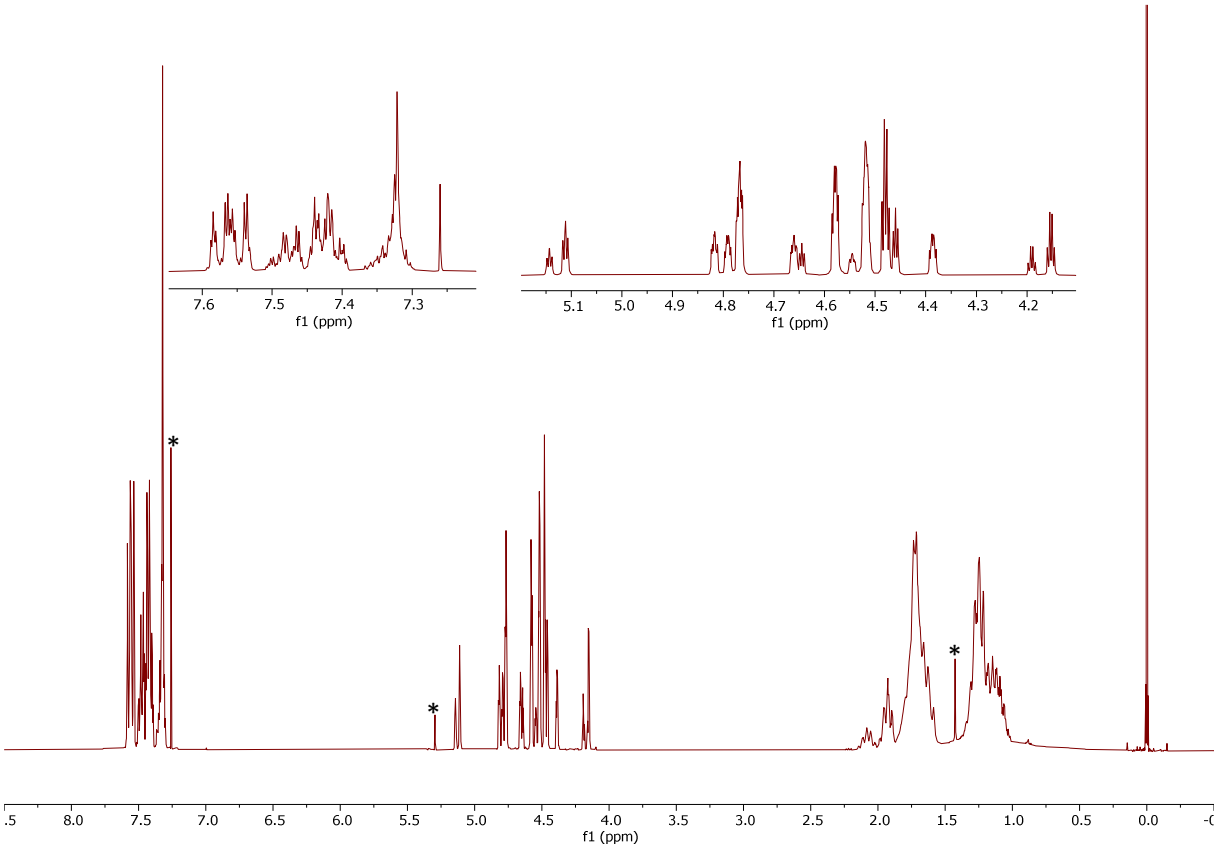

Figure S16. ^{1}H NMR spectrum (400 MHz, $CDCl_3$) of **2·BH$_3$**.

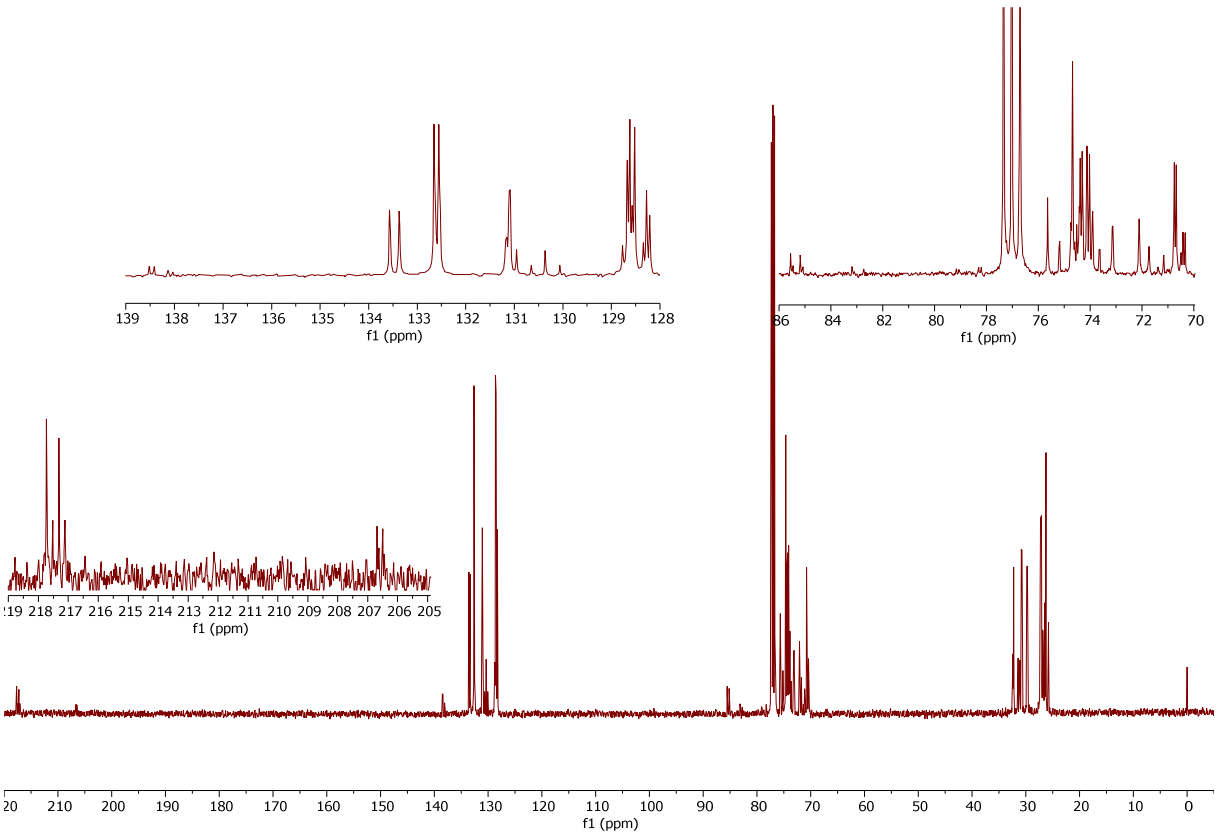

Figure S17. ^{13}C{^{1}H} NMR spectrum (101 MHz, $CDCl_3$) of **2·BH$_3$**.

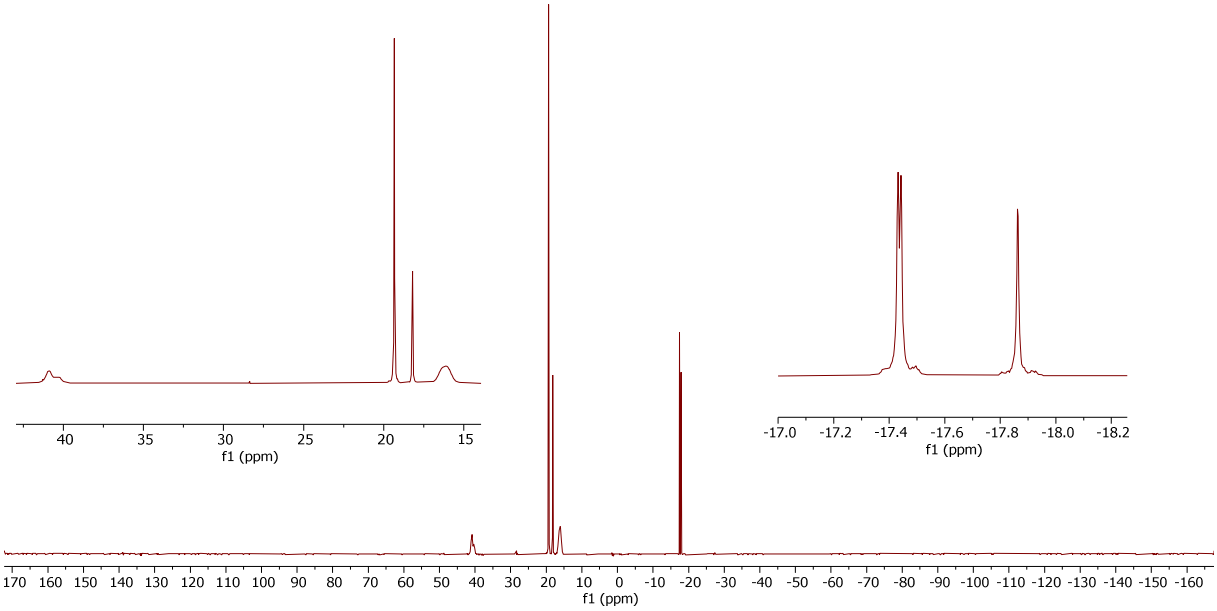

Figure S18. $^{31}P\{^{1}H\}$ NMR spectrum (162 MHz, $CDCl_3$) of **2·BH$_3$**.

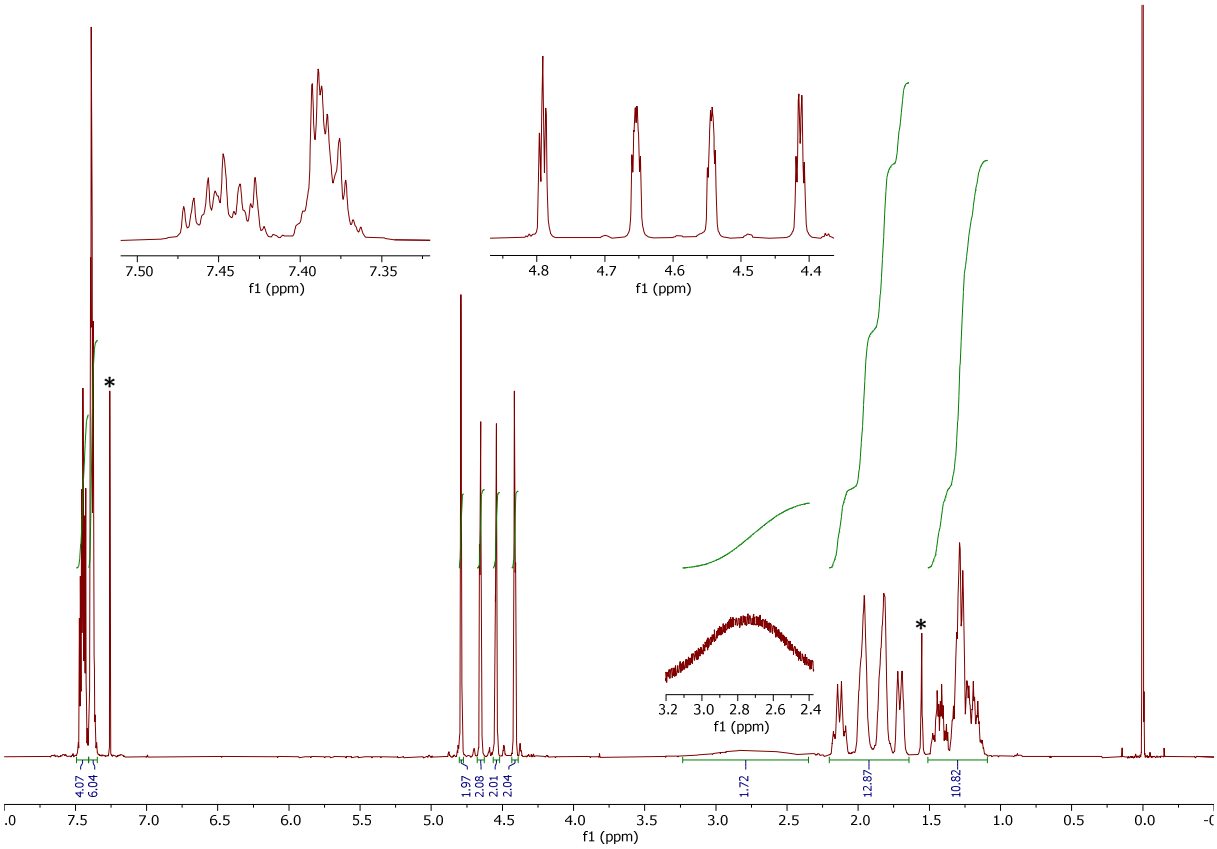

Figure S19. ^{1}H NMR spectrum (400 MHz, $CDCl_3$) of **3·BH$_2$Cl**.

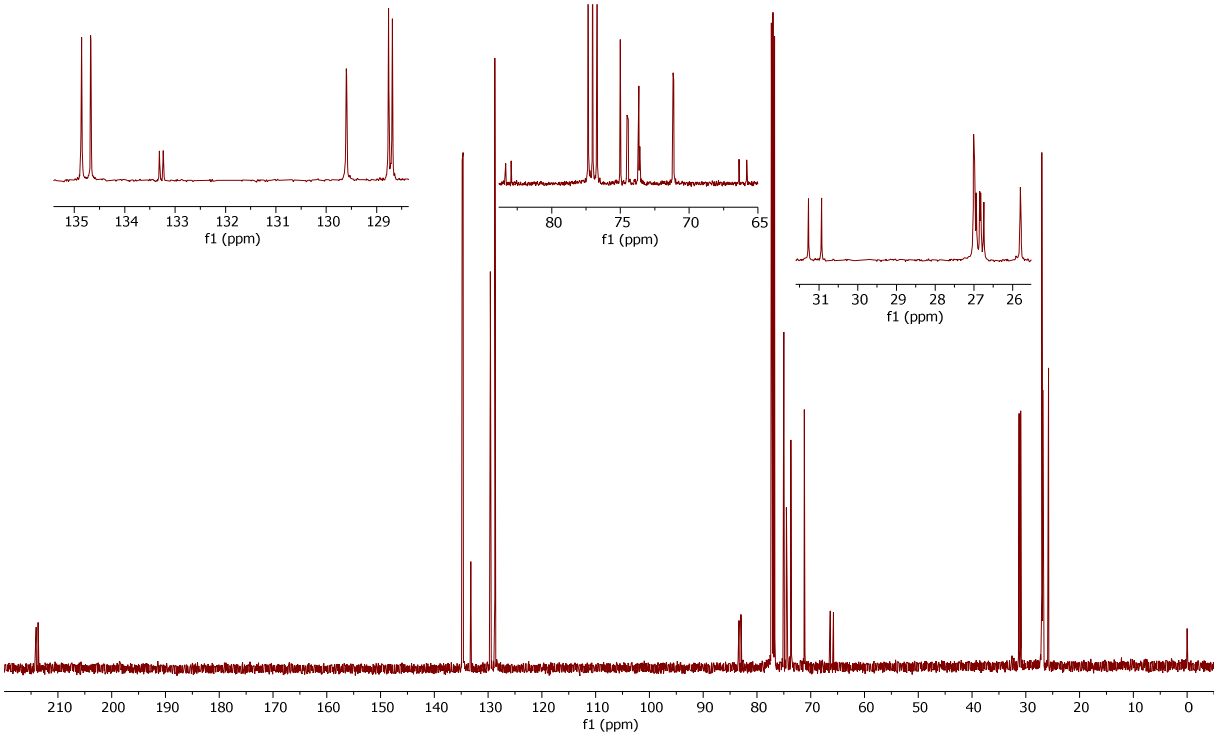

Figure S20. ^{13}C{^{1}H} NMR spectrum (101 MHz, $CDCl_3$) of **3·BH$_2$Cl**.

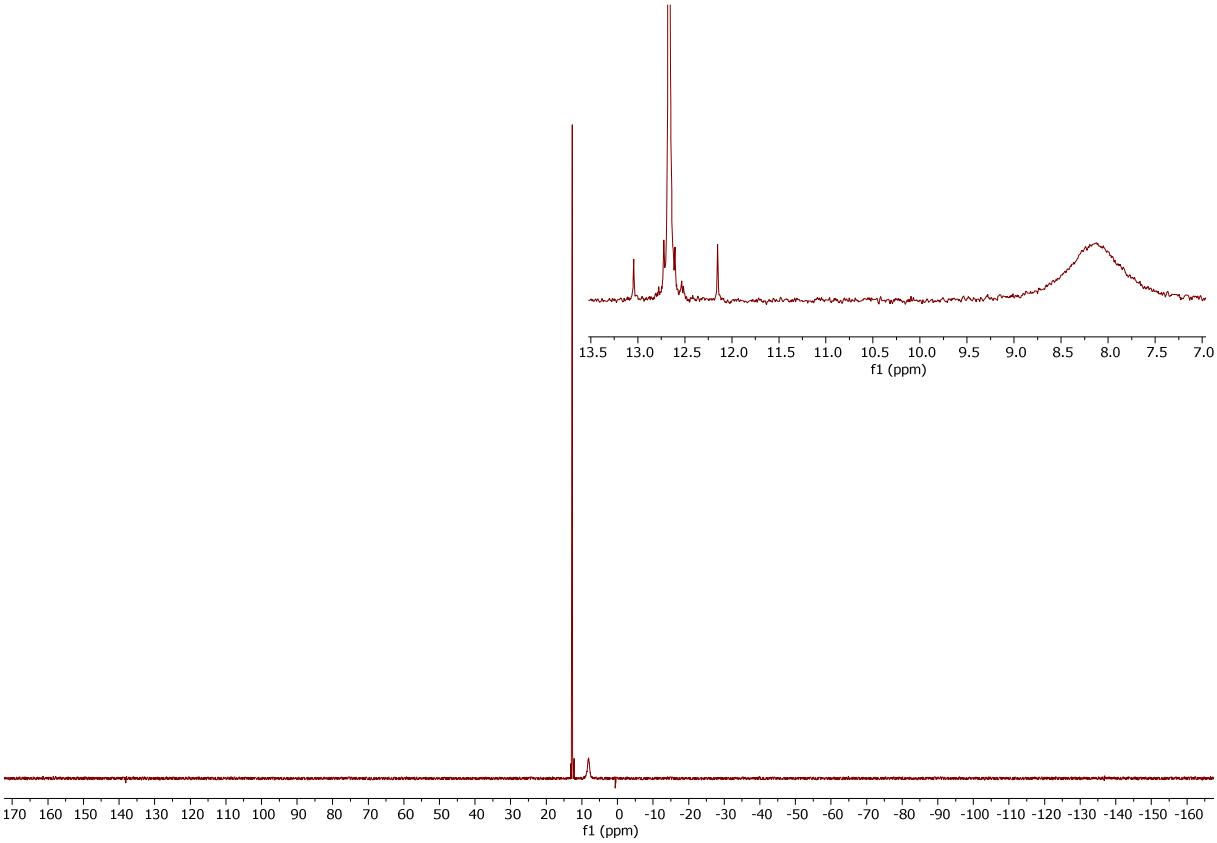

Figure S21. $^{31}P\{^{1}H\}$ NMR spectrum (162 MHz, $CDCl_3$) of **3·BH_2Cl**.

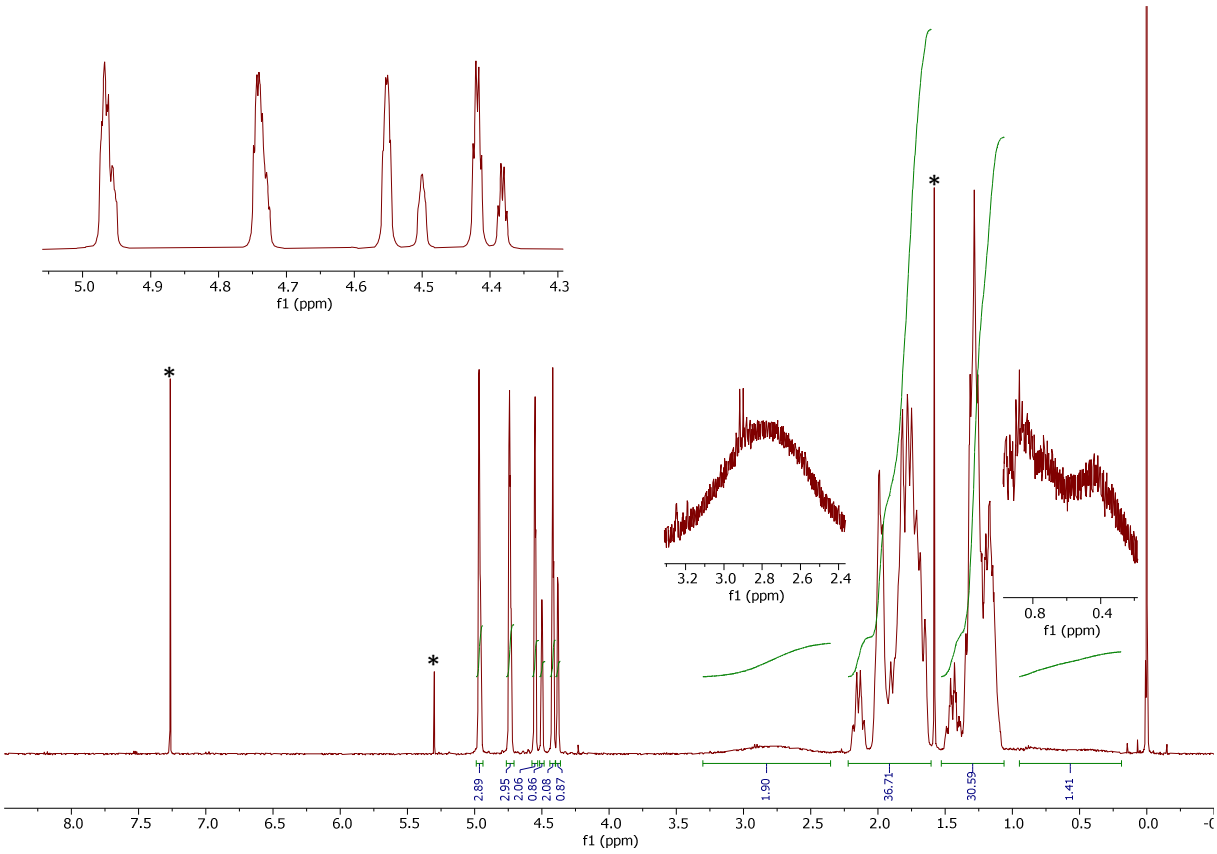

Figure S22. ^{1}H NMR spectrum (400 MHz, $CDCl_3$) of **4·BH$_2$Cl/4·BH$_3$**.

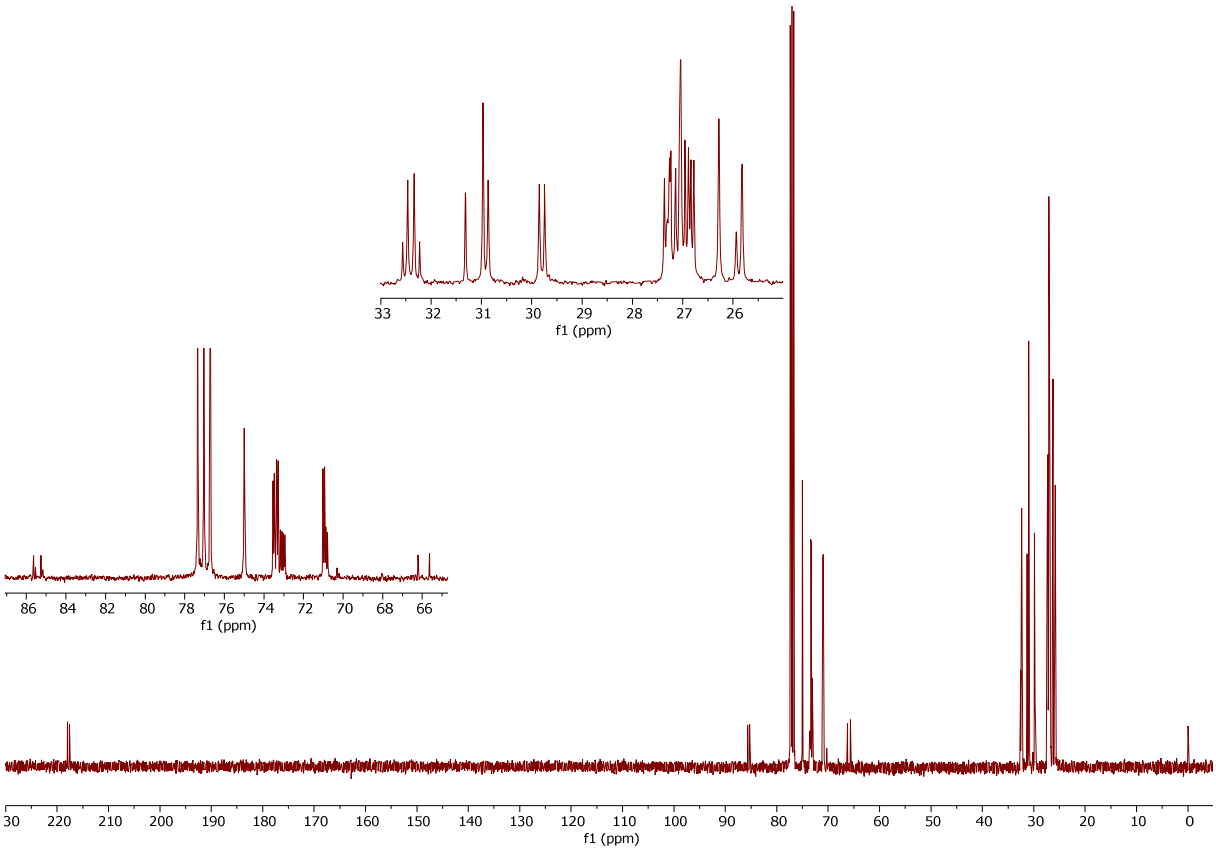

Figure S23. ^{13}C{^{1}H} NMR spectrum (101 MHz, $CDCl_3$) of **4·BH$_2$Cl/4·BH$_3$**.

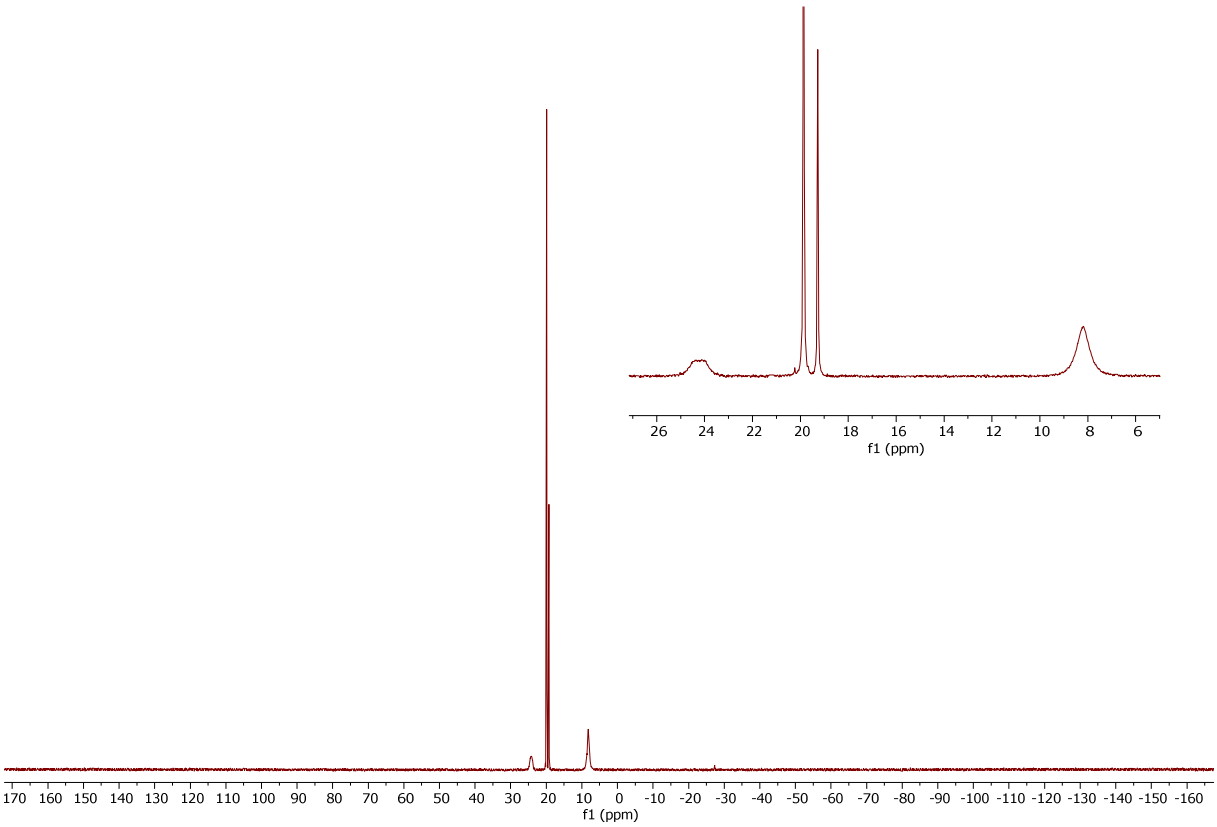

Figure S24. $^{31}P\{^{1}H\}$ NMR spectrum (162 MHz, $CDCl_3$) of **4·BH_2Cl/4·BH_3**.

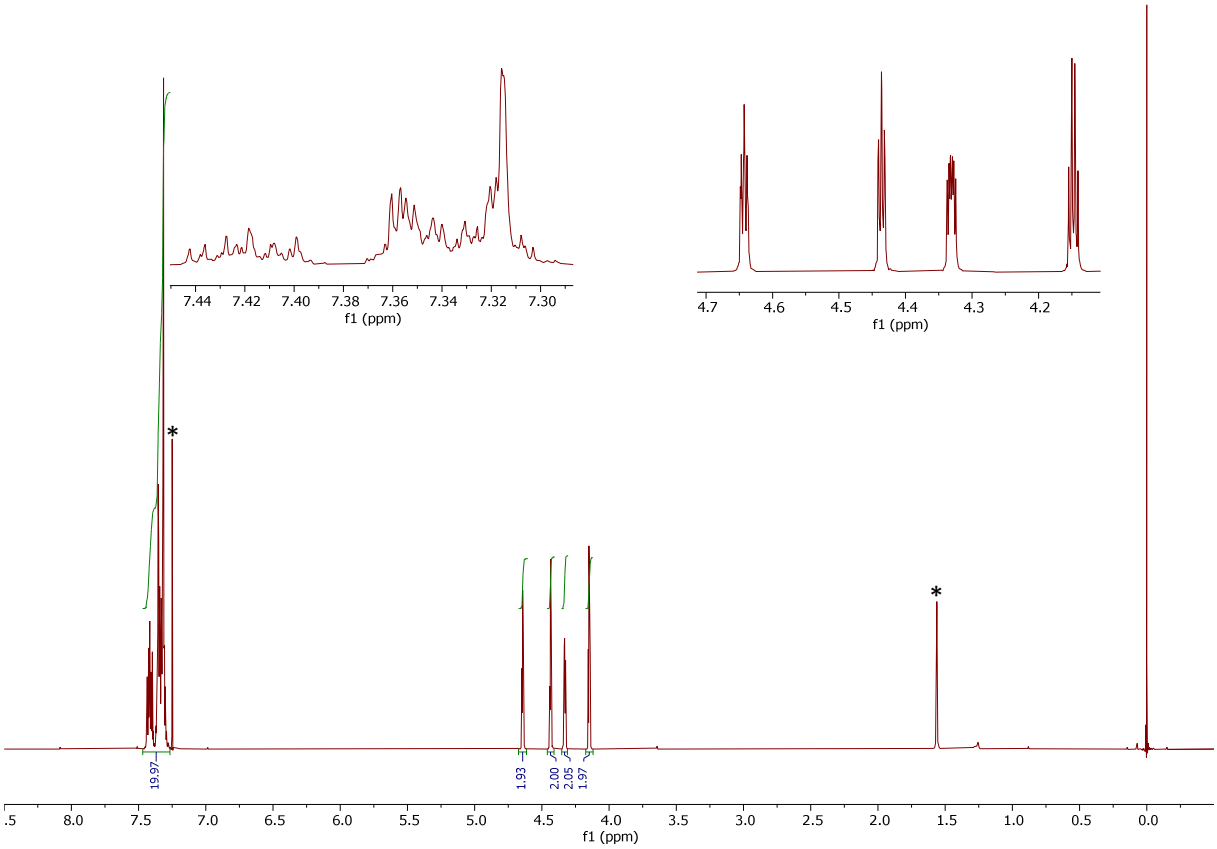

Figure S25. ^{1}H NMR spectrum (400 MHz, $CDCl_3$) of **1**.

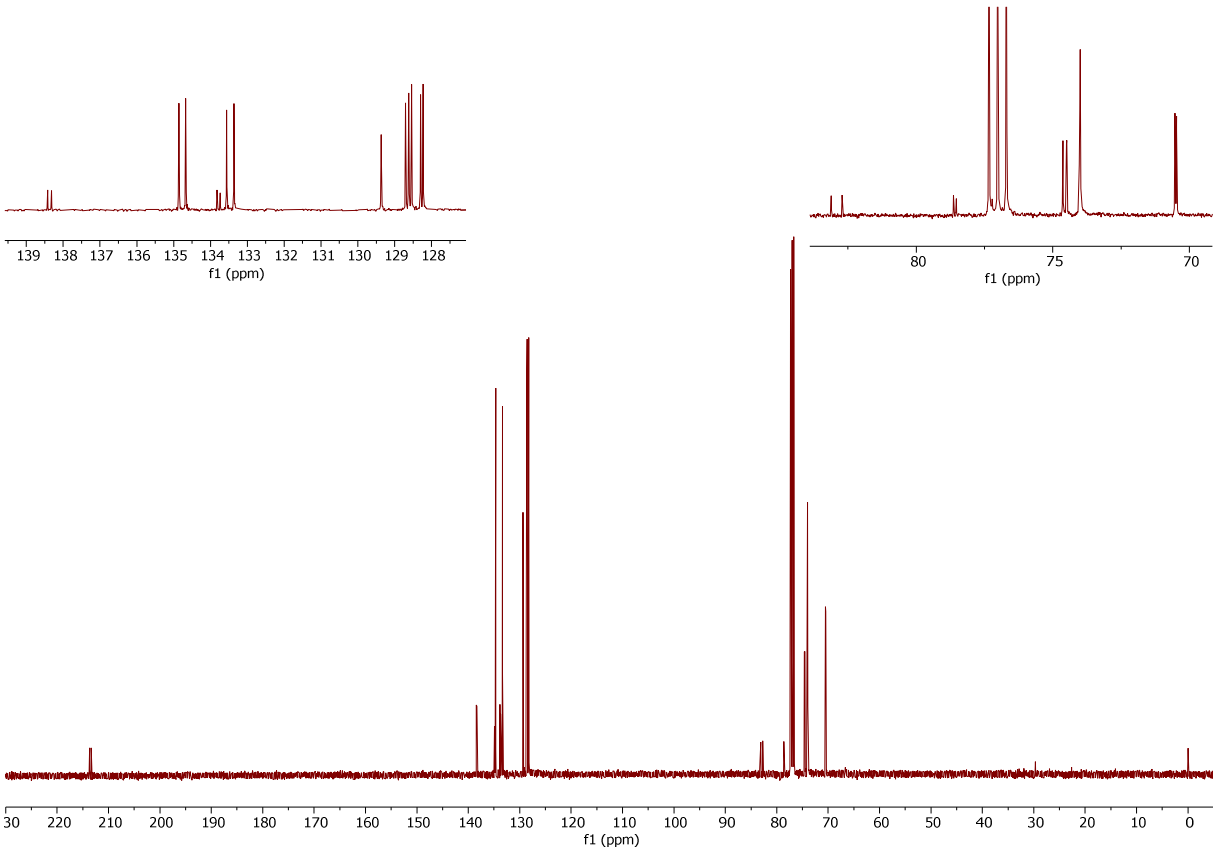

Figure S26. $^{13}C\{^{1}H\}$ NMR spectrum (101 MHz, $CDCl_3$) of **1**.

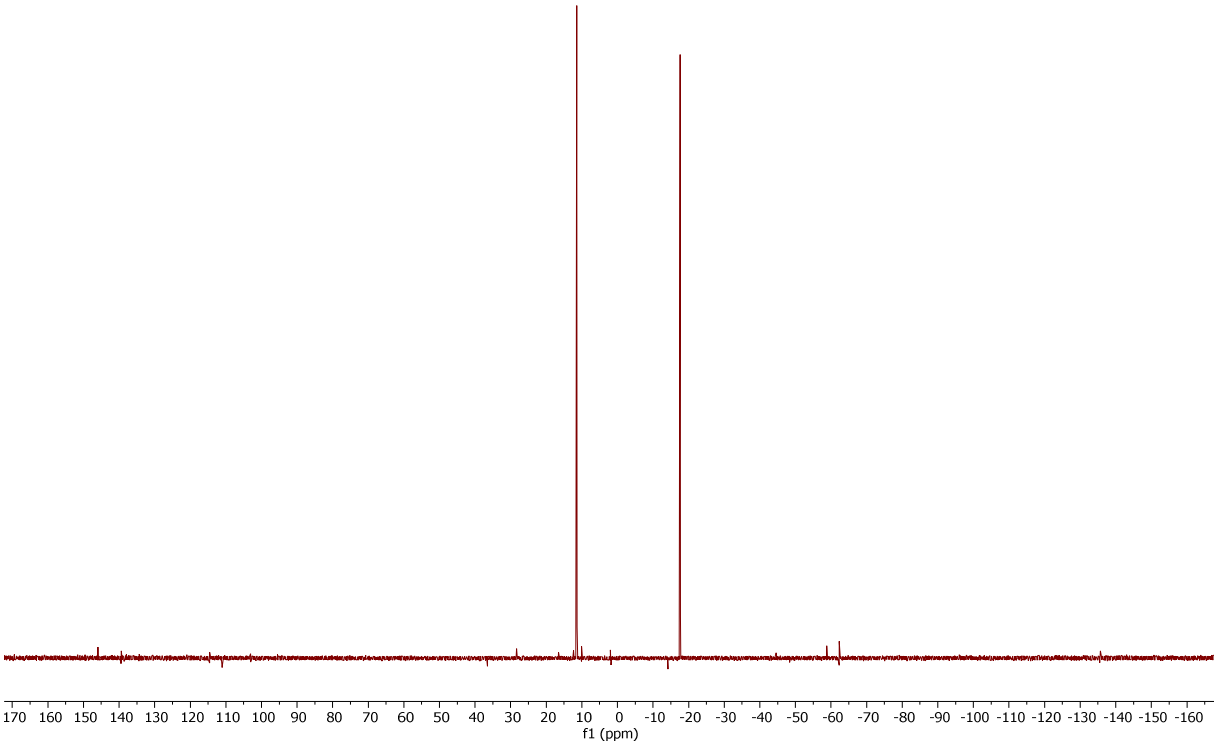

Figure S27. $^{31}P\{^{1}H\}$ NMR spectrum (162 MHz, $CDCl_3$) of **1**.

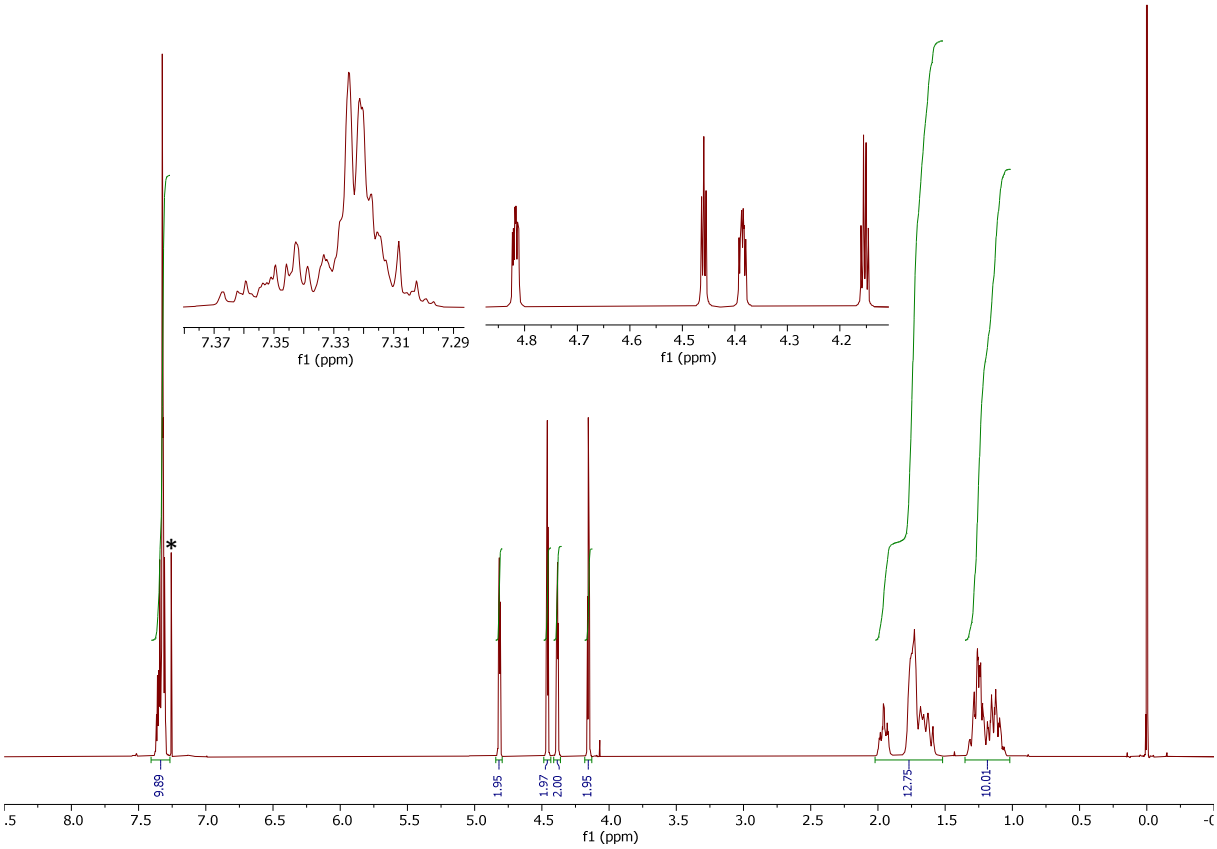

Figure S28. ^{1}H NMR spectrum (400 MHz, $CDCl_3$) of **2**.

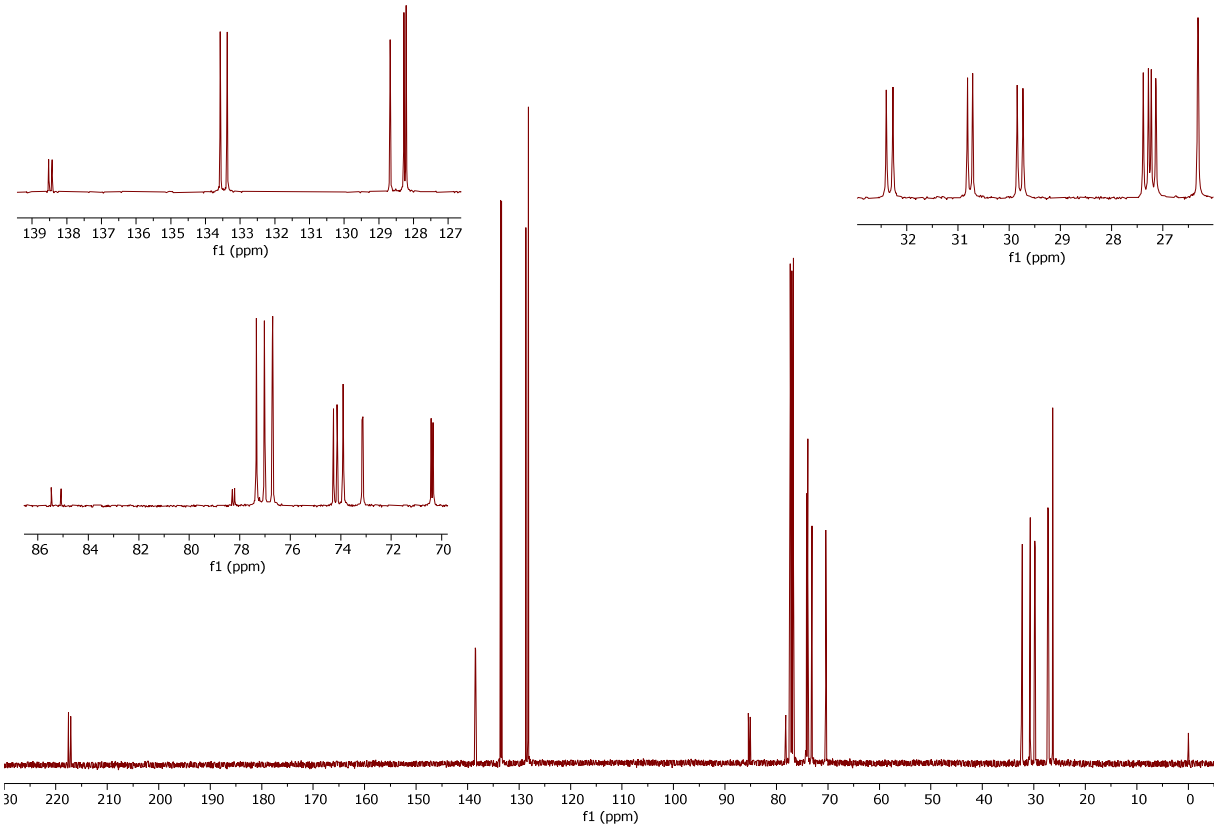

Figure S29. $^{13}C\{^{1}H\}$ NMR spectrum (101 MHz, $CDCl_3$) of **2**.

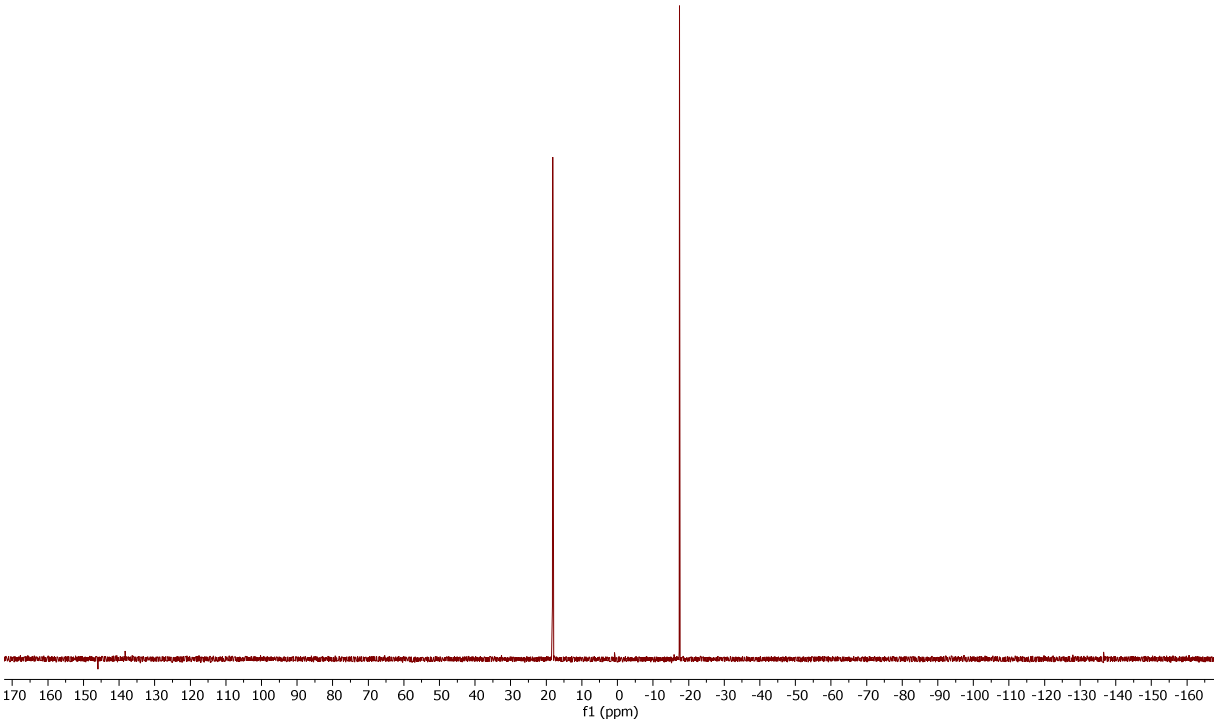

Figure S30. $^{31}P\{^{1}H\}$ NMR spectrum (162 MHz, $CDCl_3$) of **2**.

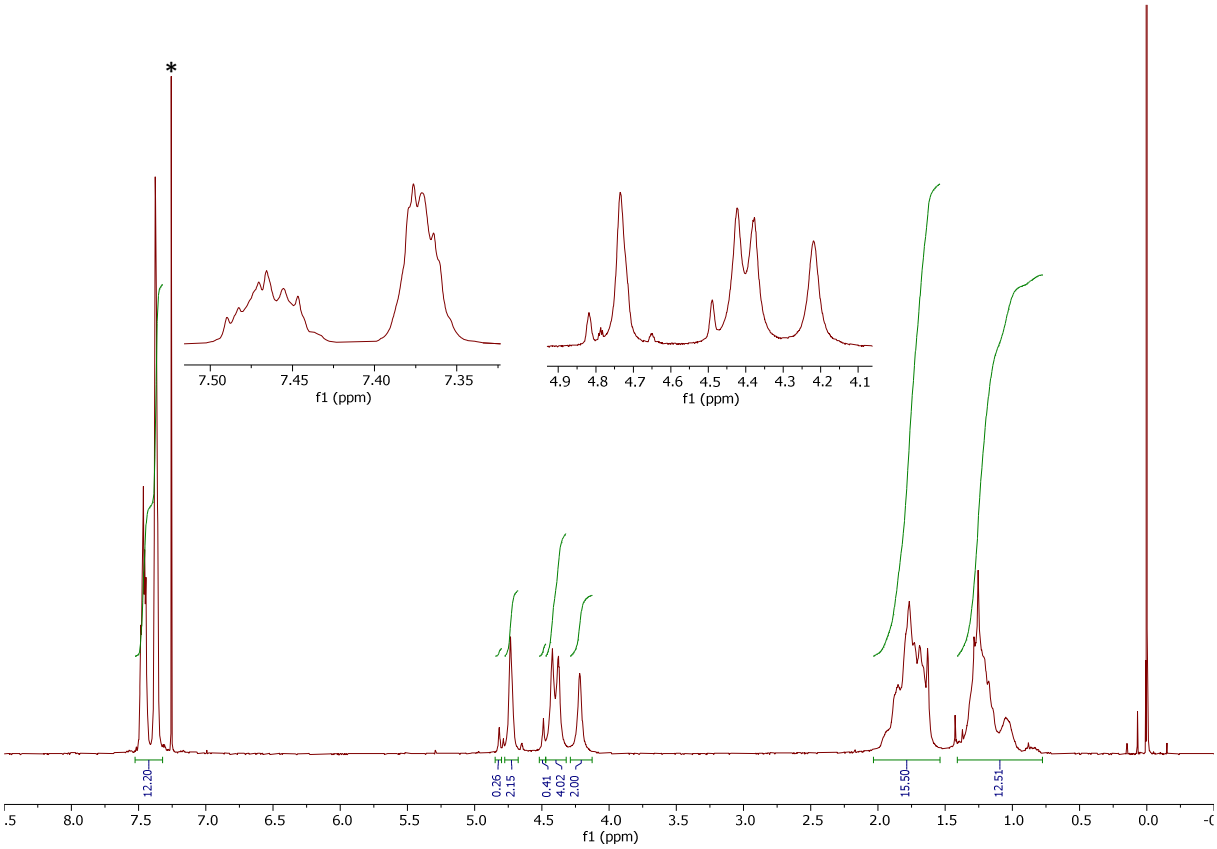

Figure S31. ^{1}H NMR spectrum (400 MHz, $CDCl_3$) of **3**.

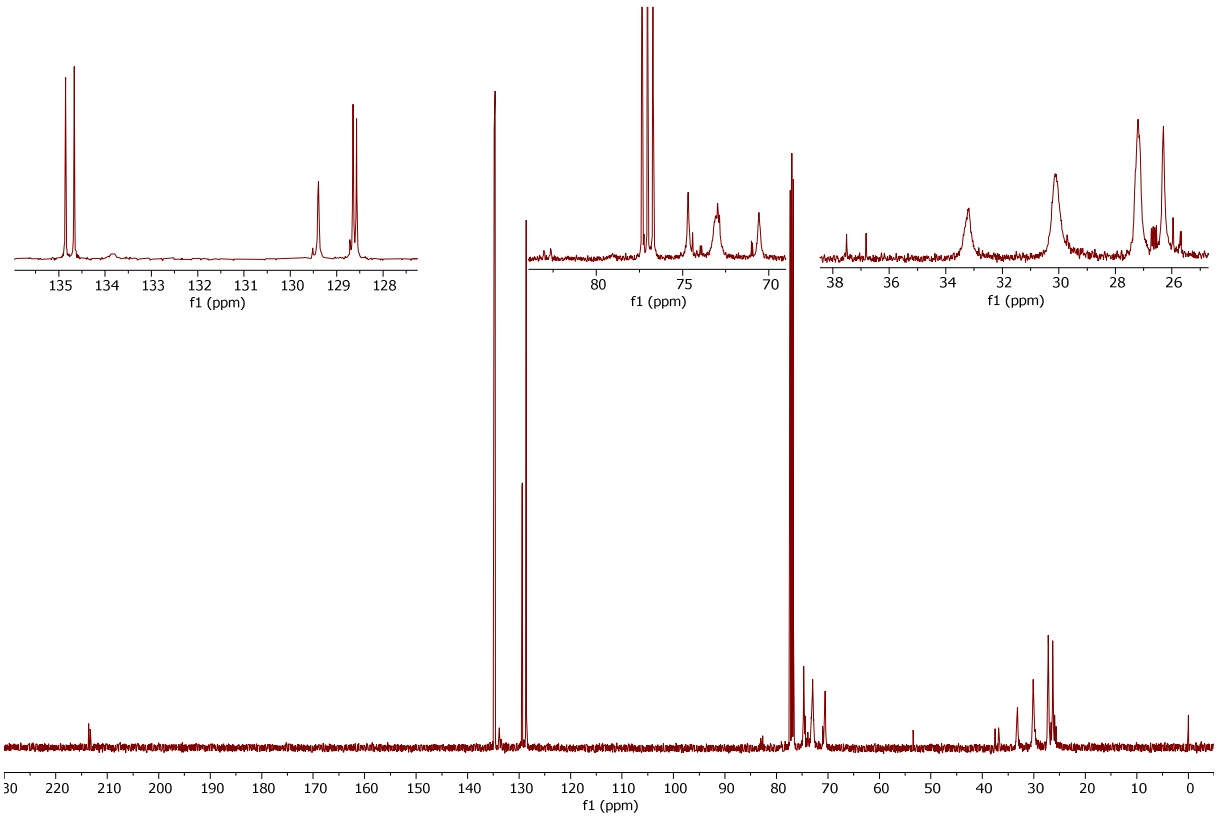

Figure S32. $^{13}C\{^{1}H\}$ NMR spectrum (101 MHz, $CDCl_3$) of **3**.

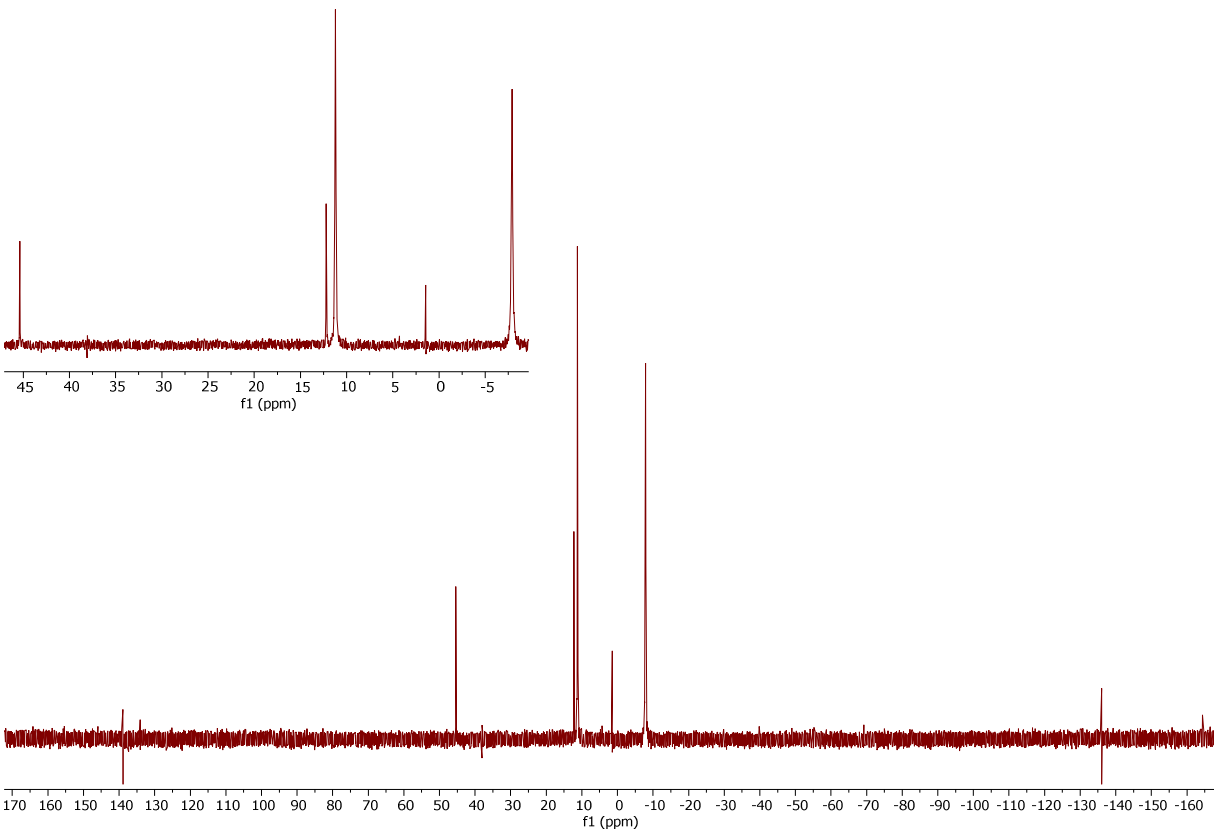

Figure S33. $^{31}P\{^{1}H\}$ NMR spectrum (162 MHz, $CDCl_3$) of **3**.

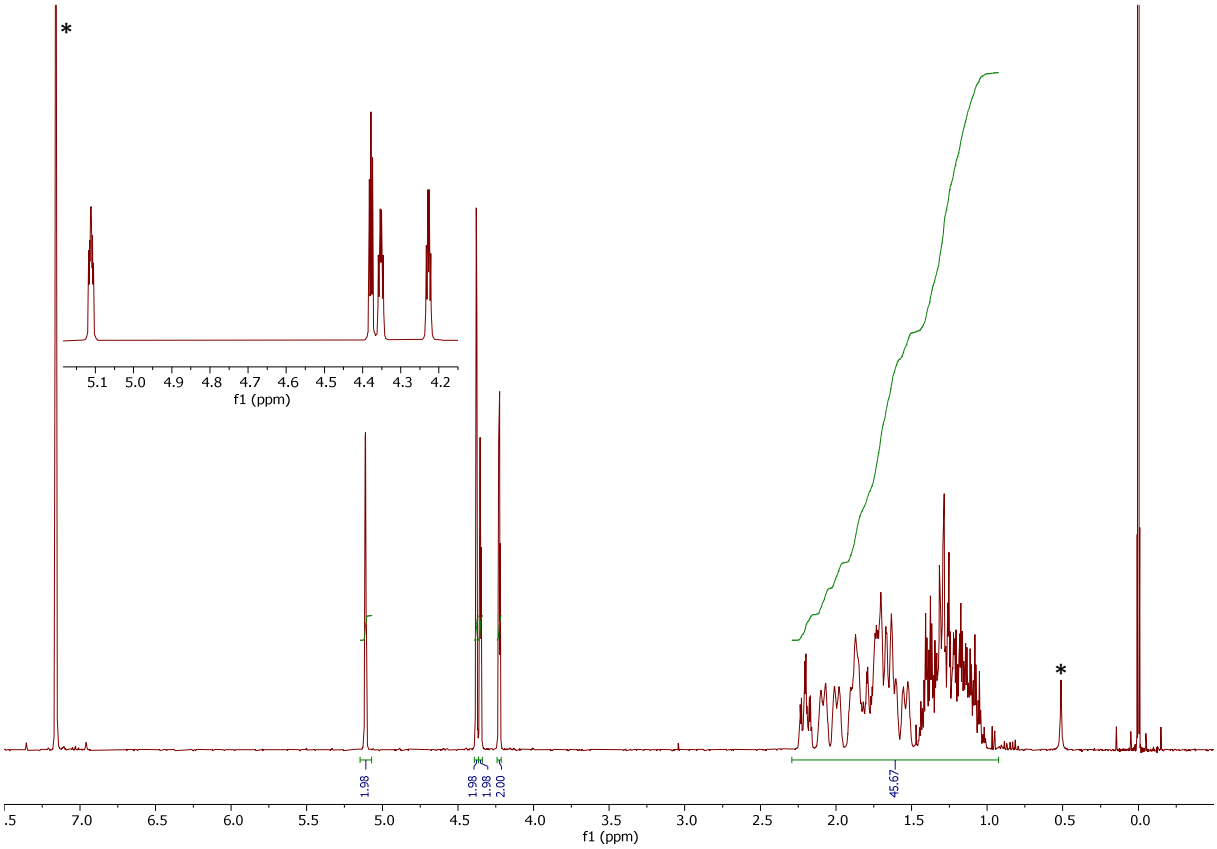

Figure S34. ^{1}H NMR spectrum (400 MHz, $CDCl_3$) of **4**.

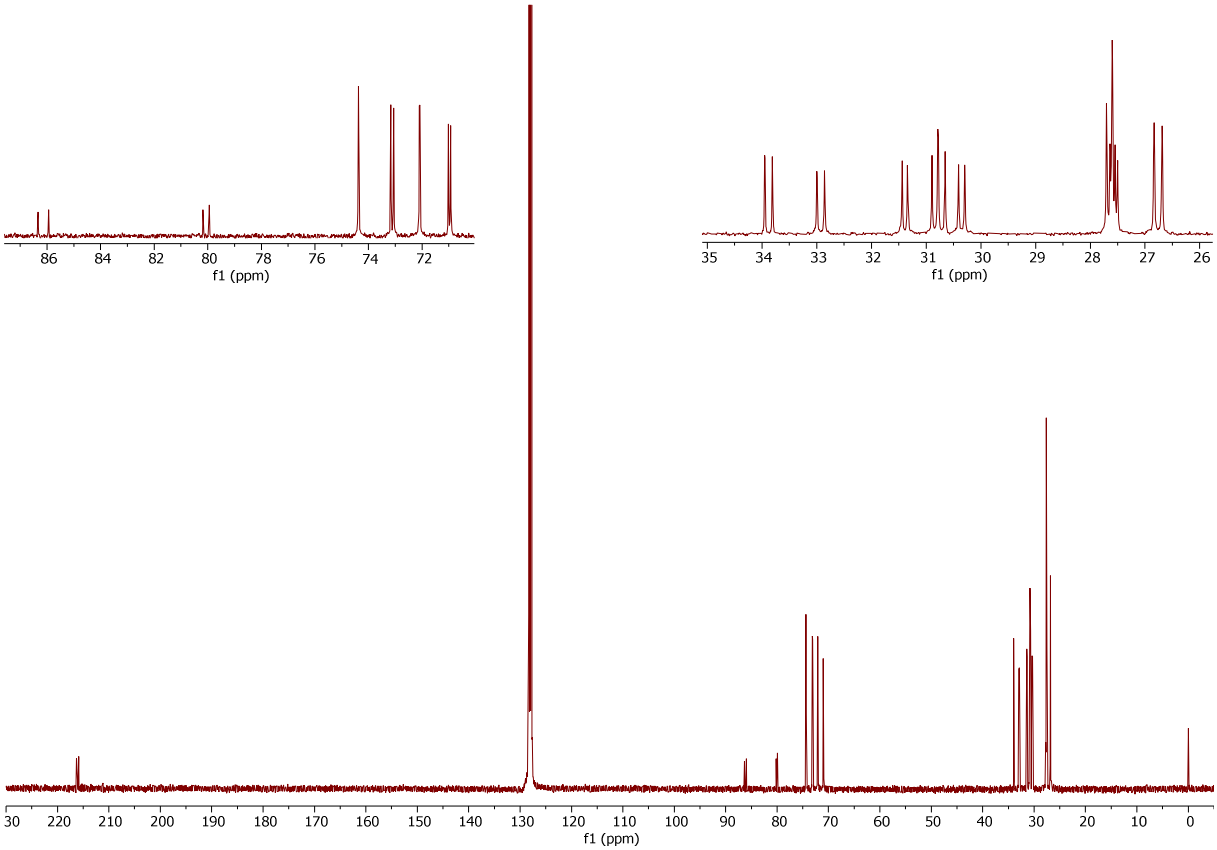

Figure S35. ^{13}C{^{1}H} NMR spectrum (101 MHz, $CDCl_3$) of **4**.

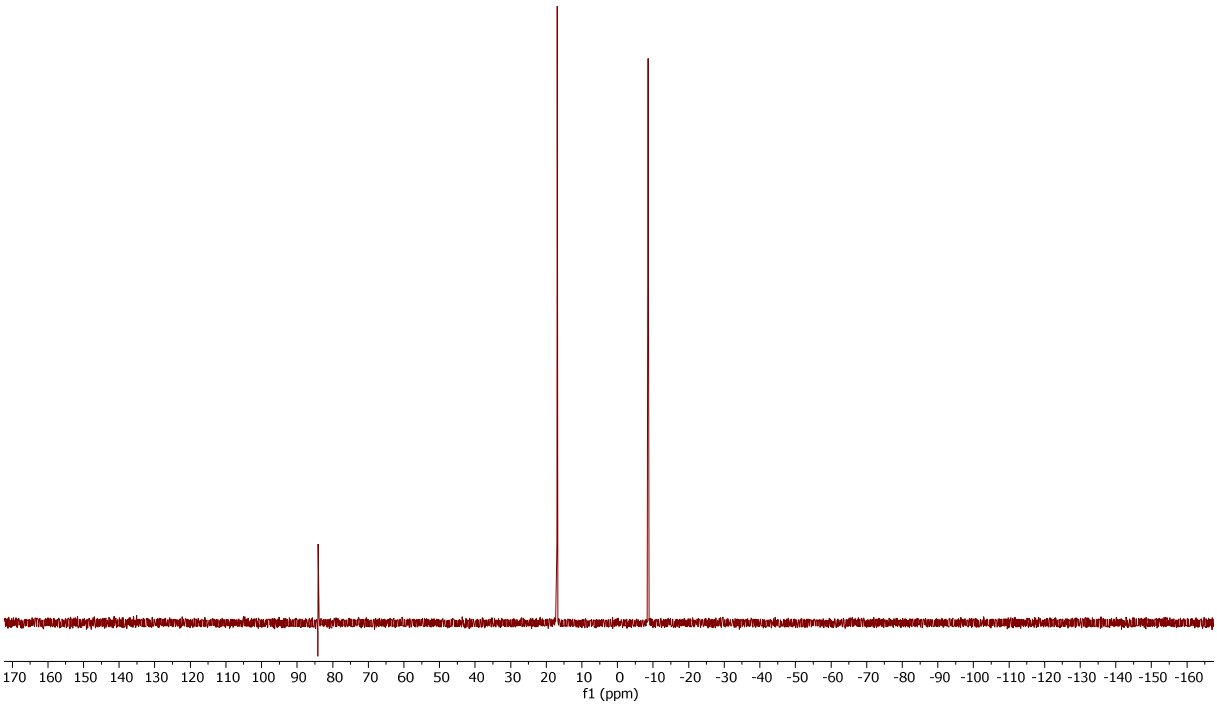

Figure S36. $^{31}P\{^{1}H\}$ NMR spectrum (162 MHz, $CDCl_3$) of **4**.

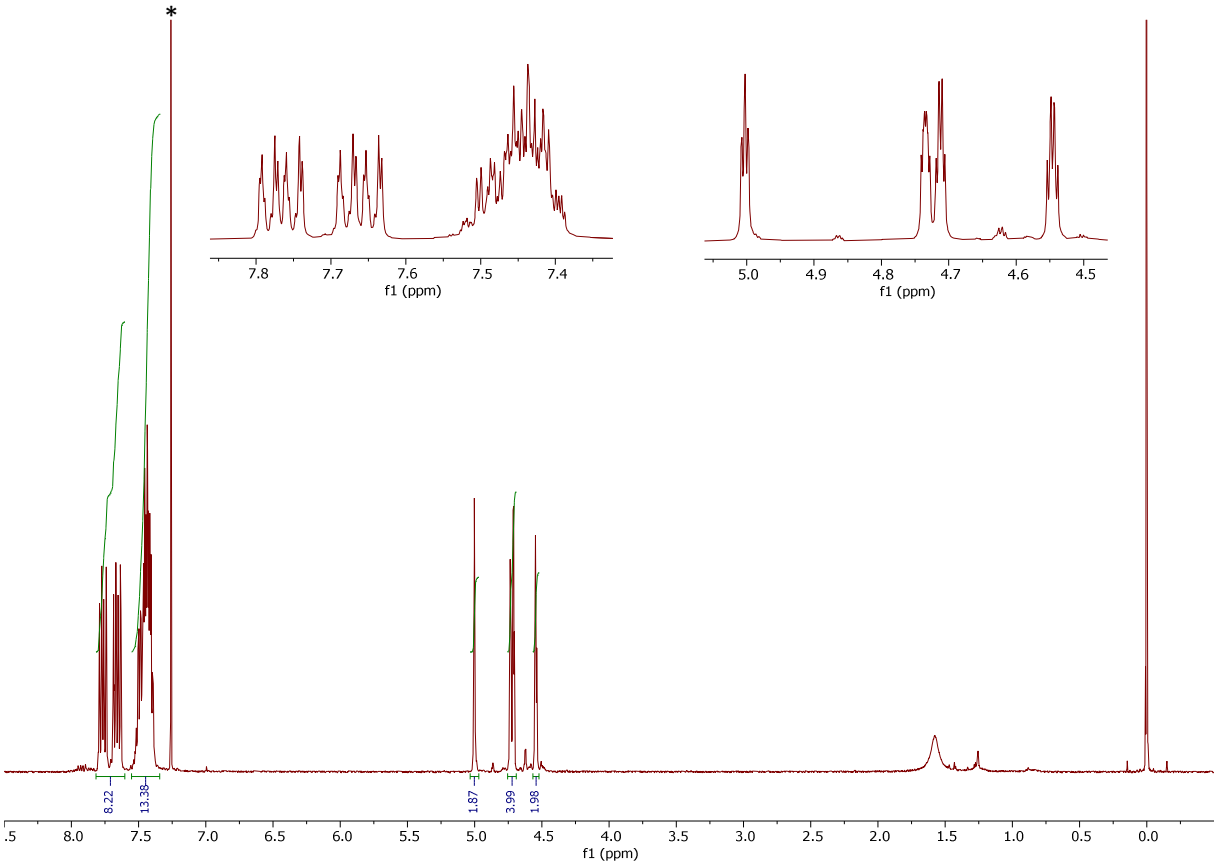

Figure S37. ^{1}H NMR spectrum (400 MHz, $CDCl_3$) of **7**.

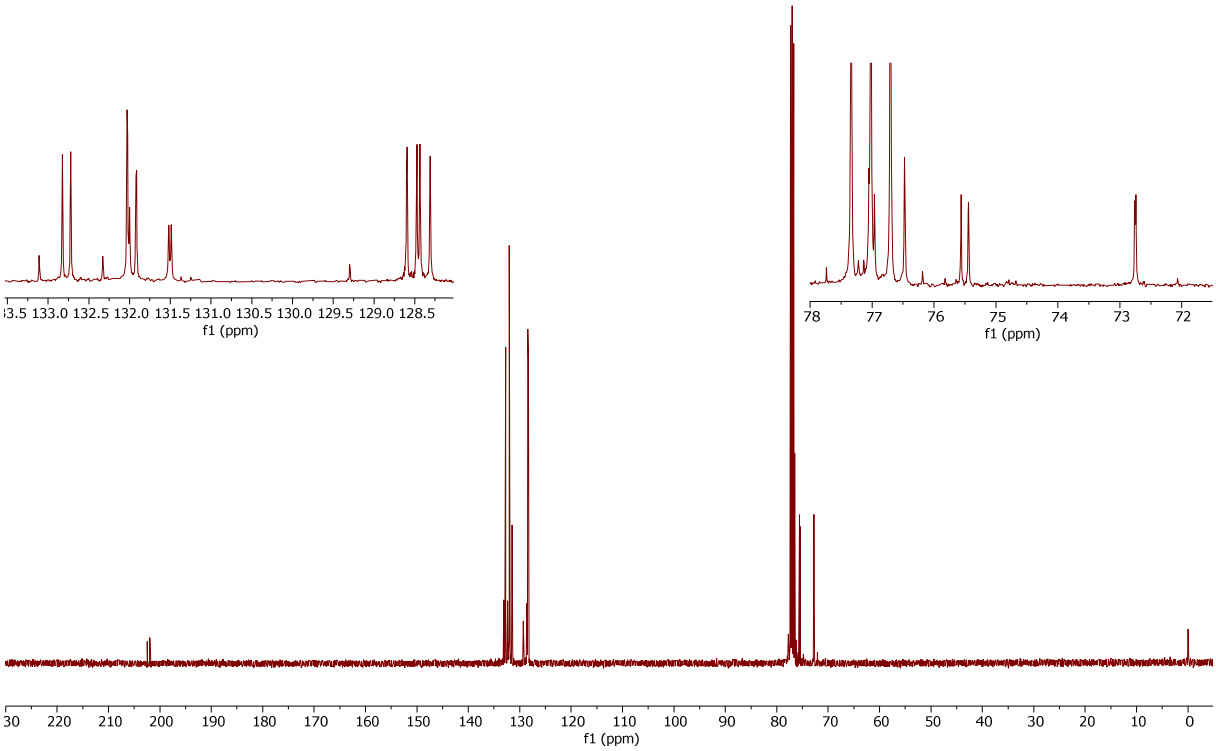

Figure S38. ^{13}C{^{1}H} NMR spectrum (101 MHz, $CDCl_3$) of **7**.

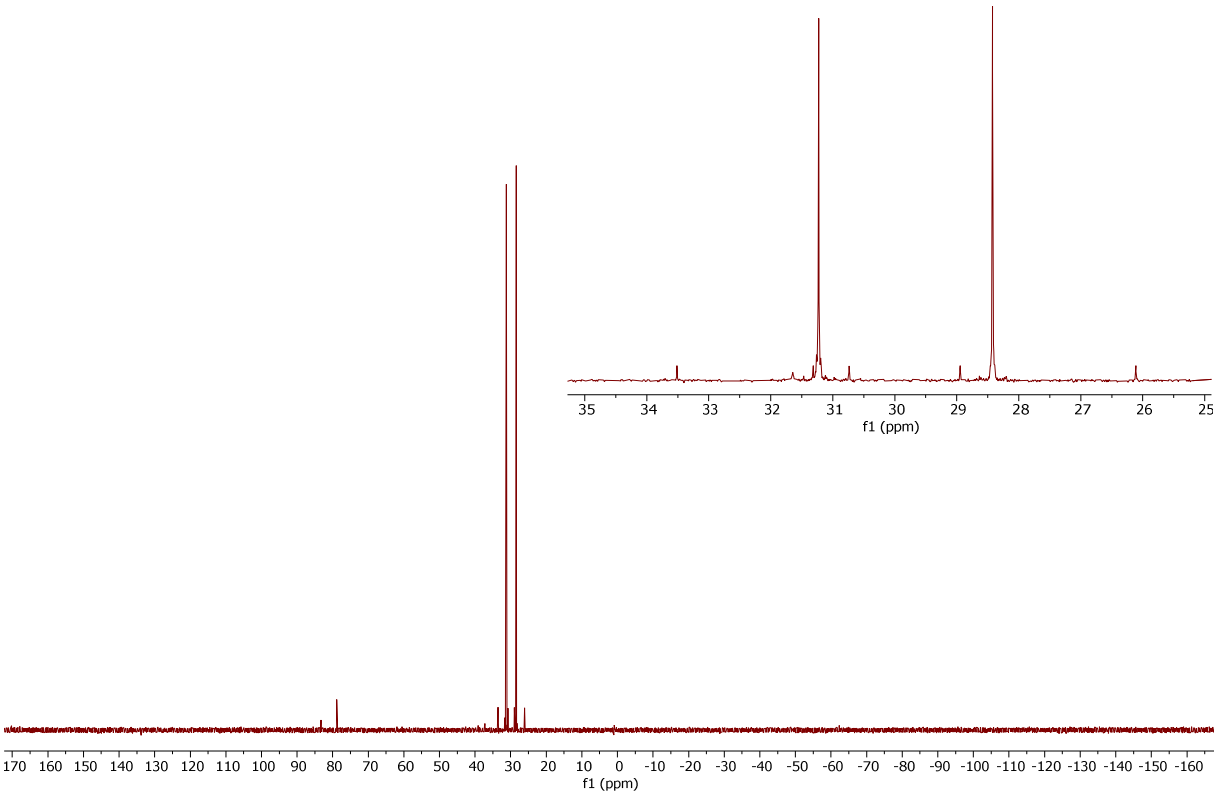

Figure S39. $^{31}P\{^{1}H\}$ NMR spectrum (162 MHz, $CDCl_3$) of **7**.

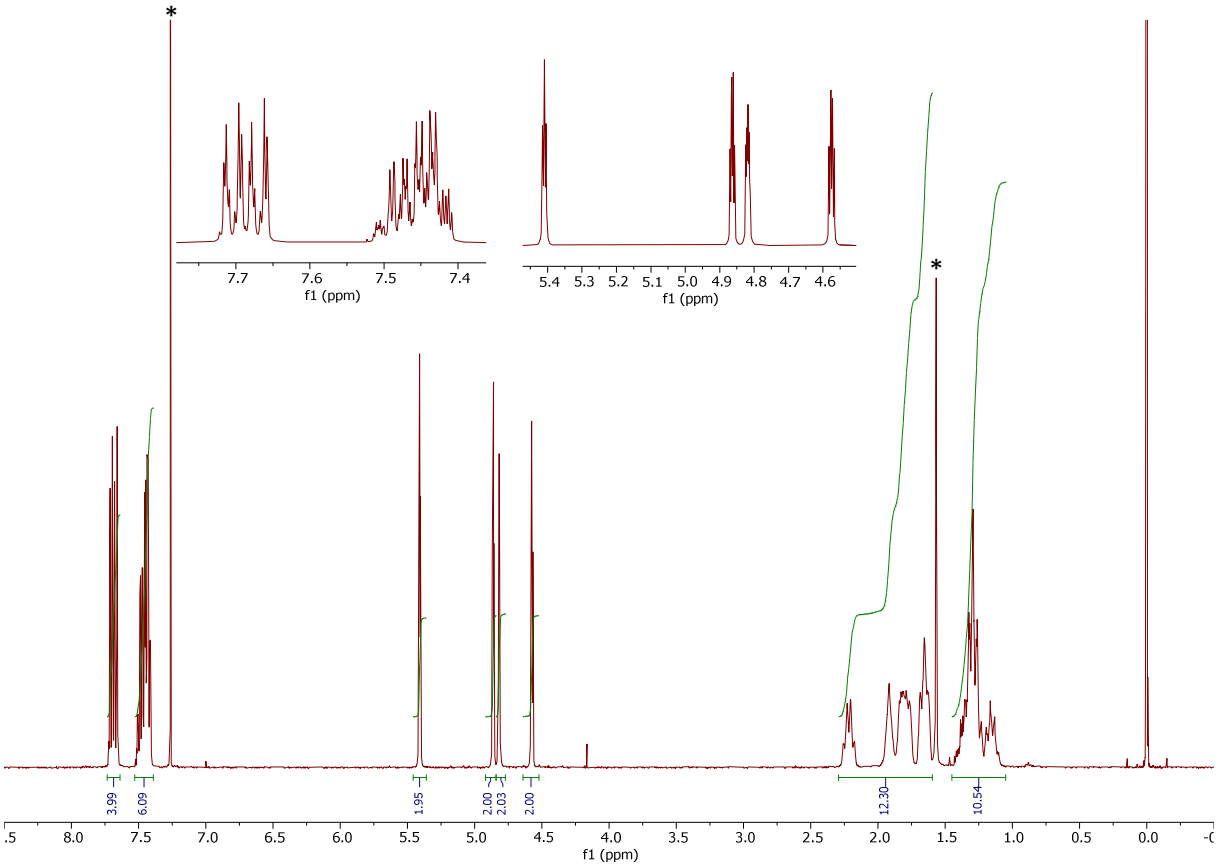

Figure S40. ^{1}H NMR spectrum (400 MHz, $CDCl_3$) of **8**.

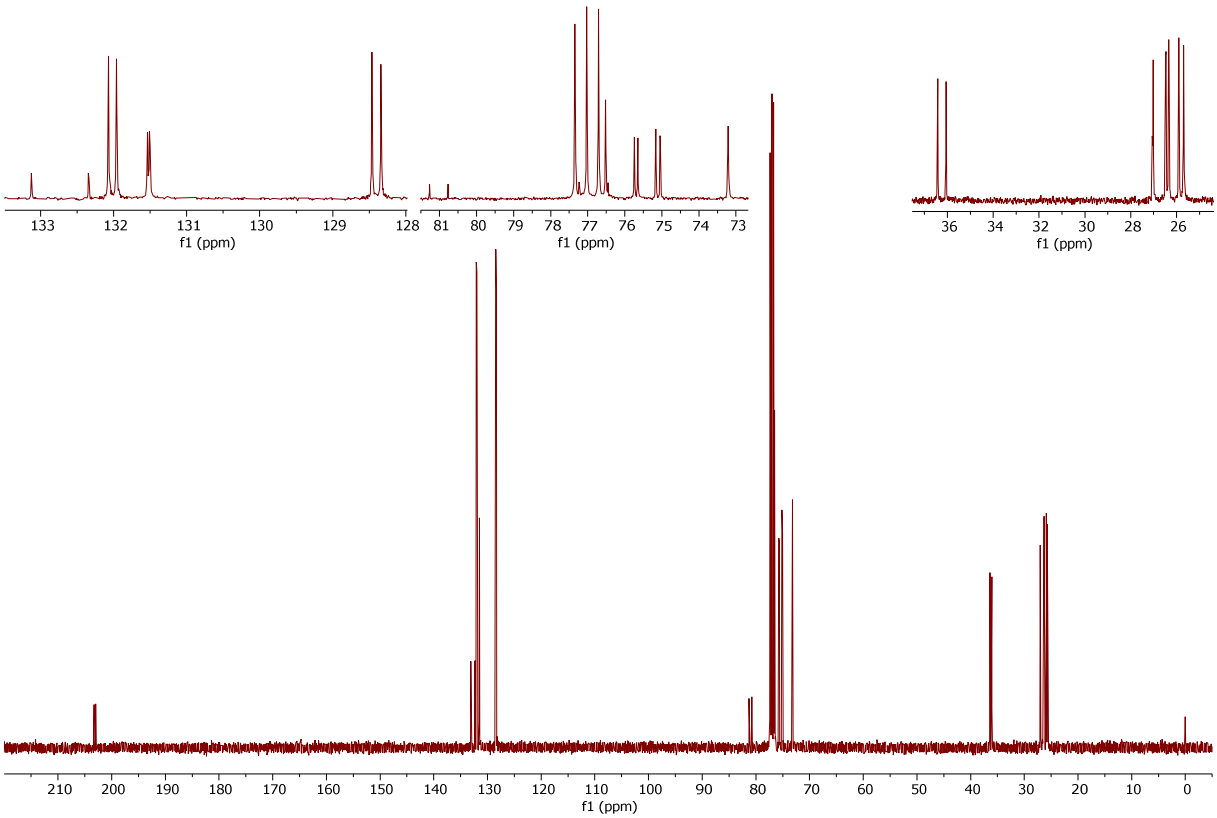

Figure S41. ^{13}C{^{1}H} NMR spectrum (101 MHz, $CDCl_3$) of **8**.

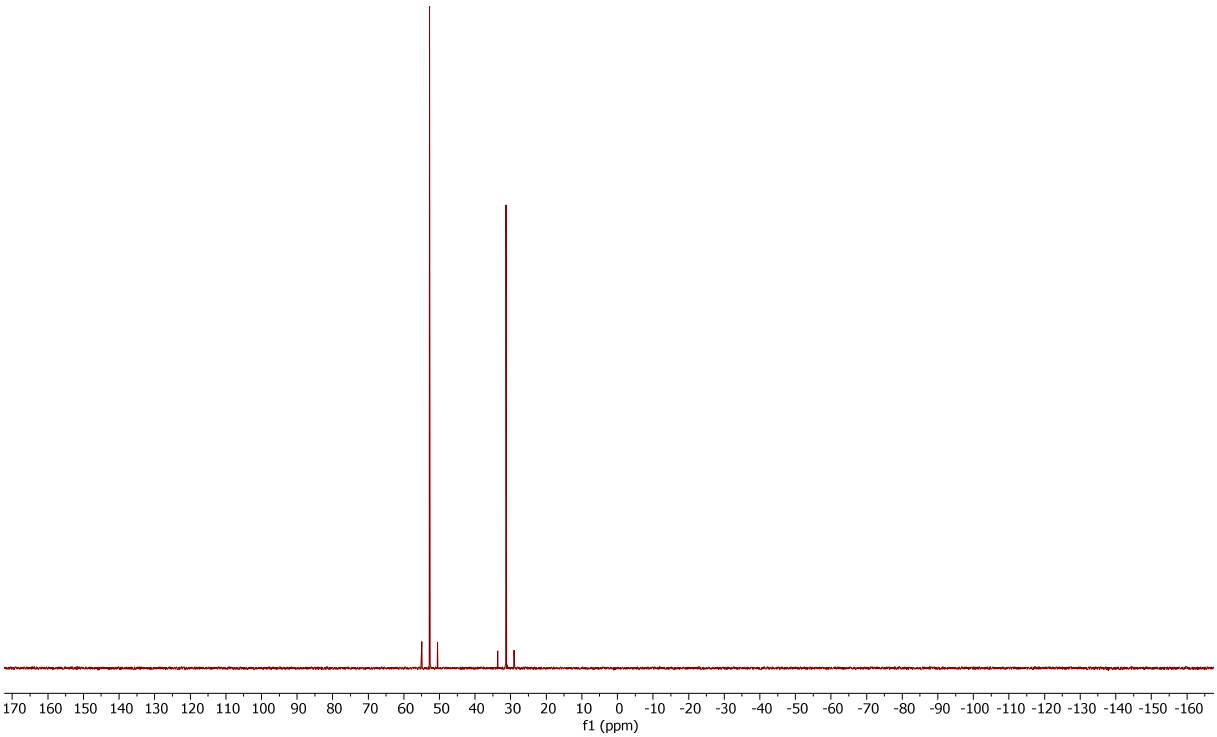

Figure S42. $^{31}P\{^{1}H\}$ NMR spectrum (162 MHz, $CDCl_3$) of **8**.

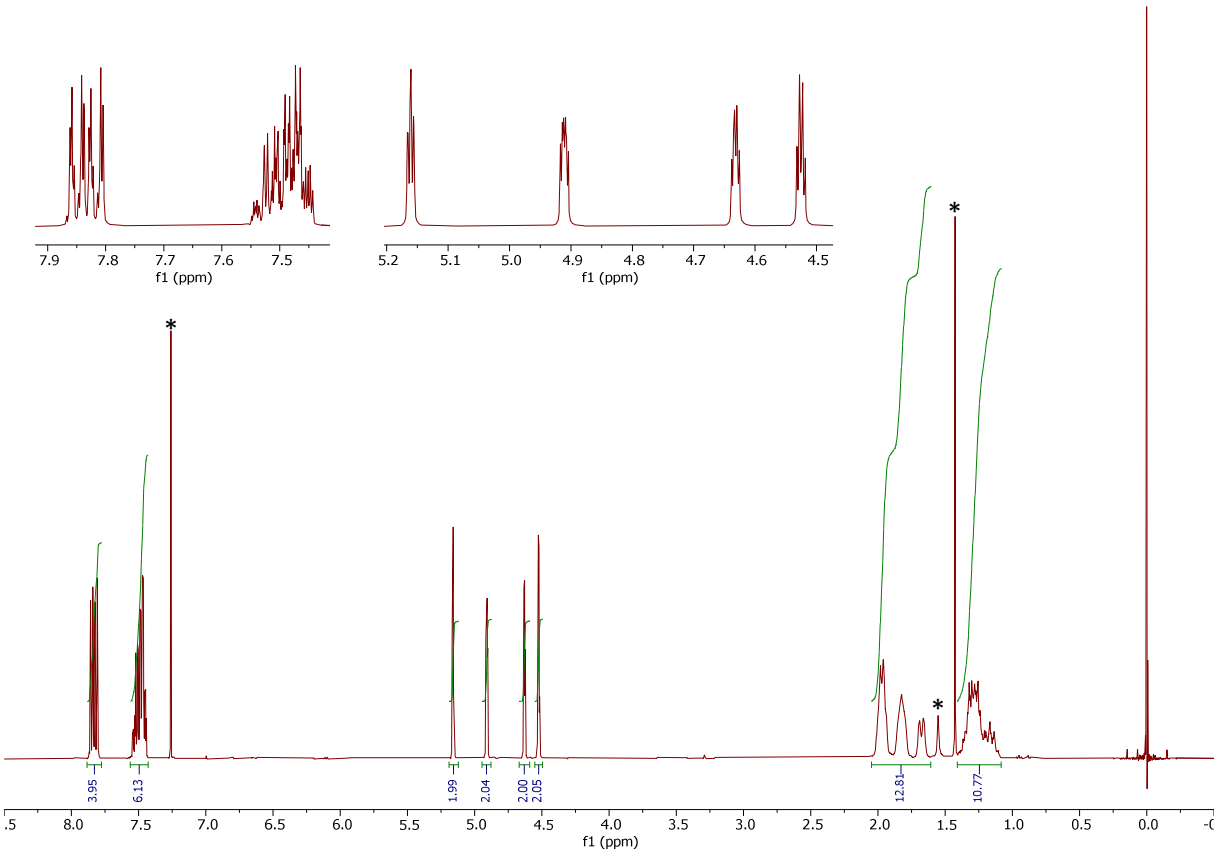

Figure S43. ^{1}H NMR spectrum (400 MHz, $CDCl_3$) of **9**.

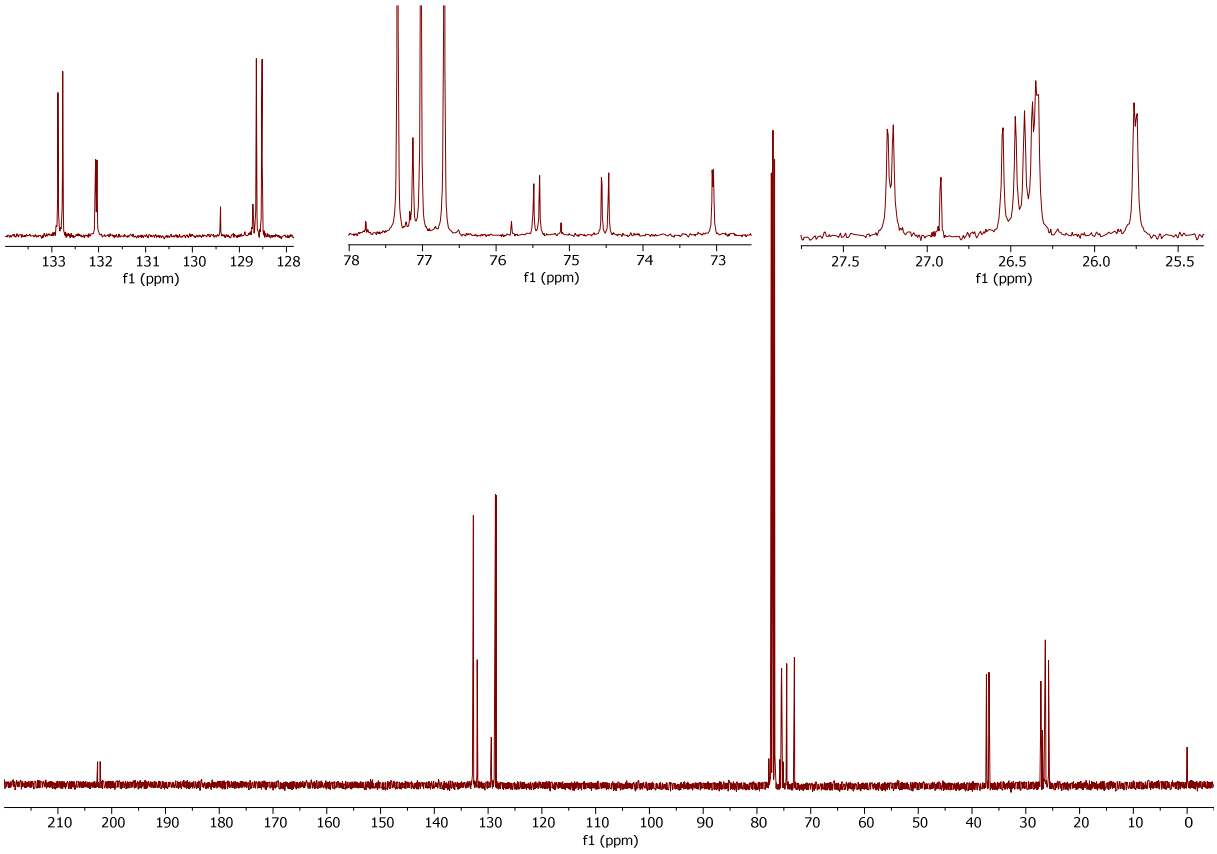

Figure S44. ^{13}C{^{1}H} NMR spectrum (101 MHz, $CDCl_3$) of **9**.

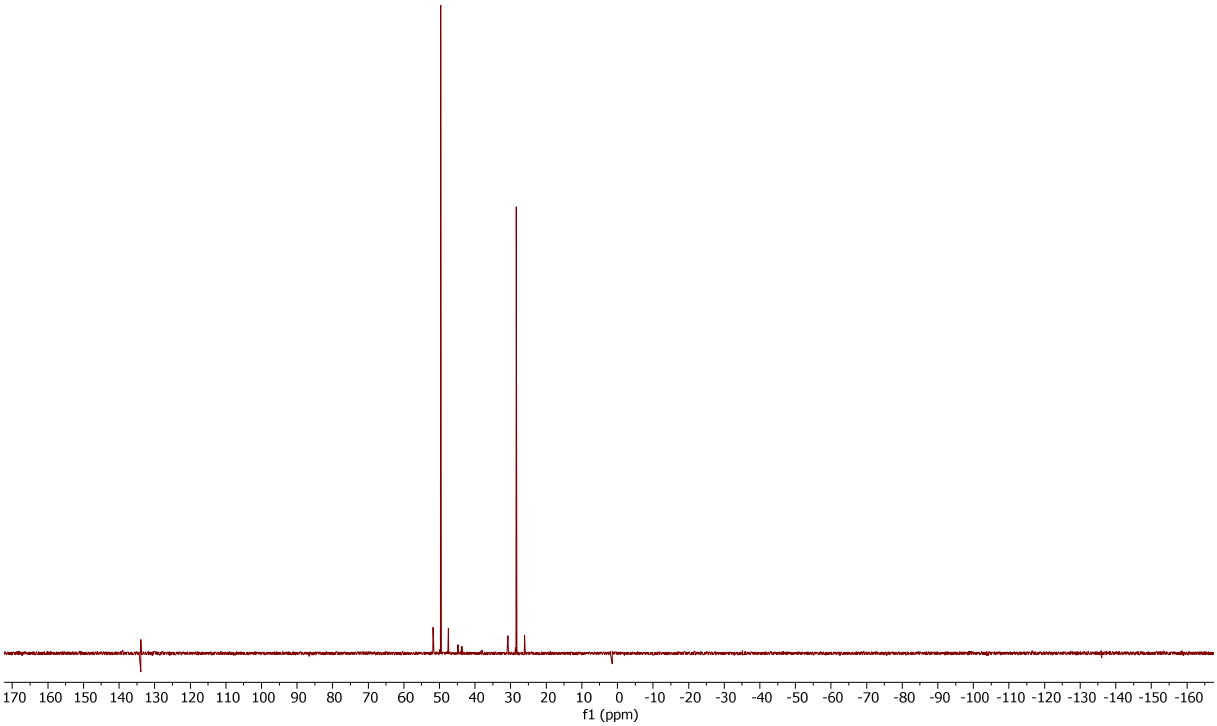

Figure S45. $^{31}P\{^{1}H\}$ NMR spectrum (162 MHz, $CDCl_3$) of **9**.

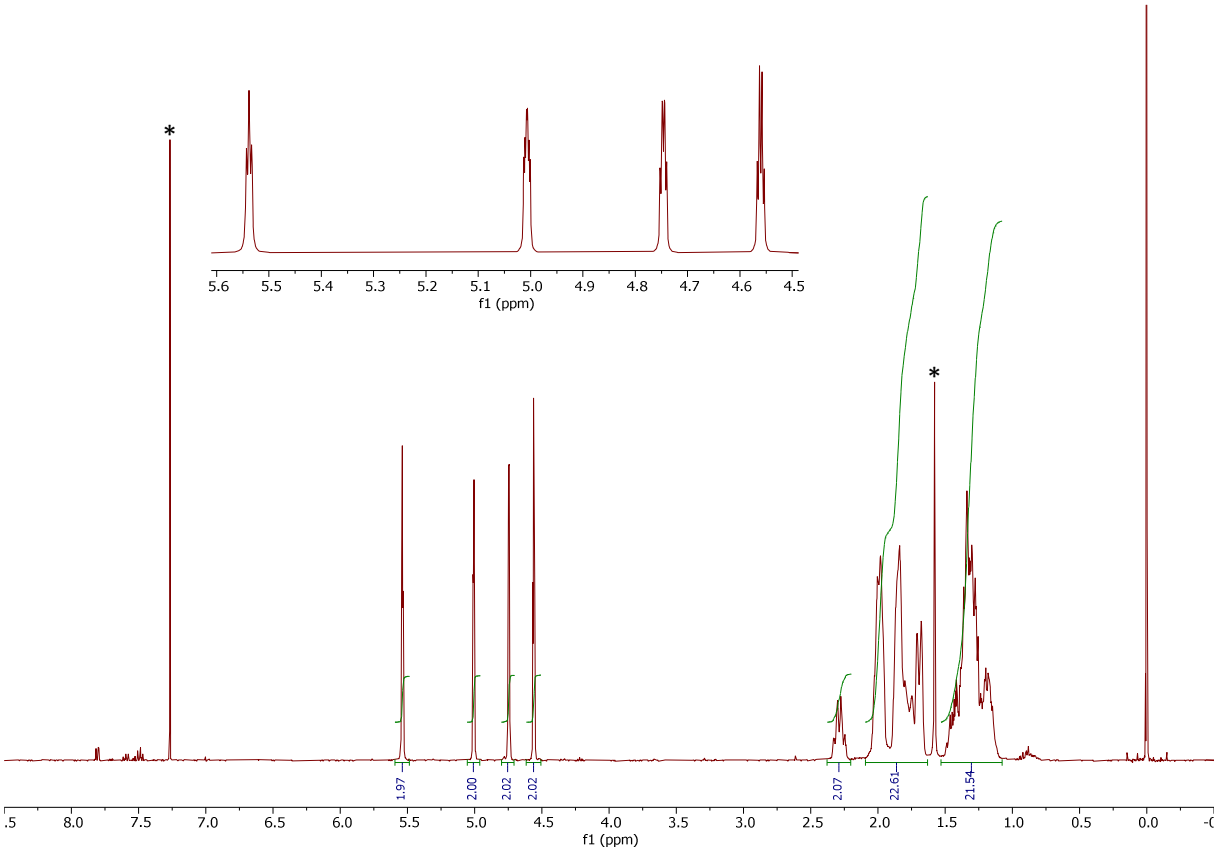

Figure S46. ^{1}H NMR spectrum (400 MHz, $CDCl_3$) of **10**.

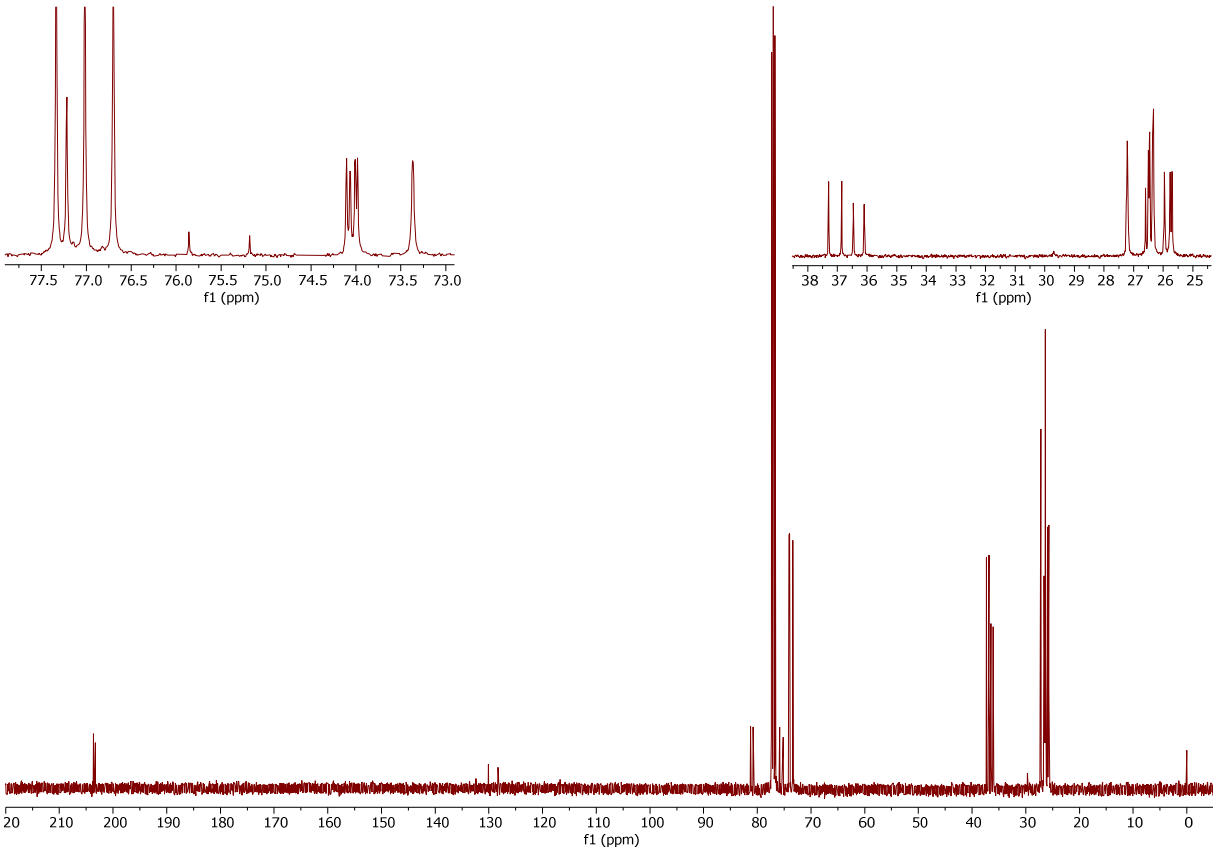

Figure S47. ^{13}C{^{1}H} NMR spectrum (101 MHz, $CDCl_3$) of **10**.

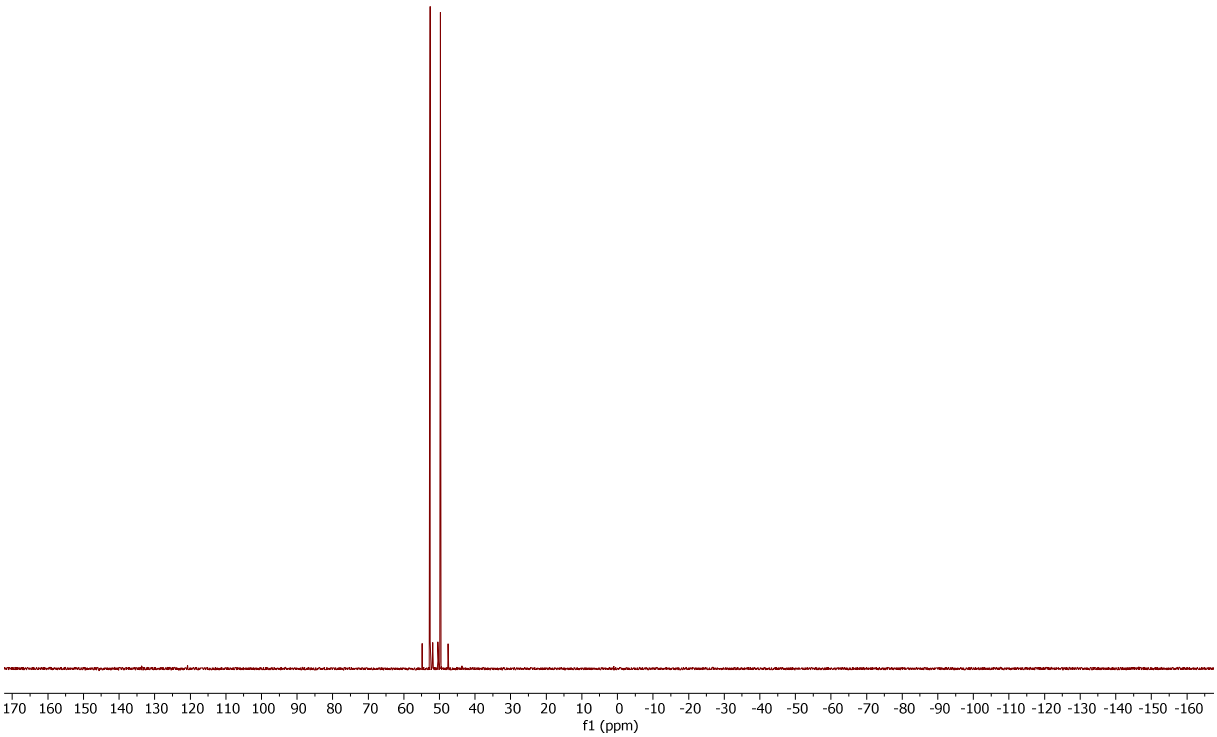

Figure S48. $^{31}P\{^{1}H\}$ NMR spectrum (162 MHz, $CDCl_3$) of **10**.

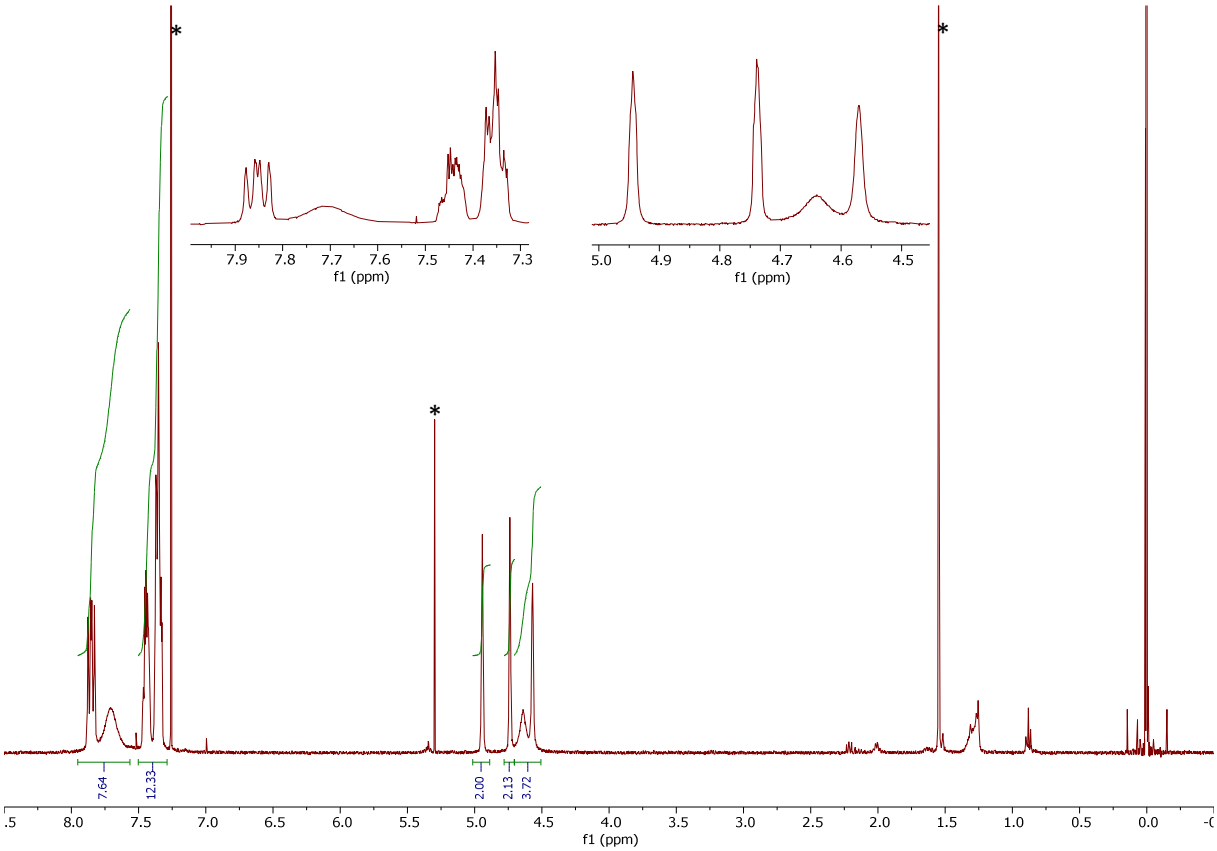

Figure S49. ^{1}H NMR spectrum (400 MHz, $CDCl_3$) of **11**.

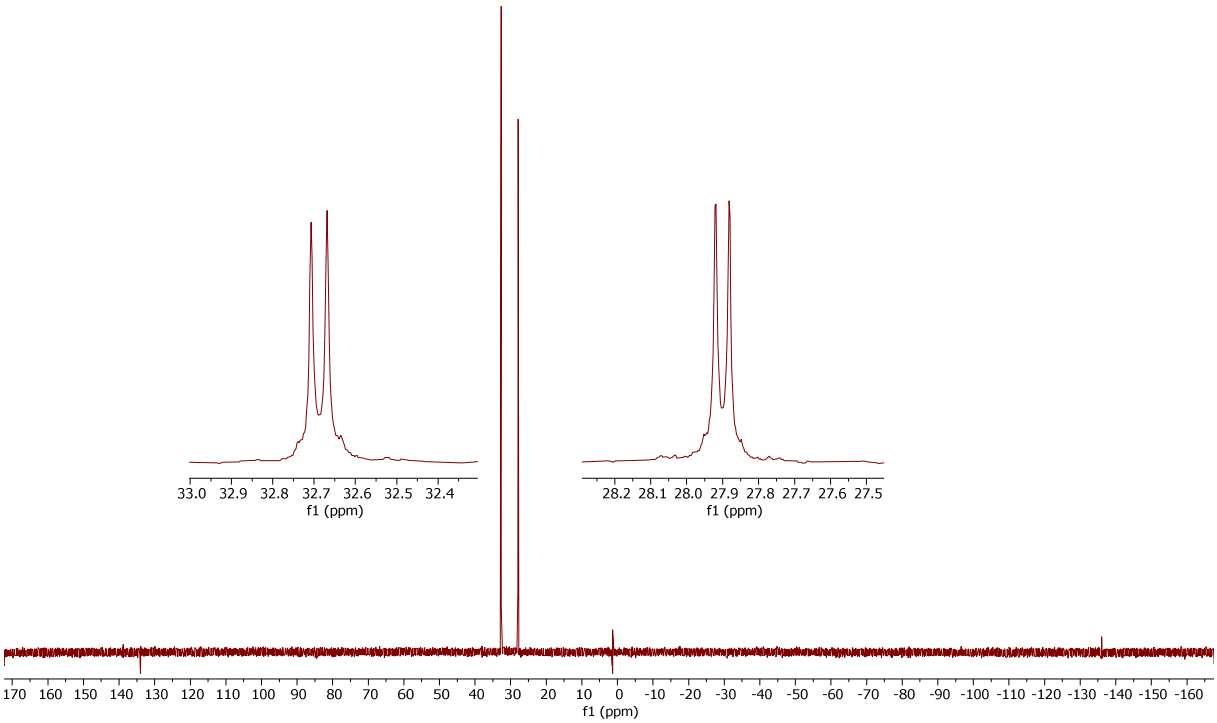

Figure S50. ^{31}P{^{1}H} NMR spectrum (162 MHz, $CDCl_3$) of **11**.

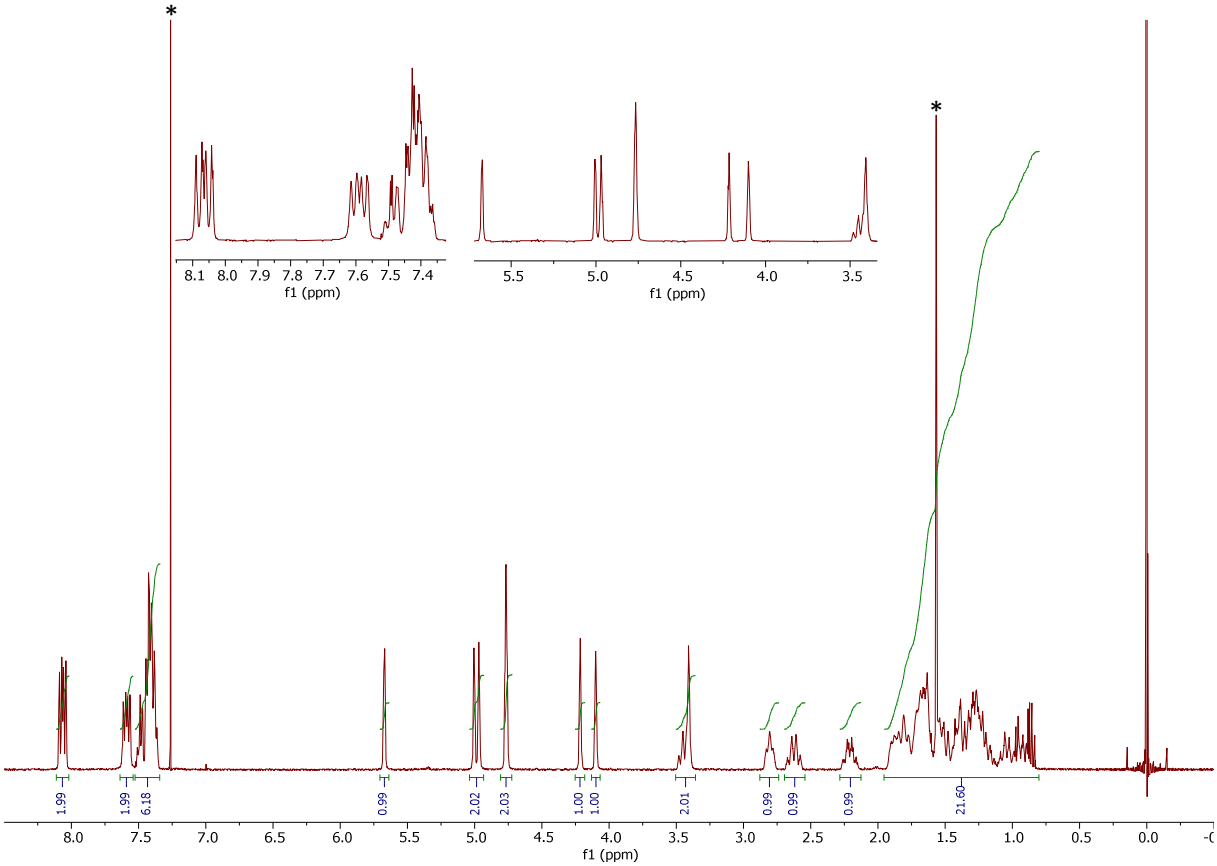

Figure S51. ^{1}H NMR spectrum (400 MHz, $CDCl_3$) of **12**.

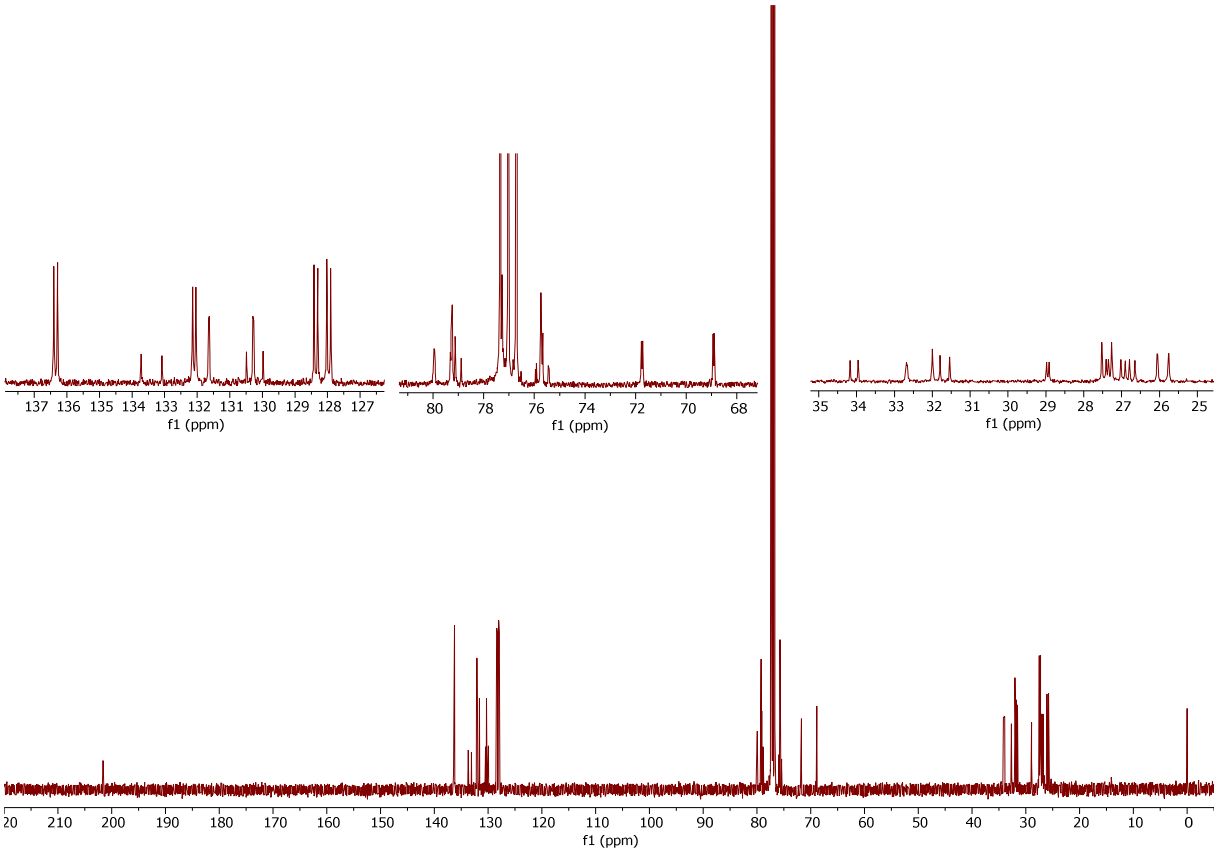

Figure S52. ^{13}C{^{1}H} NMR spectrum (101 MHz, $CDCl_3$) of **12**.

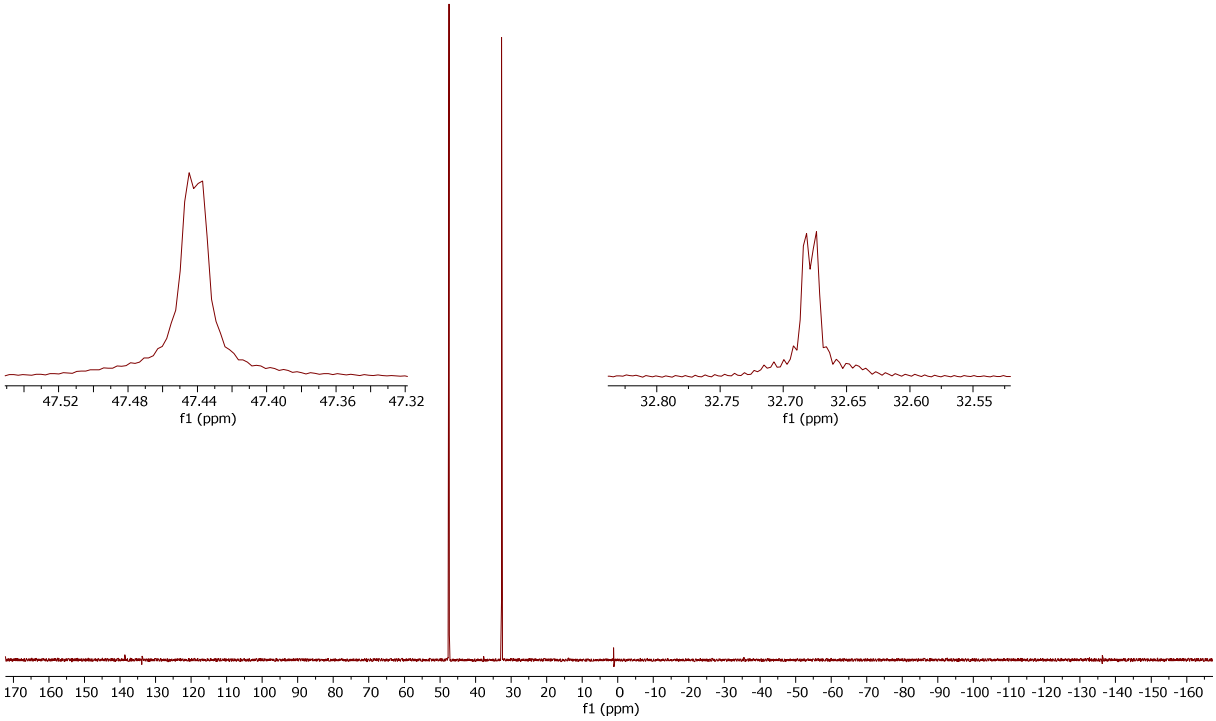

Figure S53. $^{31}P\{^{1}H\}$ NMR spectrum (162 MHz, $CDCl_3$) of **12**.

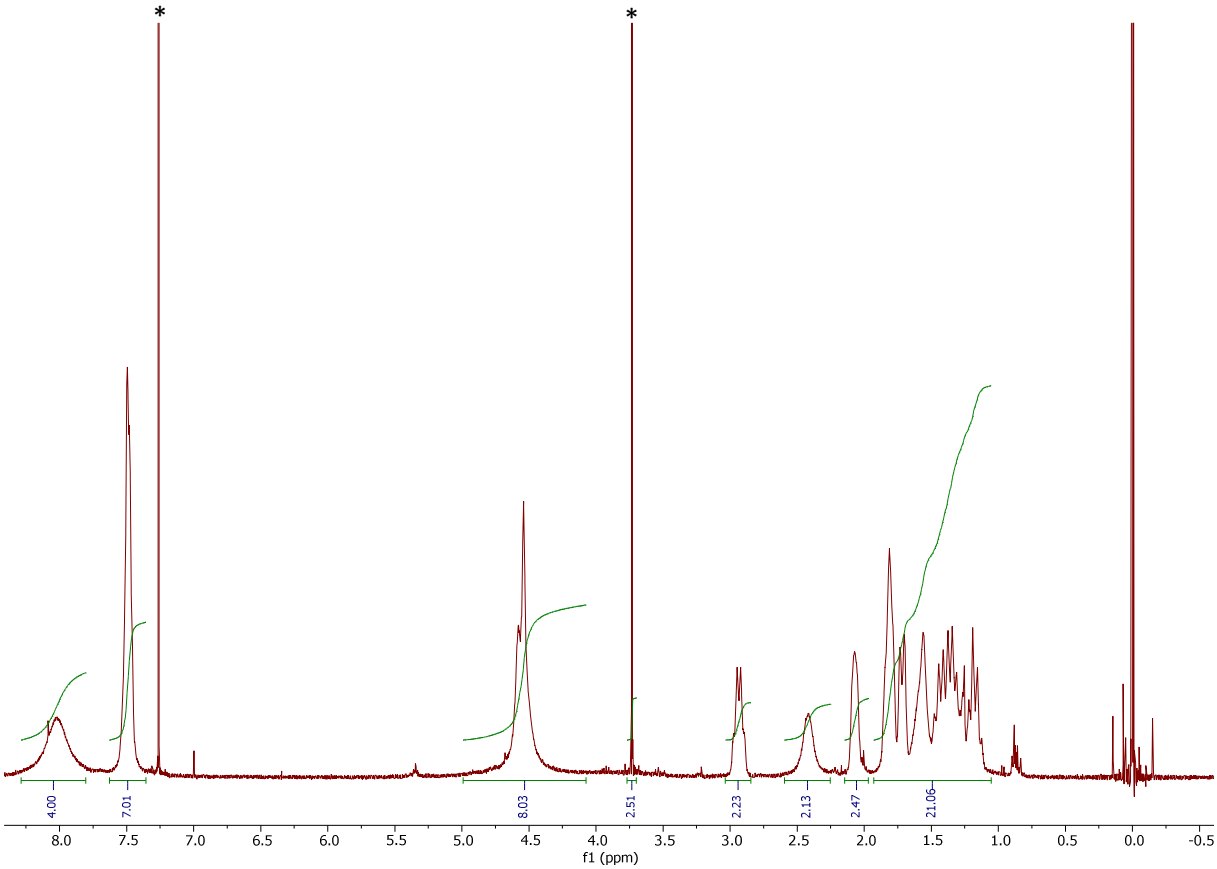

Figure S54. ^{1}H NMR spectrum (400 MHz, $CDCl_3$) of **13**.

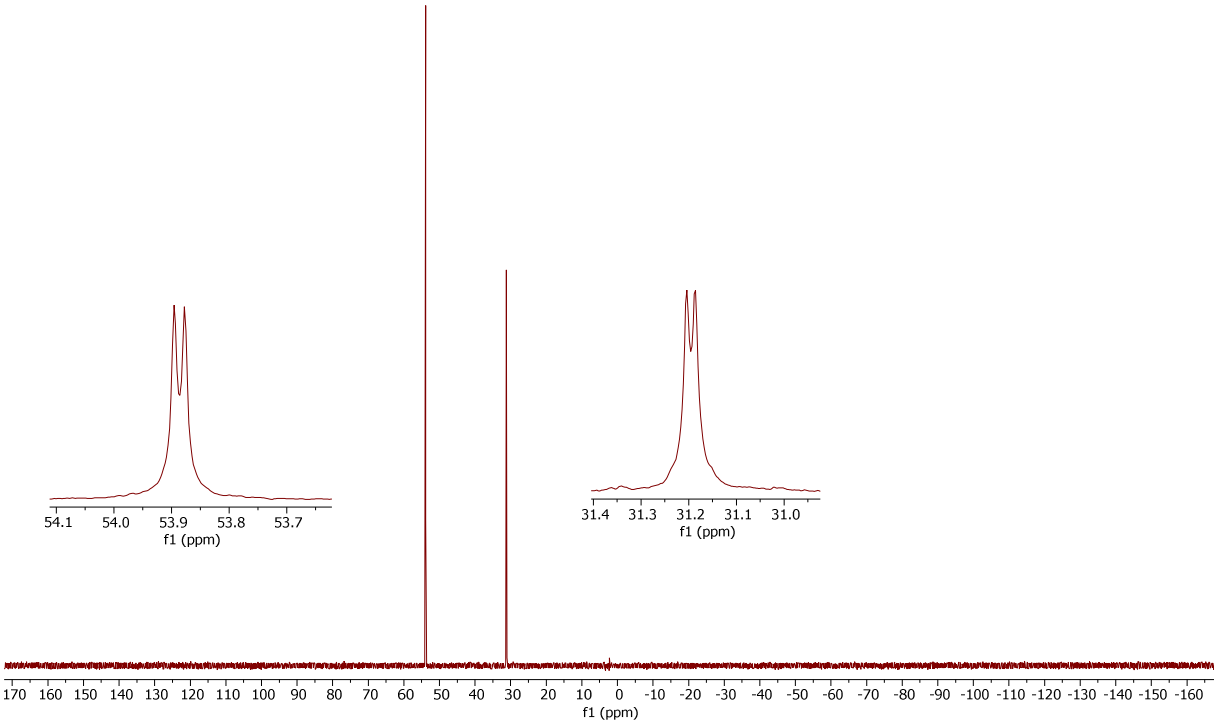

Figure S55. $^{31}P\{^{1}H\}$ NMR spectrum (162 MHz, $CDCl_3$) of **13**.

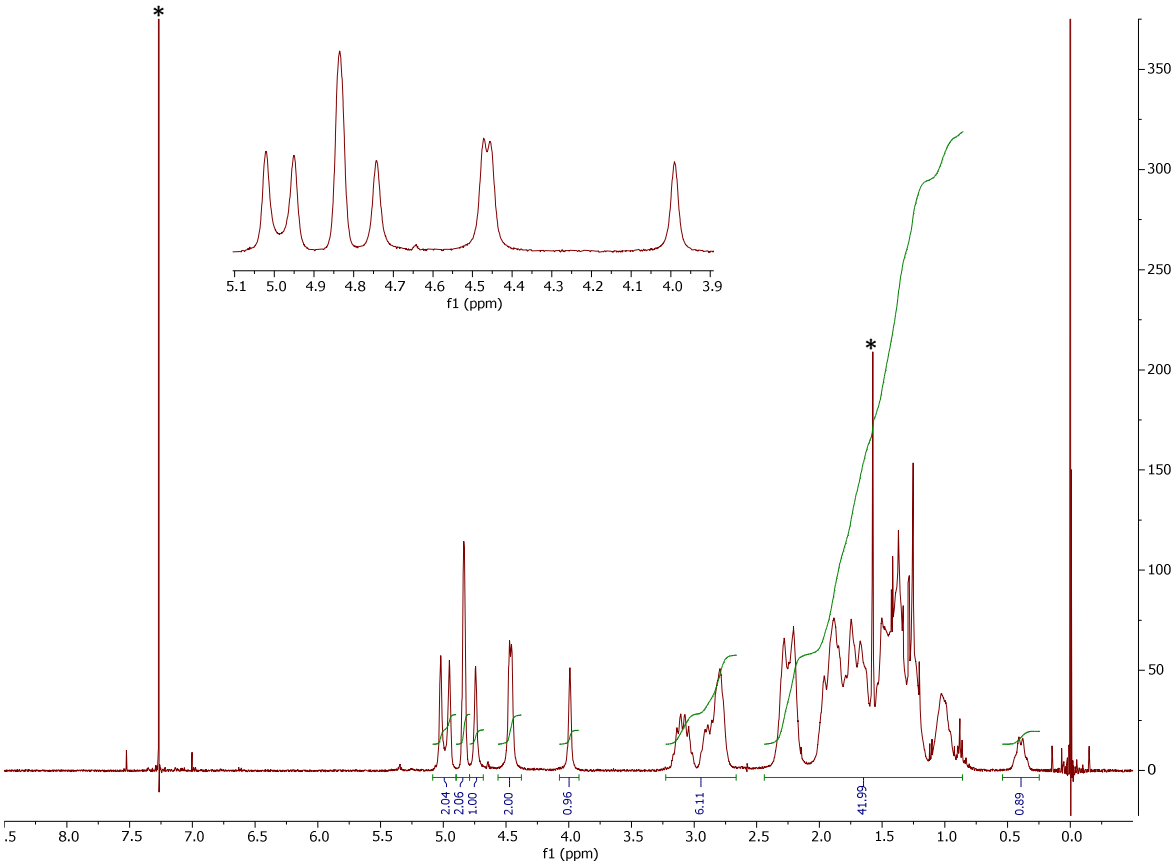

Figure S56. ^{1}H NMR spectrum (400 MHz, $CDCl_3$) of **14a**.

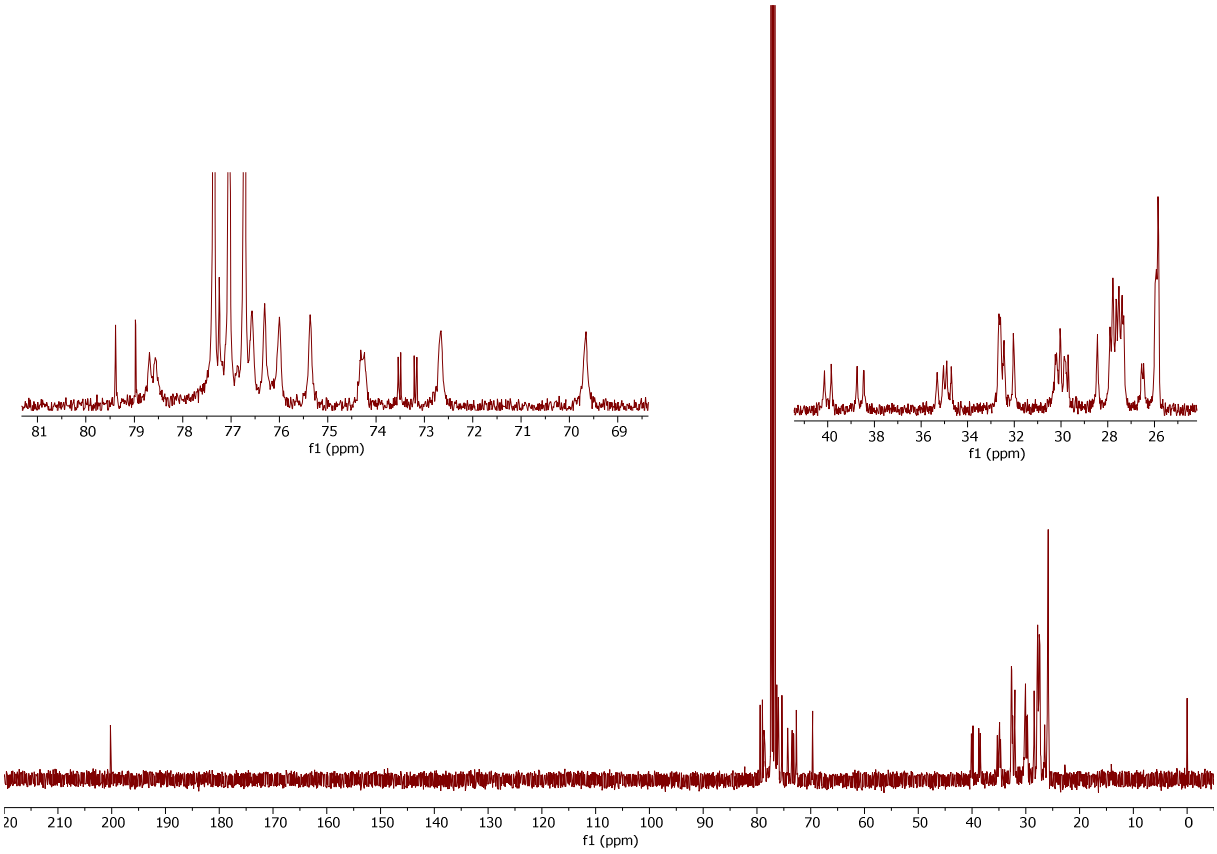

Figure S57. ^{13}C{^{1}H} NMR spectrum (101 MHz, $CDCl_3$) of **14a**.

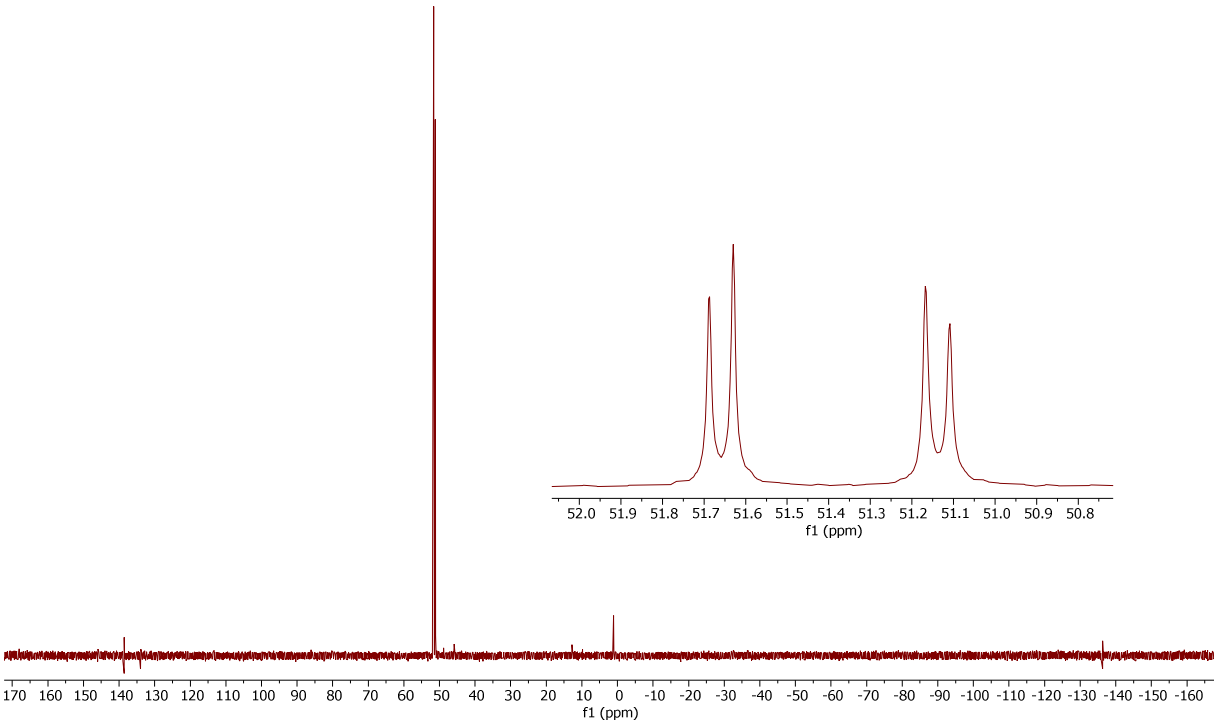

Figure S58. $^{31}P\{^{1}H\}$ NMR spectrum (162 MHz, $CDCl_3$) of **14a**.

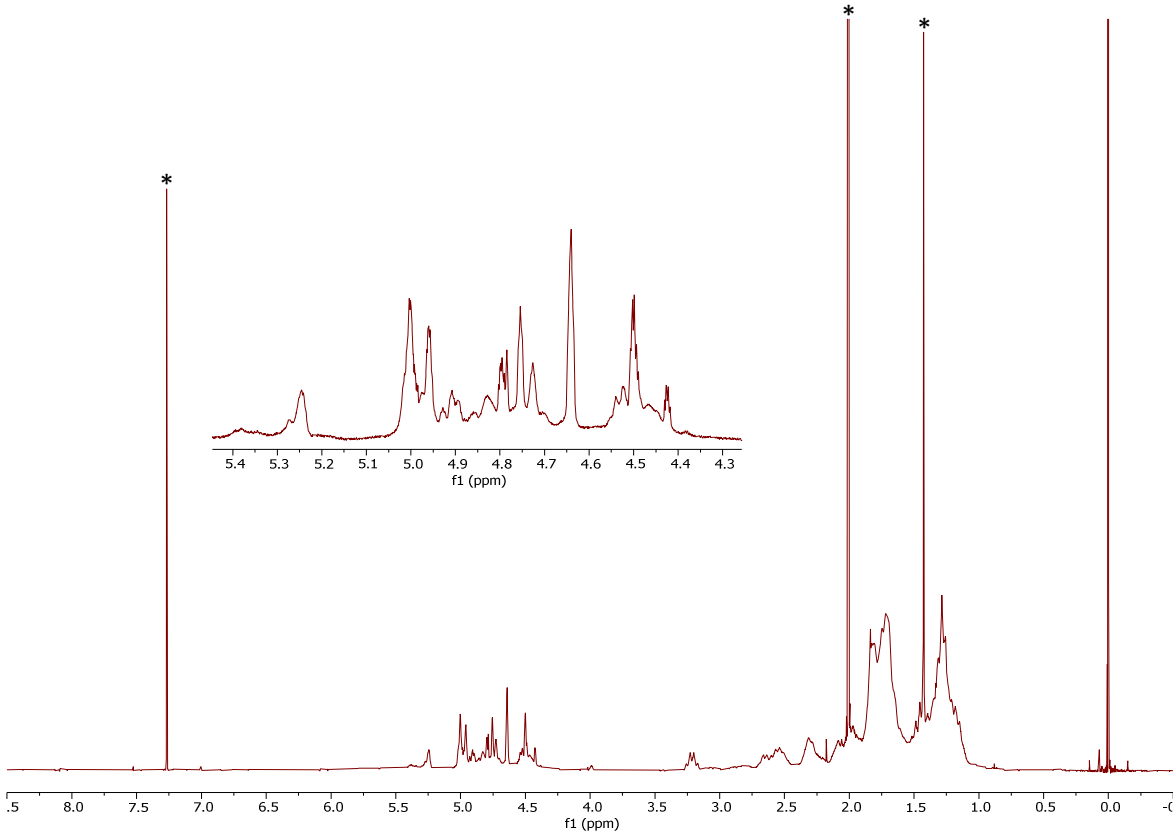

Figure S59. ^{1}H NMR spectrum (400 MHz, $CDCl_3$) of mixture **14a** and **14b** measured 10 min after mixing.

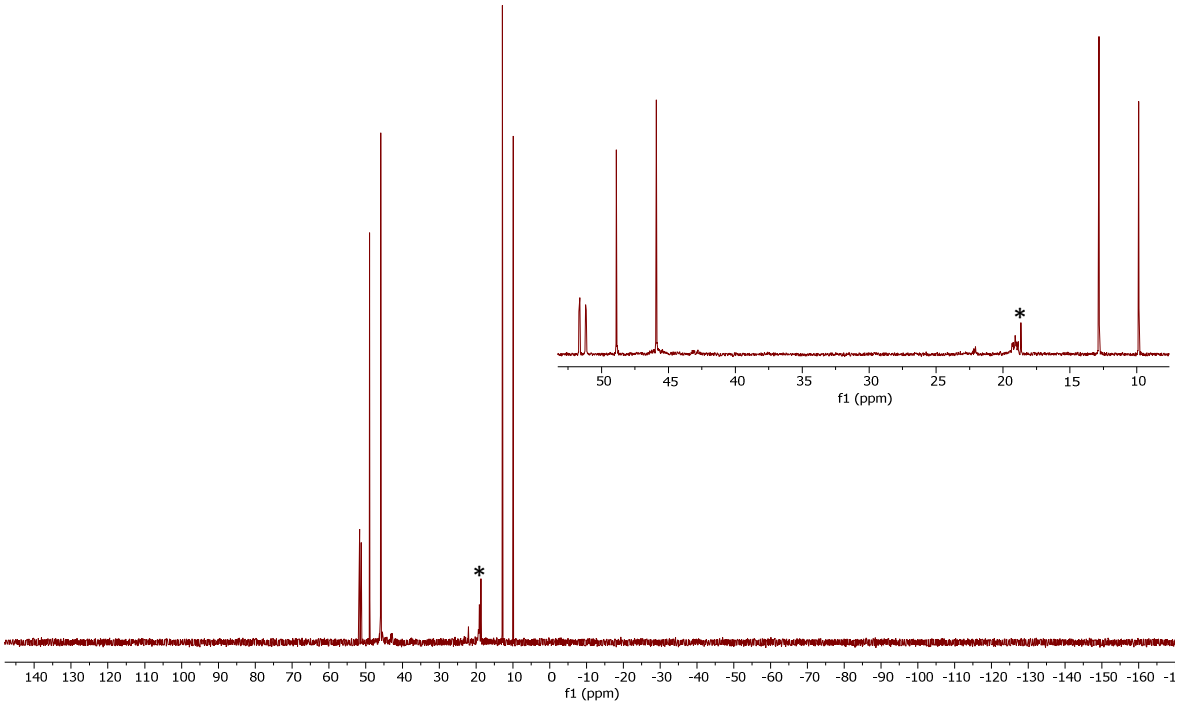

Figure S60. ^{31}P{^{1}H} NMR spectrum (162 MHz, $CDCl_3$) of mixture **14a** and **14b** measured 10 min after mixing.

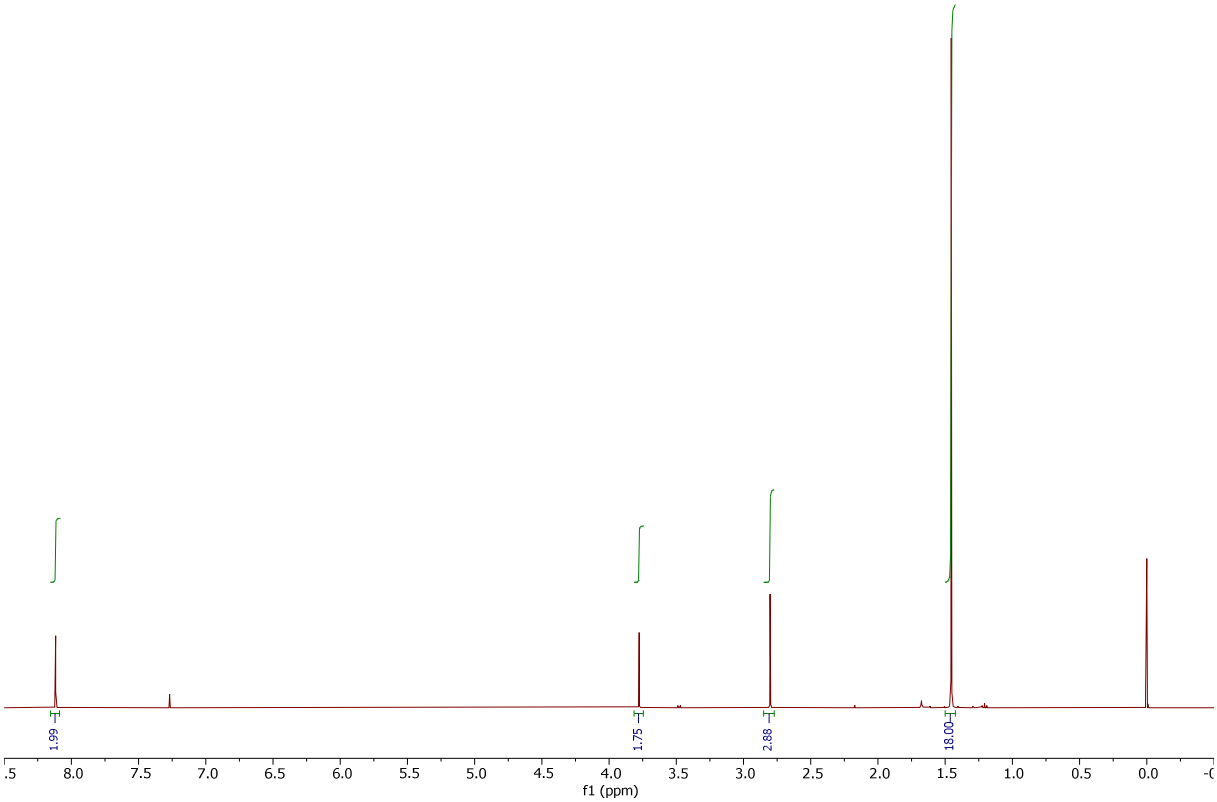

Figure S61. ^{1}H NMR spectrum (400 MHz, $CDCl_3$) of **15**.

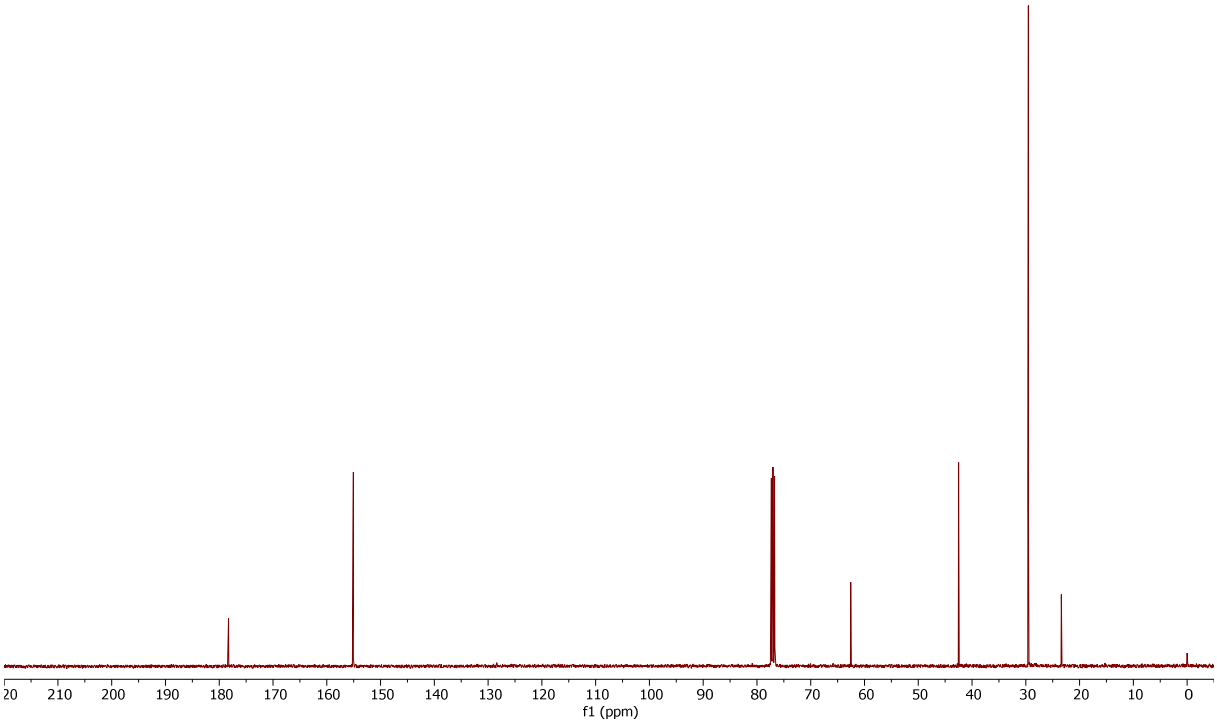

Figure S62. $^{13}C\{^{1}H\}$ NMR spectrum (101 MHz, $CDCl_3$) of **15**.

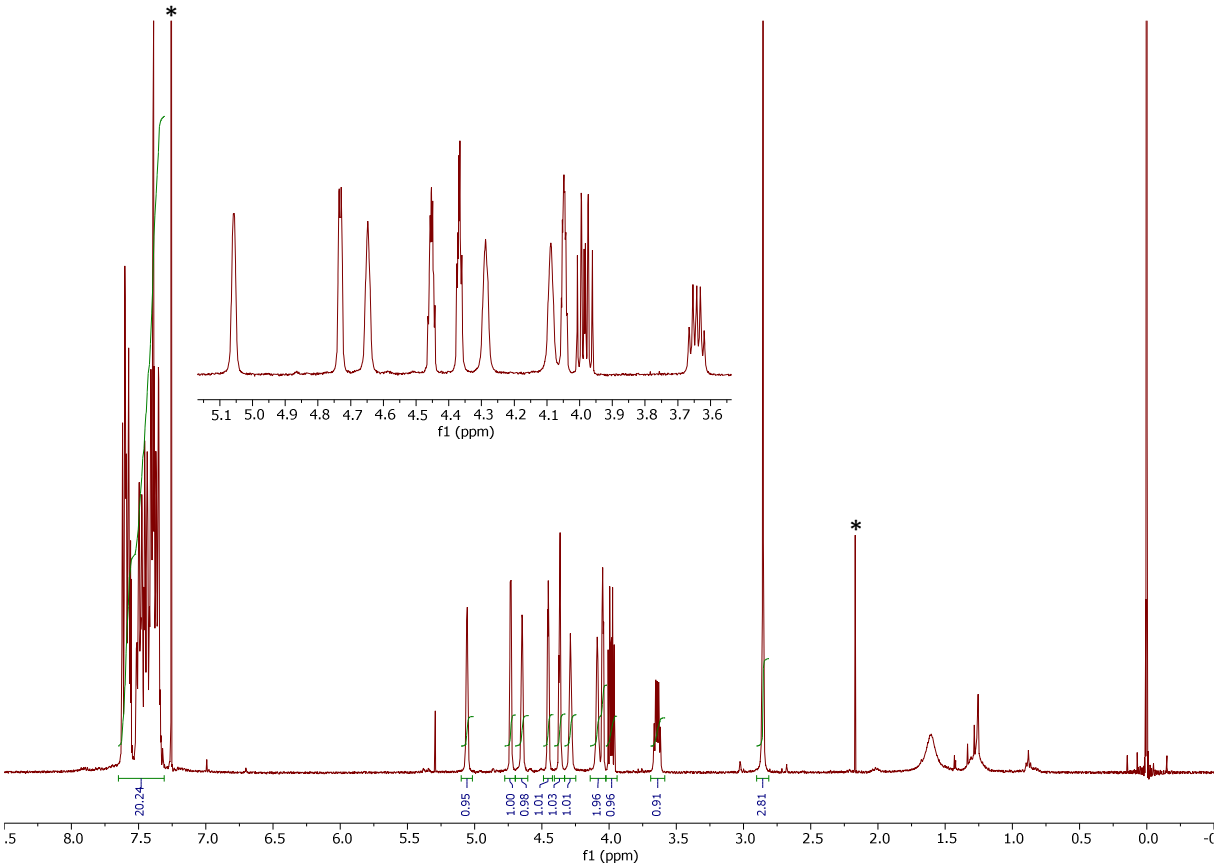

Figure S63. ^{1}H NMR spectrum (400 MHz, $CDCl_3$) of **16**.

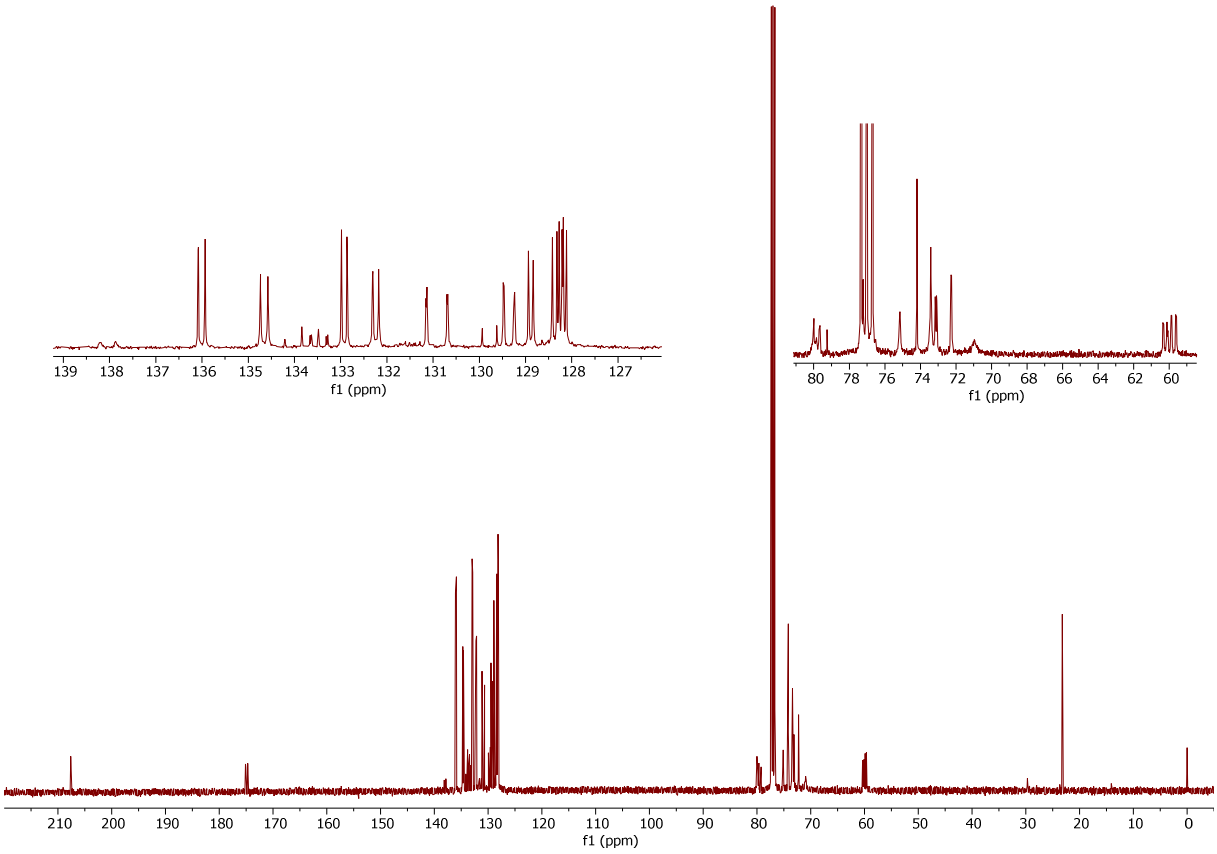

Figure S64. $^{13}C\{^{1}H\}$ NMR spectrum (101 MHz, $CDCl_3$) of **16**.

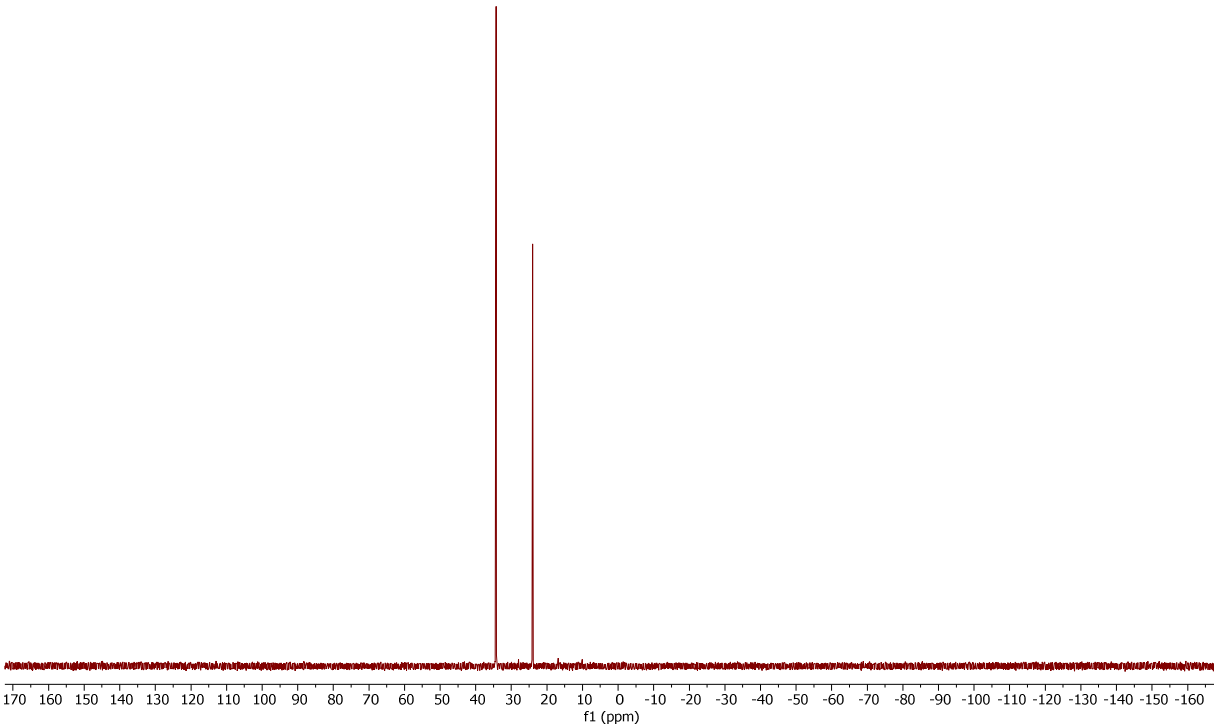

Figure S65. $^{31}P\{^{1}H\}$ NMR spectrum (162 MHz, $CDCl_3$) of **16**.

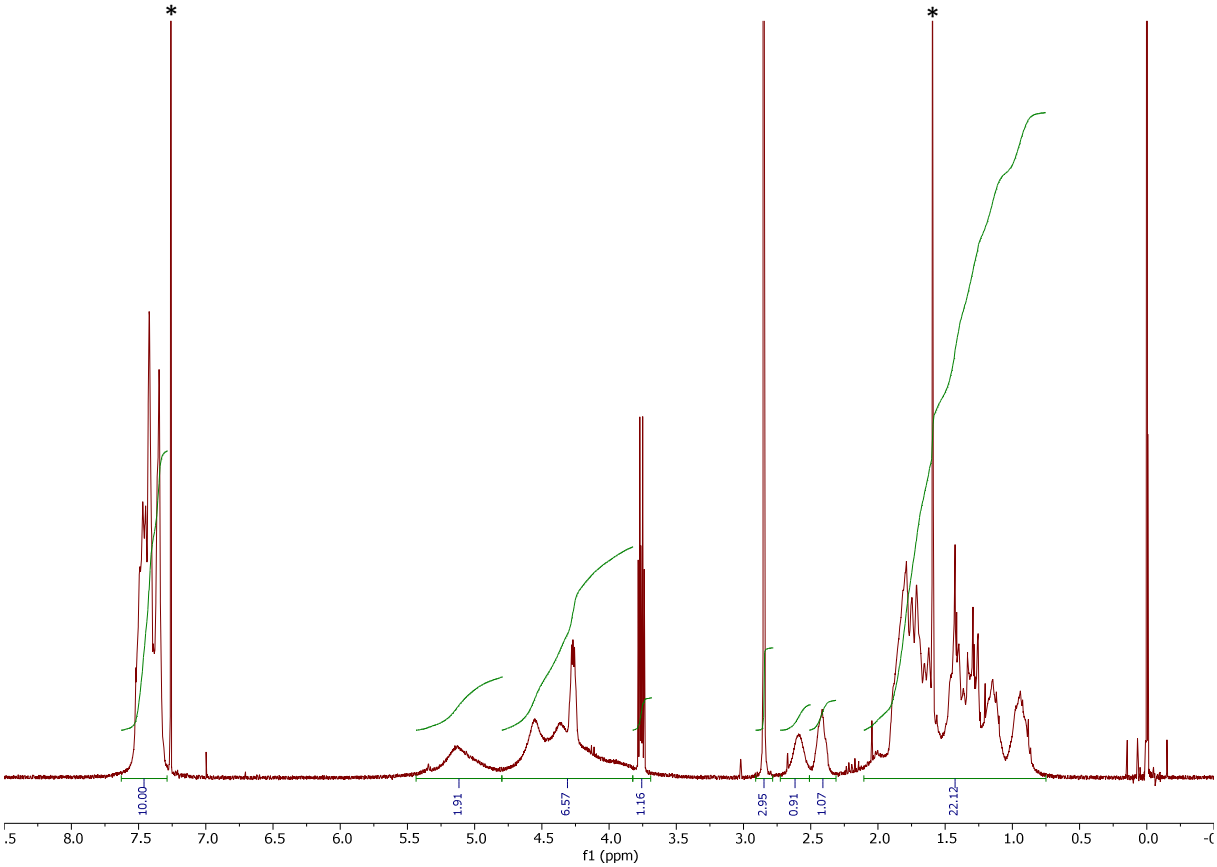

Figure S66. ^{1}H NMR spectrum (400 MHz, $CDCl_3$, 25 °C) of **17**.

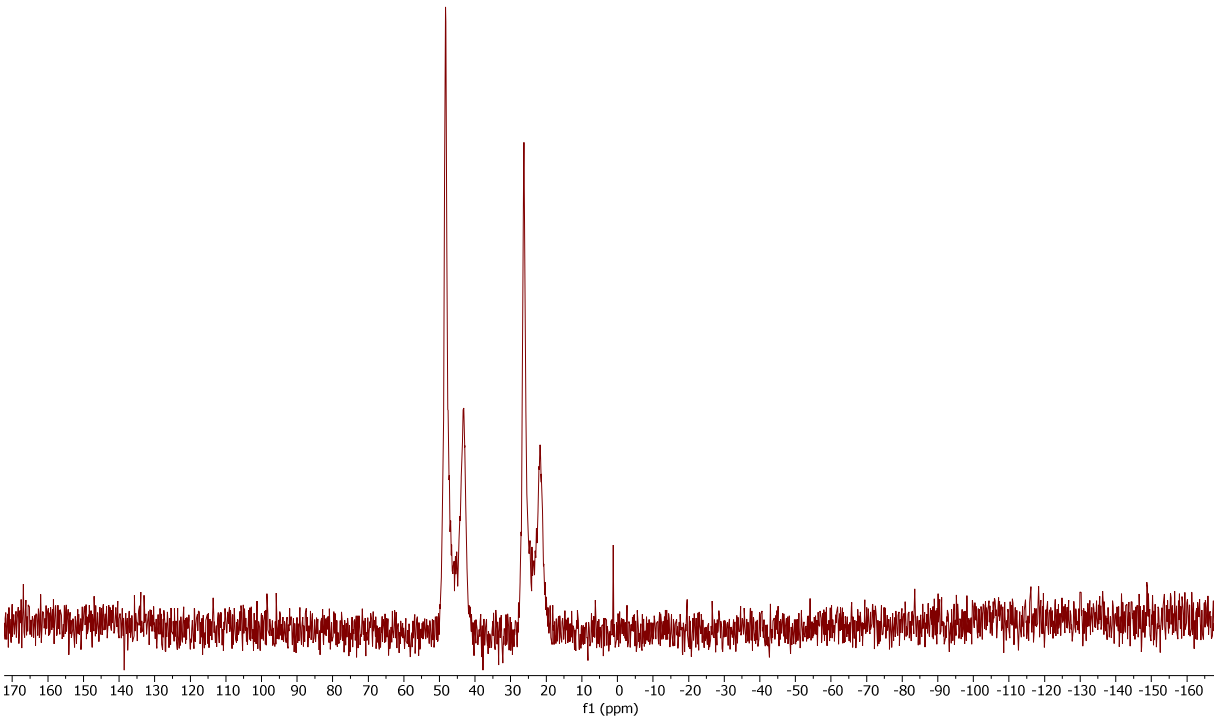

Figure S67. ^{31}P{^{1}H} NMR spectrum (162 MHz, $CDCl_3$, 25 °C) of **17**.

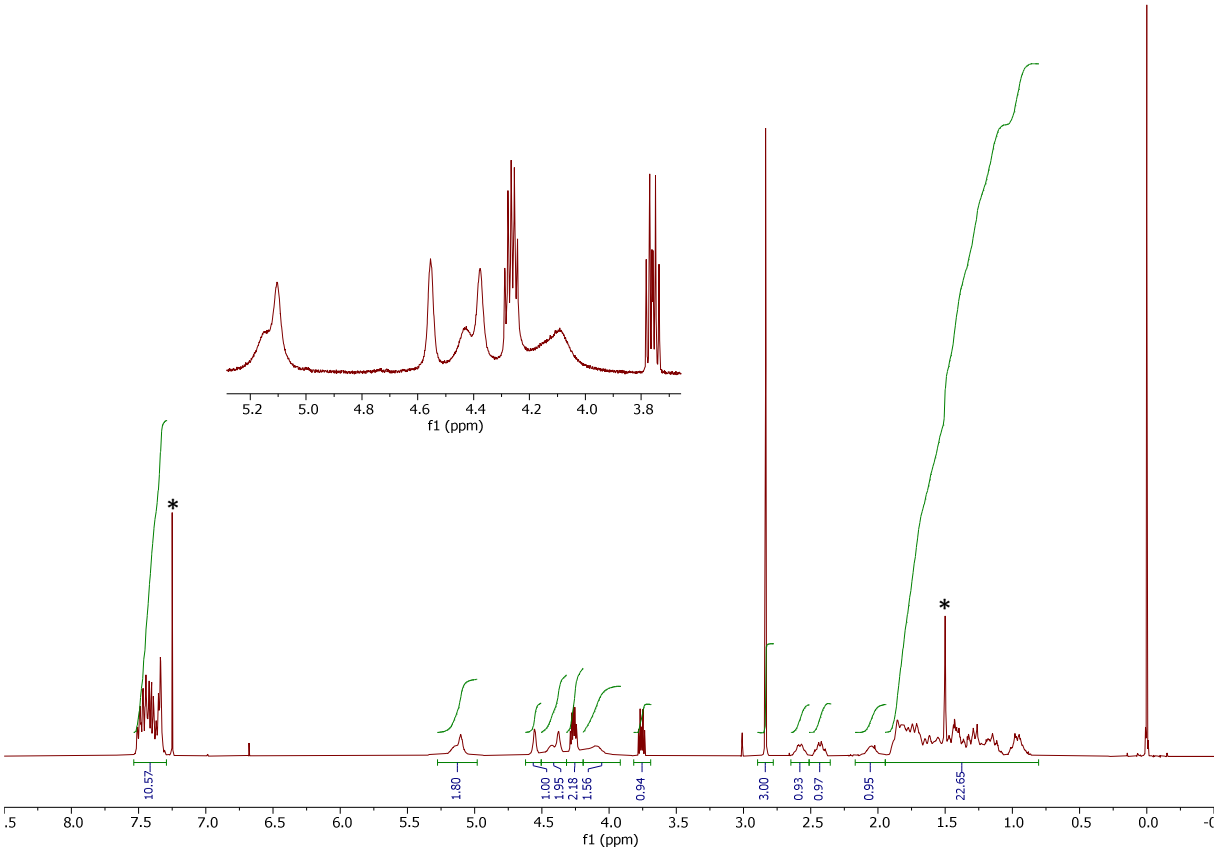

Figure S68. ^{1}H NMR spectrum (400 MHz, $CDCl_3$, 50 °C) of **17**.

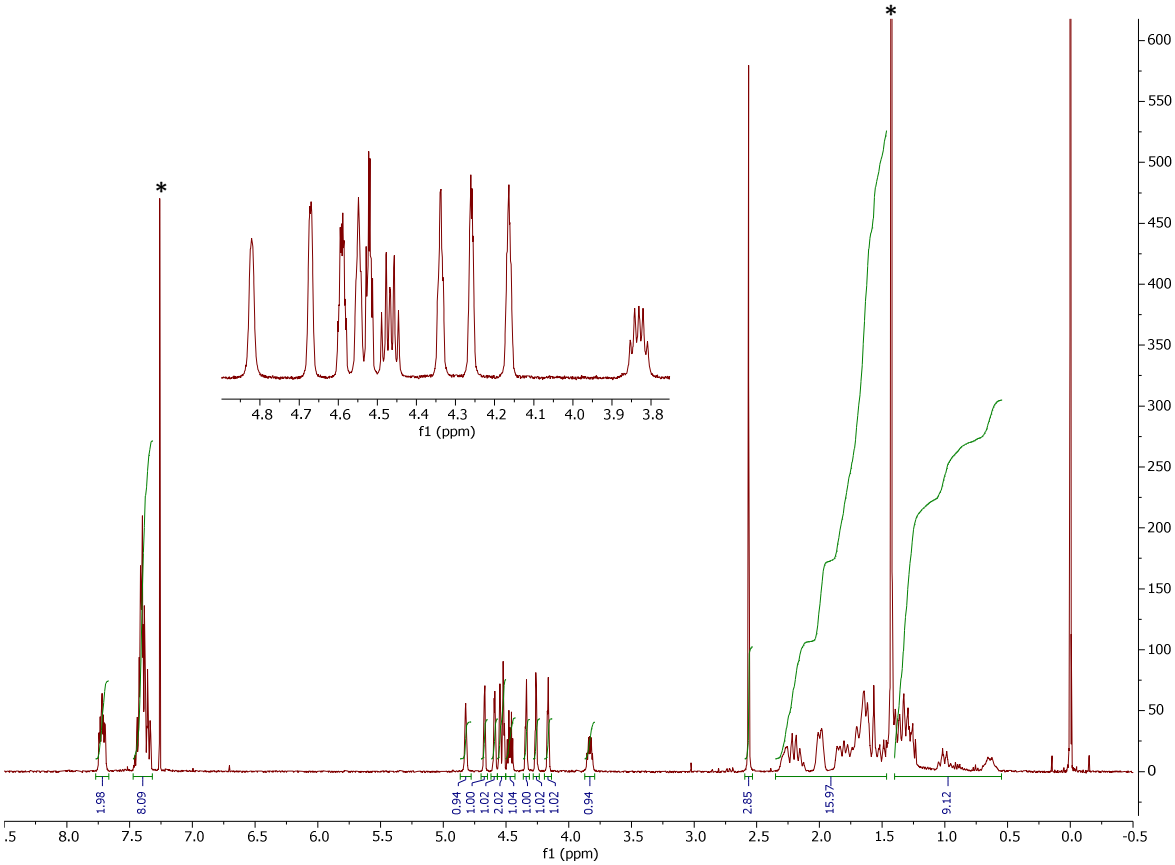

Figure S69. ^{1}H NMR spectrum (400 MHz, $CDCl_3$) of **18**.

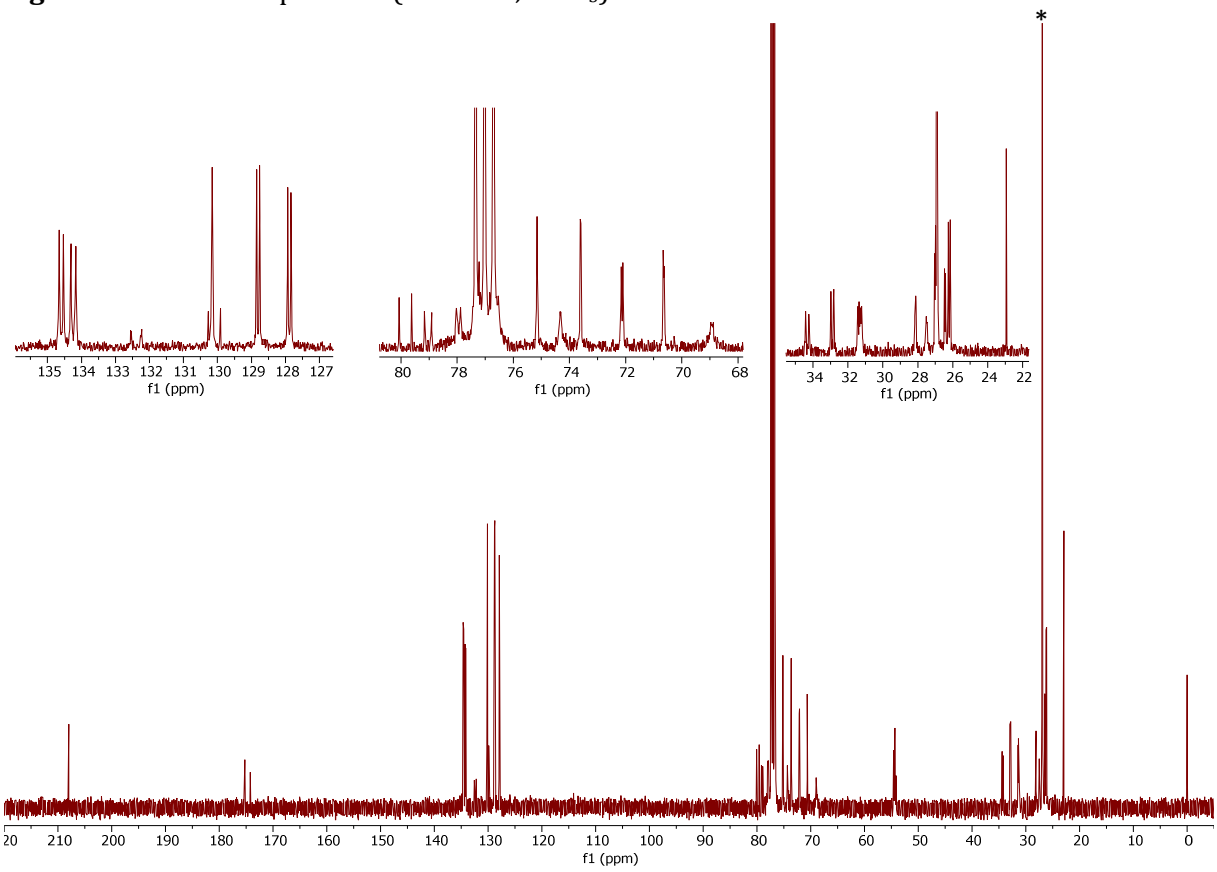

Figure S70. ^{13}C{^{1}H} NMR spectrum (101 MHz, $CDCl_3$) of **18**.

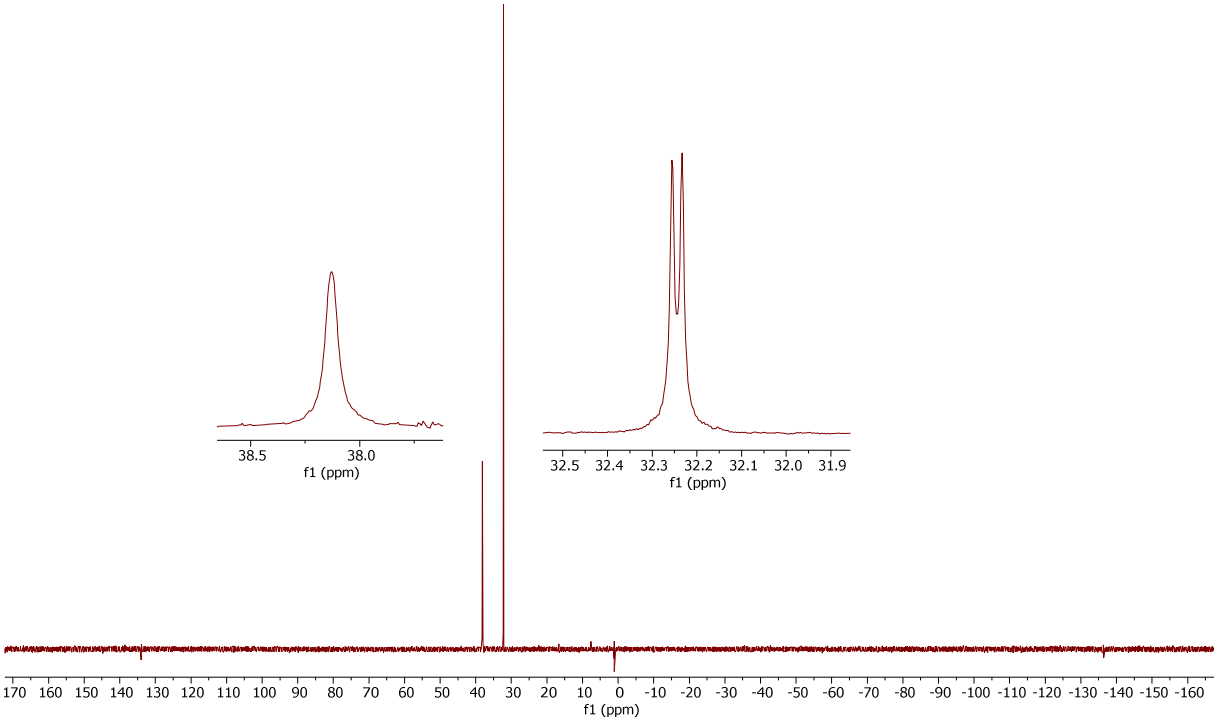

Figure S71. $^{31}P\{^{1}H\}$ NMR spectrum (162 MHz, $CDCl_3$) of **18**.

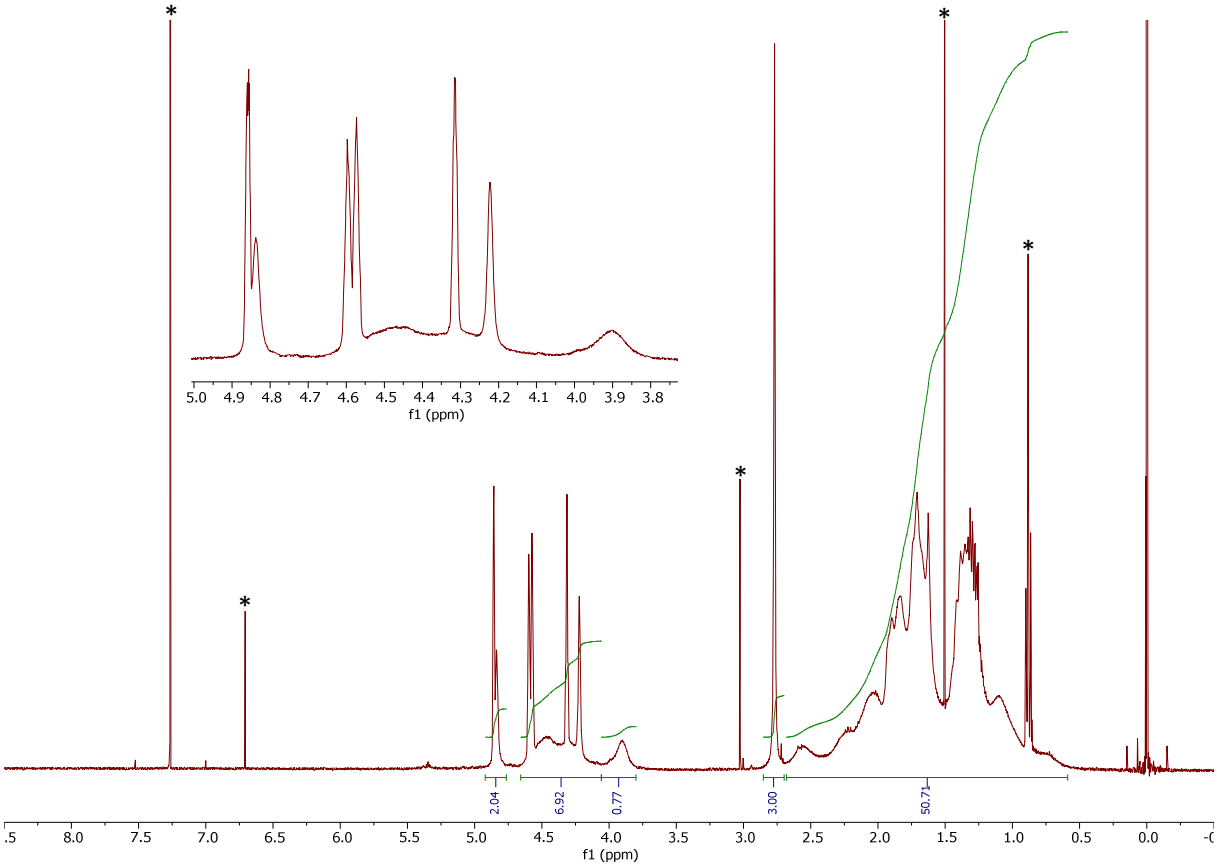

Figure S72. ^{1}H NMR spectrum (400 MHz, $CDCl_3$, 25 °C) of **19**.

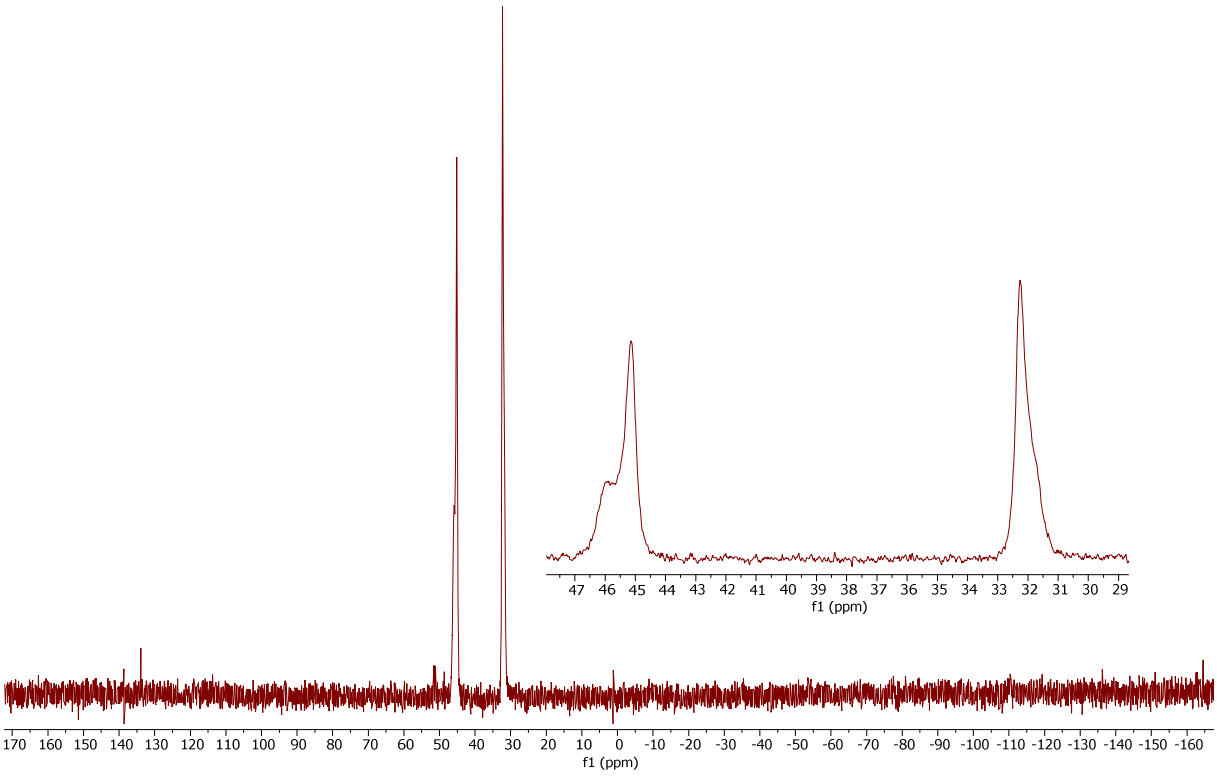

Figure S73. ^{31}P{^{1}H} NMR spectrum (162 MHz, $CDCl_3$, 25 °C) of **19**.

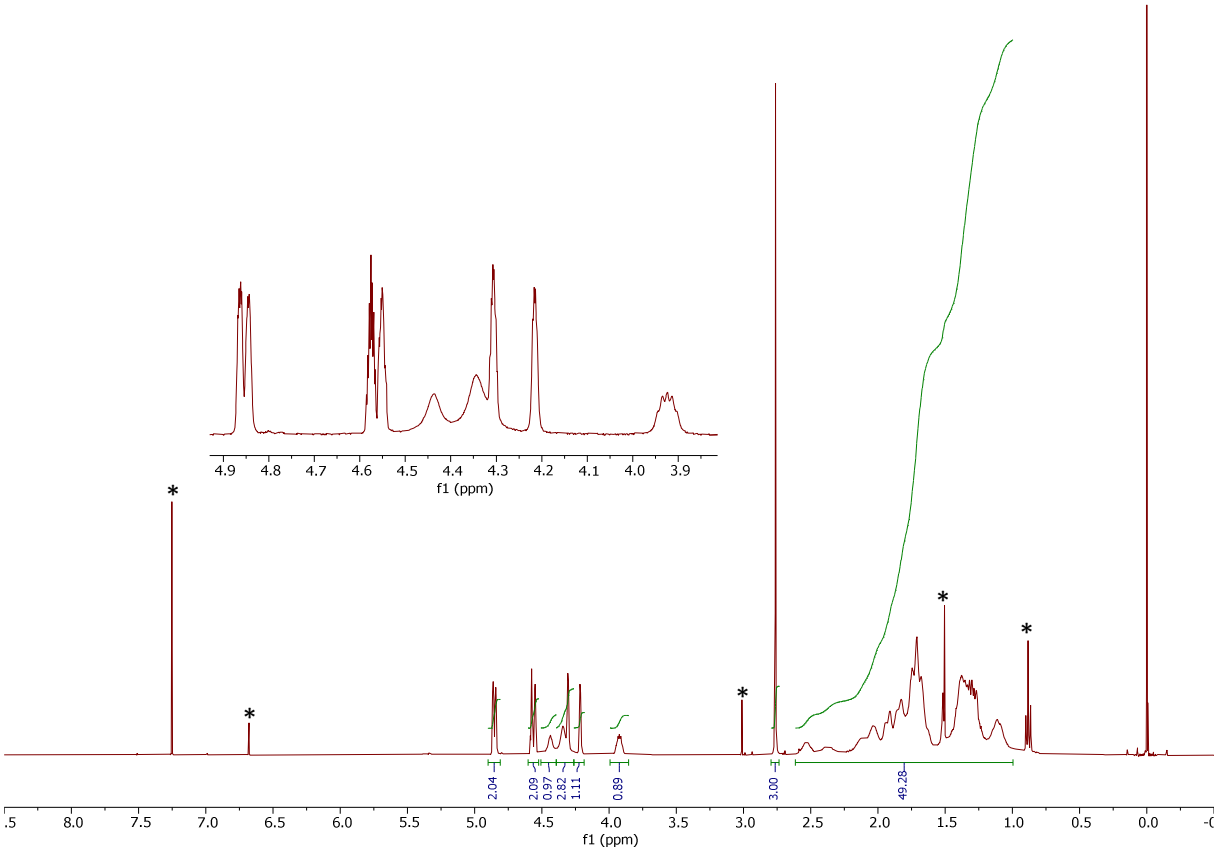

Figure S74. ^{1}H NMR spectrum (400 MHz, $CDCl_3$, 50 °C) of **19**.

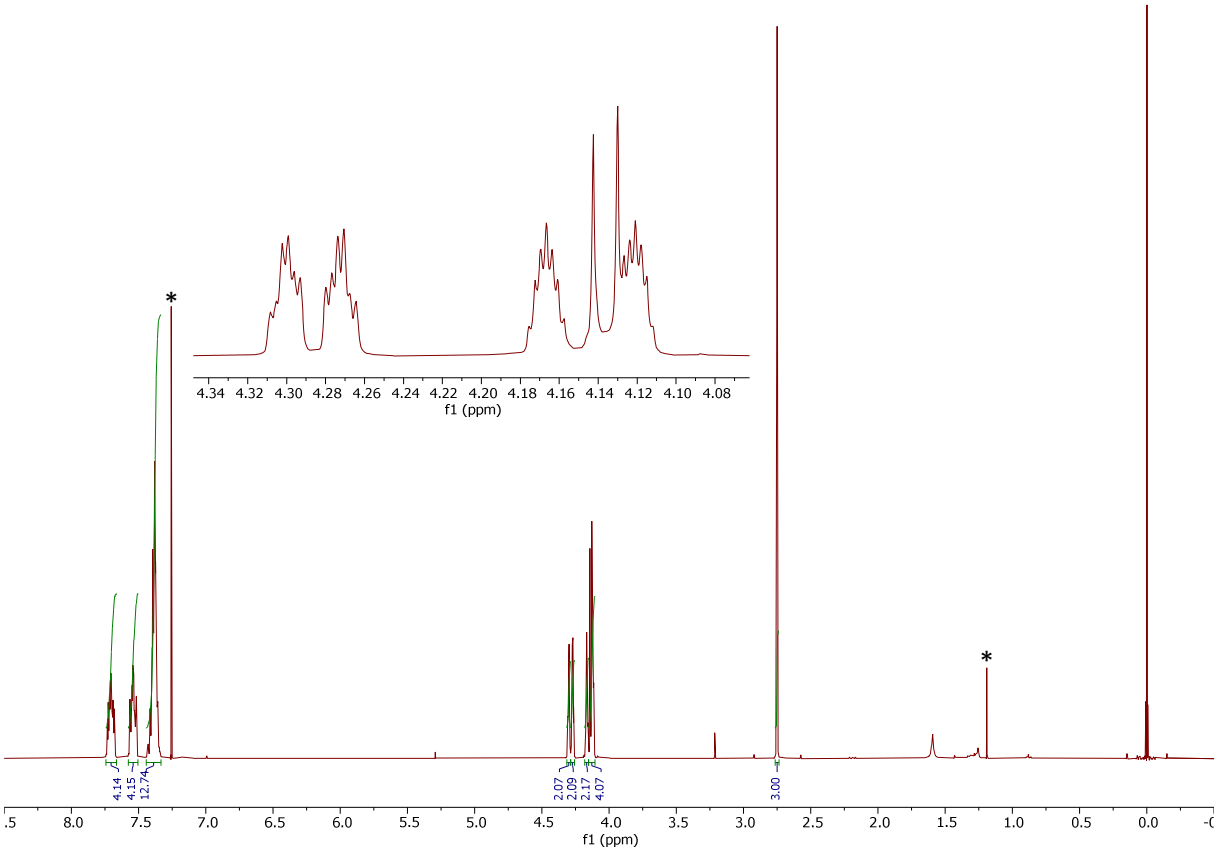

Figure S75. ^{1}H NMR spectrum (400 MHz, $CDCl_3$) of **20**.

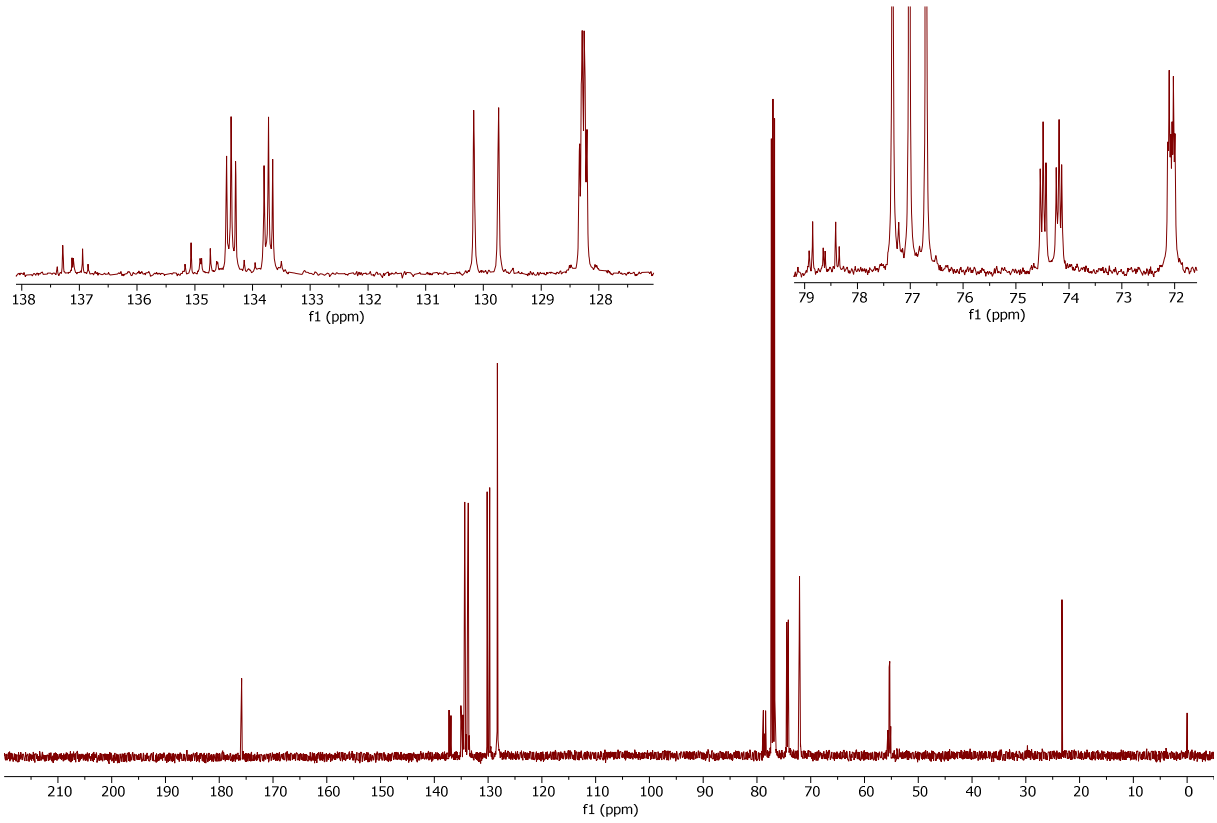

Figure S76. ^{13}C{^{1}H} NMR spectrum (101 MHz, $CDCl_3$) of **20**.

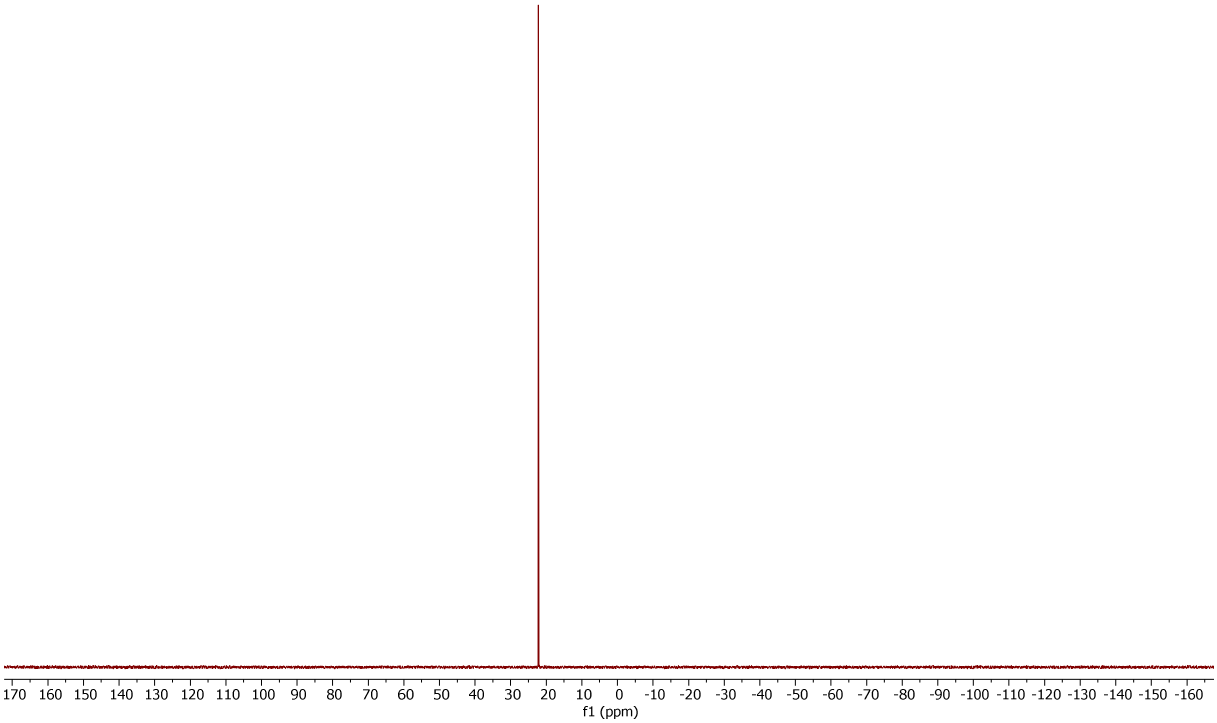

Figure S77. $^{31}P\{^{1}H\}$ NMR spectrum (162 MHz, $CDCl_3$) of **20**.

References

1 J. J. M. de Pater, D. S. Tromp, D. M. Tooke, A. L. Spek, B.-J. Deelman, G. van Koten, C. J. Elsevier, *Organometallics*, 2005, **24**, 6411.

2 P. Hauwert, R. Boerleider, S. Warsink, J. J. Weigand, C. J. Elsevier, *J. Am. Chem. Soc.,* 2010, **132**, 16900.

3 K. Dong, R. Sang, X. Fang, R. Franke, A. Spannenberg, H. Neumann, R. Jackstell, M. Beller, *Angew. Chem. Int. Ed.*, 2017, **56**, 5267.